Transcriptional and Epigenetic States Underlying Drug Resistance in Malignant Melanoma

Master Thesis

For the attainment of the academic degree

Master of Science

From the University of Applied Sciences FH Campus Wien

Submitted by:
Melanie Allram

Personal identity code
1810544045

Supervisor:
Dr. Leonard Zon
Boston Children's Hospital and Harvard University
Boston, Massachusetts
United States of America

Submitted on:
25. 02. 2021

Abstract (English)

Melanoma is a cancer of melanocytes, the pigment producing cells in the human body, and is the deadliest form of skin cancer. Molecular classification has revealed the activating *BRAFV600E* mutation as a major driver of melanoma. Targeted inhibitors of the MAPK signalling pathway have greatly improved patient outcomes, but resistance is almost universal within one year of initiating treatment. Understanding of molecular mechanisms driving drug resistance in malignant melanoma is of great importance to identify novel therapeutic approaches. Melanoma exhibits a high degree of both inter- and intratumoral heterogeneity and the arrival of single-cell sequencing techniques has allowed characterization of distinct phenotypic tumor states. To further define disease relevant tumor states we investigated primary melanoma samples on two levels: transcriptionally by applying single-cell RNA sequencing (scRNA-seq) and epigenetically by single-cell ATAC sequencing (scATAC-seq) during treatment with MAPK pathway inhibitors. For modelling *BRAFV600E* driven melanoma, we used a *BRAFV600E;tp53*$^{-/-}$ driven zebrafish model of melanoma that was previously established in the Zon lab. Primary tumors were generated and drug treated with the BRAF inhibitor dabrafenib. Resistant tumors arose with variable kinetics and samples from several disease relevant time points were obtained for both scRNA-seq and scATAC-seq to identify candidate transcriptional and epigenetic states characteristic of phases of drug response to MAPK pathway inhibition. Our data suggests that an initial dedifferentiation takes place, followed by acquisition of a neural crest/“stress-like” state in minimal disease cells. Pseudotime trajectory analysis revealed two distinct cell states in resistant cells: a differentiated cell state and a neural crest/ “stress-like” state. The *in vitro* validation of the “stress-like” state revealed differential expression of candidate genes in a resistant and sensitive cell line upon inhibition of stress signalling using pharmacologic inhibition. Bulk ATAC-seq showed higher accessibility of several stress related genes in the resistant cell line. Collectively, our study demonstrated the acquisition of a “stress-like” subpopulation in melanoma upon BRAF inhibition and provides a refinement of transcriptional and epigenetic cell states at respective disease-relevant time points.

Abstract (German)

Melanom ist ein Krebs der Melanozyten, jene Zellen, die im menschlichen Körper Pigment produzieren. Diese Krebsart gilt als einer der tödlichsten Hautkrebsarten. Molekulare Tumorklassifizierung hat gezeigt, dass die aktivierende *BRAFV600E*-Mutation eine wesentliche Drivermutation von Melanom ist. Gezielte Inhibitoren des MAPK Signalweges haben eine gute Wirkung auf den Heilungsprozess von Patienten gezeigt. Eine Resistent tritt aber in fast allen Fällen innerhalb eines Jahres nach Beginn der Behandlung ein. Das Wissen über die molekularen Mechanismen, die zur einer Medikamentenresistenz bei einem malignen Melanom führen, ist von zentraler Bedeutung, um zukünftige Therapieansätze verbessern zu können. Das Melanom weist ein hohes Maß an inter- und intratumoralen Heterogenität auf und das Einbringen von Einzelzell-Sequenzierungstechniken hat die Differenzierung verschiedener Tumorphänotypen wesentlich vorangetrieben. Für weitere Tumordefinitionen wandten wir zwei unterschiedliche Methoden zur Untersuchung primärer Melanomproben an: transkriptionell durch Anwendung von Einzelzell-RNA-Sequenzierung (scRNA-seq) und epigenetisch durch Einzelzell-ATAC-Sequenzierung (scATAC-seq), während der Behandlung mit MAPK-Signalweg-Inhibitoren. Für die Modellierung des *BRAFV600E*-getriebenen Melanoms wurde ein im Zon-Labor etabliertes *BRAFV600E;tp53* getriebenes Zebrafischmodell des malignen Melanoms verwendet. Primärtumore wurden generiert, medikamentös behandelt und scRNA-seq und scATAC-seq wurden durchgeführt, um den transkriptionellen und epigenetischen Status zu identifizieren, die charakteristisch für die Phasen der Medikamentenwirkung auf die Inhibition des MAPK-Signalweges sind. Resistente Tumore entstanden mit variabler Kinetik und in einem weiteren Schritt wurden Proben von mehreren krankheitsrelevanten Stadien genommen. Unsere Daten deuten darauf hin, dass eine anfängliche Dedifferenzierung stattfindet, gefolgt vom Erwerb eines Neuralleisten/Stress Zustandes in den Zellen mit minimaler Krankheit. Die Pseudozeitanalyse zeigte zwei unterschiedliche Zellstatus in den resistenten Zellen: einen differenzierten Zellstatus und einen Neuralleisten-/Stress Status. Die *in vitro*-Validierung des Stressstatus ergab eine differentielle Expression von Kandidatengenen in einer resistenten und sensitiven humanen Melanom-Zelllinie bei Hemmung der Stresssignalwege durch pharmakologische Inhibition. Die ATAC-Sequenzierung demonstrierte eine höhere Zugänglichkeit mehrerer „Stressgene“ in der resistenten Zelllinie. Zusammenfassend zeigt unsere Studie die Akquisition einer „stressähnlichen" Subpopulation im Melanom nach BRAF-Inhibierung und stellt eine genaue Analyse der transkriptionellen und epigenetischen Zellstatus in krankheitsrelevanten Stadien dar.

Table of Contents

1 List of abbreviations

CAFs	Cancer-associated fibroblasts
cDNA	Complementary DNA
DMEM	Dulbecco's Modified Eagle Medium
DNA	Deoxyribonucleic acid
DNA	Copy-number alterations
ECM	Extra-cellular matrix
ER	Endoplasmic reticulum
hrs	Hours
IF	Immunofluorescence
kb	Kilo base
M	Mole
MCR:EGFP	MiniCoopR: Enhanced green fluorescent protein
MRD	Minimal residual disease
mRNA	Messenger RNA
NCSC	Neural crest stem cells
ng	Nano gram
NK cells	Natural killer
nM	Nanomole
PBS	Phosphate-buffer saline
PCA	Principal component analysis
PCR	Polymerase chain reaction
PDX	Patient-derived xenograft
pg	Pico gram
QC	Quality control
qPCR	Quantitative polymerase chain reaction
RNA	Ribonucleic acid
ROS	Reactive oxygen species

scATAC-seq	Single-cell assay for transposase-accessible chromatin using sequencing
scRNA-seq	Single-cell ribonucleic acid sequencing
SMC	„Starved“-like melanoma cells
TCGA	The Cancer Genome Atlas
Tg	Transgenic
TME	Tumor micro environment
T-SNE	T-distributed stochastic neighbor embedding
uM	Micromole
UMAP	Uniform manifold approximation and projection
UV	Ultraviolet
V600E	Valine (V) is substituted by glutamic acid (E) at amino acid 600
V600K	Valine (V) is substituted by lysine (K) at amino acid 600
WT	Wild type

2 Introduction

2.1 Molecular classification of melanoma

The skin is the largest human organ and fulfils a barrier function for external forces as well as maintaining chemicals and nutrients inside the body. It consists of several layers: the epidermis which is the visible top layer, the dermis, and subcutaneous fat as the bottom layer. The epidermis consists predominantly of three cell types: keratinocytes, melanocytes and Langerhans cells. In development, melanocytes derive from the neural crest and migrate to the skin and other sites (Costin and Hearing 2007). Their primary function is to produce the pigment melanin, which acts to protect cells from ultraviolet (UV) radiation. UV radiation can lead to cellular and genetic damage and is one of the leading risk factors for most types of skin cancer (Tobin 2006). UV radiation leads to the generation of reactive oxygen species (ROS) that promote free radical mediated damage to nucleotides and mutagenesis of G/C pairs to A/T pairs. UV radiation can trigger adjacent pyrimidines to form aberrant covalent bonds and form highly mutagenic dimers (D'Orazio et al. 2013). Thus, UV radiation is one of major risk factors for the development of nearly all types of skin cancer. The three most common forms of skin cancers include: basal cell carcinoma, squamous cell carcinoma, and melanoma. This work focuses on cutaneous melanoma, which is a cancer of the melanocytes, and the most deadly form of skin cancer (Diepgen and Mahler 2002).

The genetic and environmental risk factors and why some melanocytes undergo transformation are not fully understood. The triggers for malignant transformation and proliferative/invasive/metastatic behaviour of melanoma cells need to be further investigated. The development of therapies for melanoma patients has greatly progressed over the last decade - with the development of targeted small molecule inhibitors of the MAPK pathway and and immune checkpoint blockade therapies. Yet, it remains to be elucidated why some melanomas respond to certain therapies and some do not, eventually develop metastasis or acquire resistance to established treatments.

In an attempt to understand the molecular mechanisms that drive melanoma, several risk factors and the genetic/hereditary component of the disease have been investigated. 10% of patients with melanoma have a strong family history. This hereditary form of melanoma is often characterized by either recurring cases of melanoma in the family history, a relatively

early development of melanoma or multiple primary tumors within a patient (Gandini et al. 2005).

As in other malignancies, several tumor suppressors have been implicated in the development of melanoma. Among germline mutations, the cell-cycle regulating protein retinoblastoma (RB) is a master regulator of the G1/S checkpoint and disruptions in RB and p53 signalling are considered highly predisposing for melanoma formation (Hodis et al. 2012; Yang et al. 2005).

Markers for pigmentation were also subject to investigation of mutations in melanoma. The melanocortin-1 receptor (MC1R) is a G-protein coupled receptor that activates adenylate cyclase and subsequently the second major player in pigmentation, the microphthalmia-associated transcription factor (MITF) which has been found to be amplified in some melanomas (Tsao et al. 2012). MITF is a helix-loop-helix leucine zipper transcription factor that is a master regulator in melanocyte development and therefore an important player in melanoma development and progression (Ploper and Robertis 2015). The expression of MITF has been shown to drive melanocyte differentiation and is involved in pigmentation processes by regulating the expression of numerous genes involved in melanin synthesis including: tyrosinase (TYR), tyrosinase-related protein 1 (TYRP1) and dopachrome-tautomerase (DCT), together with other genes. Further, MITF regulates proliferation by controlling expression of T-box transcription factor 2 (TBX2) and cyclin-dependent kinase 2 (CDK2). Among others, upstream regulators of MITF are the neural crest transcription factors of Paired box genes 3 (PAX3), cAMP-responsive element binding protein (CREB) and sex-determining region-box 10 (SOX10), in addition to being shown to be regulated through MAPK signalling (Levy et al. 2006).

With its high mutational burden, melanoma driver mutations were initially quite challenging to identify. In an attempt to molecularly classify cutaneous melanoma, The Cancer Genome Atlas program (TCGA) from the National Cancer Institute analysed 333 samples of primary and/or metastatic tumors from 331 patients on the DNA, RNA and protein level using whole exome sequencing, mRNA sequencing and reverse-phase protein array, amongst other methods. From those samples, 52% harbored a BRAF hot-spot mutation in the V600 codon (fig.1). The most prevalent substitution is V600E followed by V600K or V600R. These mutation in BRAF lead to activation of the MAPK signalling pathway (The Cancer Genome Atlas Network 2015). Under physiological condition, this pathway triggers proliferation. These mutations lead to constitutive activation of the BRAF kinase and prolonged activation of the

MAPK signalling pathway. Upon constitutive activation, the pathway triggers proliferation and survival signalling which results in abnormal cell growth and, along with loss of a tumor suppressor, can result in cancer formation (Davies et al. 2002). Samples with a BRAF V600 and K601 hot-spot mutation typically did not occur with hot-spot NRAS mutations, however, BRAF non-hot-spot mutations were correlated with RAS hot-spot and Neurofibromatosis type 1 (NF1) mutations. The second most prevalent subtype is defined by hot-spot mutations in N-, K- and H-RAS. The NF1 subtype is the third major subtype with 14% of all samples. With its GTPase activity and RAS downregulating function, over 50% of mutations in NF1 were predicted to be loss-of-function and thereby activating canonical MAPK signalling. Samples that did not harbor BRAF, RAS or NF1 mutations were categorized as triple wild-type (Triple-WT) subtype (The Cancer Genome Atlas Network 2015).

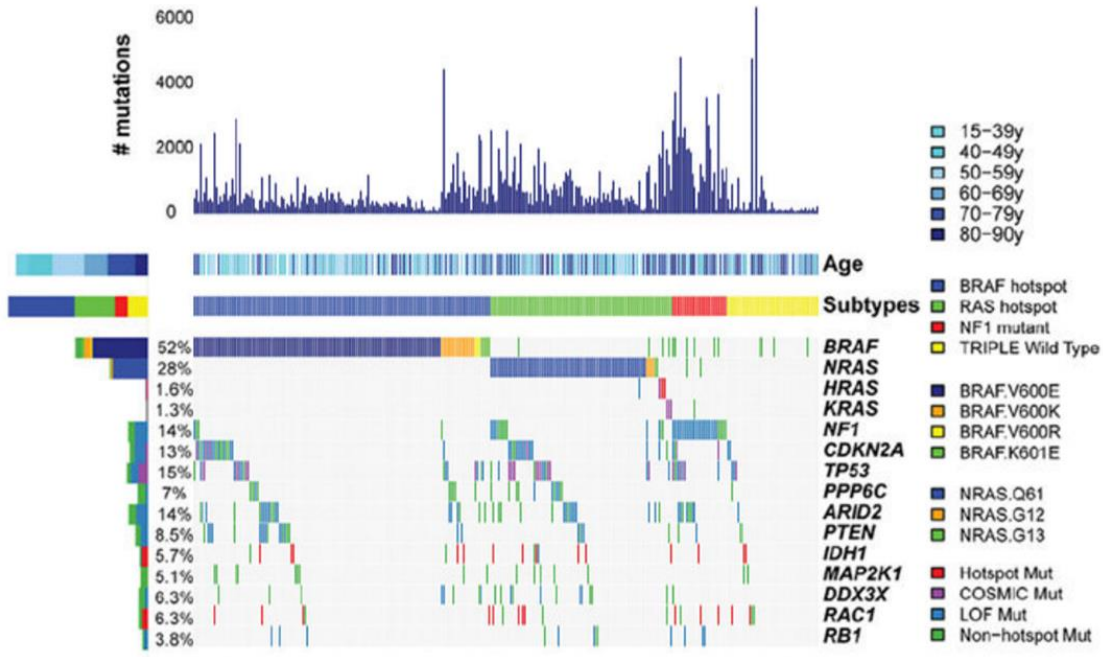

Figure 1: Molecular classification of malignant melanoma. *From top to bottom: Total number of mutations, age of melanoma accession, subtype of mutation (BRAF, RAS, NF1 and Triple-WT), colour-coded matrix of individual mutations. Figure adapted from (The Cancer Genome Atlas Network 2015).*

The samples with BRAF, RAS or NF1 hot-spot mutations had a high prevalence (90-93.5%) of UV-signature mutations, which is defined by C>T transitions at dipyrimidine sites but only 30% of Triple-WT melanomas demonstrated a UV mutational signature. Somatic copy-number alterations (CNA) and focal amplifications of known oncogenes and candidate fusion drivers were enriched in Triple-WT melanoma samples. With only 30% of Triple-WT samples harboring a UV signature and the high abundance of somatic CNAs, it is very likely that

structural rearrangements are a major driver of Triple-WT melanomas (The Cancer Genome Atlas Network 2015).

Whole genome sequencing studies of 183 melanoma samples further revealed *BRAF*, *CDKN2A*, *NRAS* and *TP53* as significantly mutated genes in cutaneous melanoma. Acral (hands and feet) and mucosal (internal body surfaces) melanoma showed higher frequency of structural variants than cutaneous melanoma. Different telomere length was observed between the samples, but not between the different melanoma subtypes. Non-coding mutations were prominent in the TERT promoter region resulting in new binding sites for the GA-binding protein transcription factor (GABPA), which ultimately regulates telomerase activity and telomere length. The loss-of-function mutations of Triple-WT melanoma subtypes were found in *CDKN2A*, *TP53* and *ARID2*. The mitogen-activated protein kinase (MAPK), phosphoinositol 3-kinase (PI3K) and receptor tyrosine kinase (RTK) were the most affected signalling pathways (Hayward et al. 2017).

The signalling pathways affected correlate with the visual and spatial appearance of melanoma. Superficial spreading and nodular melanoma often harbor *BRAF* and *NRAS* mutations affecting the MAPK pathway whereas *KIT* aberrations in acral melanoma are associated with RTK signalling (Tsao et al. 2012).

2.2 Tumor heterogeneity

The concept of tumor heterogeneity is based on the assumption that tumors do not consist of a single cell "type" that is genetically different from normal cells, but rather are made up of different populations of genetically, transcriptionally, and epigenetically definable malignant cells (fig. 2) (Burrell et al. 2013; Marusyk et al. 2012; Heppner 1984).

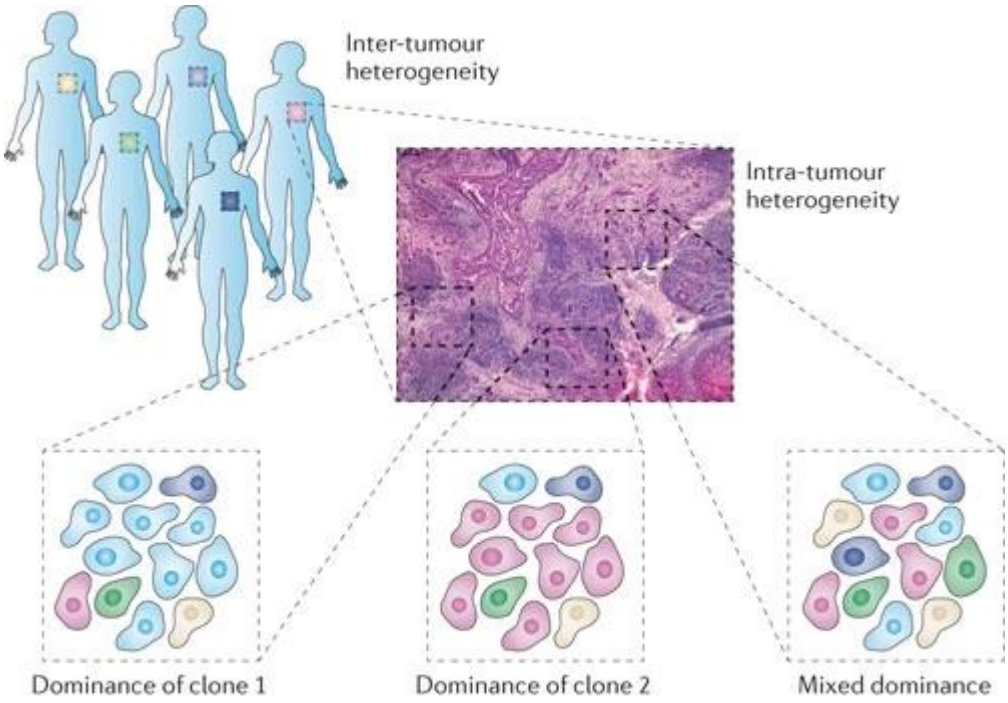

Figure 2: Melanoma patients harbor inter- and intratumoral heterogeneity. *Heterogeneity varies between and within tumors and can lead to dominance of certain phenotypes. Figure adapted from (Marusyk et al. 2012).*

Bulk sequencing of tumors identifies the dominant cell phenotype but single-cell analysis can better reflect on the composition of various subpopulations of cells within a tumor. These populations can consistent of both benign stromal elements as well as malignant cells that are all defined by distinct transcriptional and epigenetic programs that drive a certain phenotype. Single-cell sequencing techniques have emerged as a powerful tool to define cell types and programs within heterogeneous tissues. Single-cell RNA sequencing (scRNA-seq) of patient melanoma samples and dimensional reduction for instance allows clustering of non-malignant cells in their various cell types (NK, T-cells, B-cells, Macrophages, CAFs, Endothelial cells) and reveals individual clustering of malignant cells from various patients (indicated by different colour coding, fig.3) (Tirosh et al. 2016).

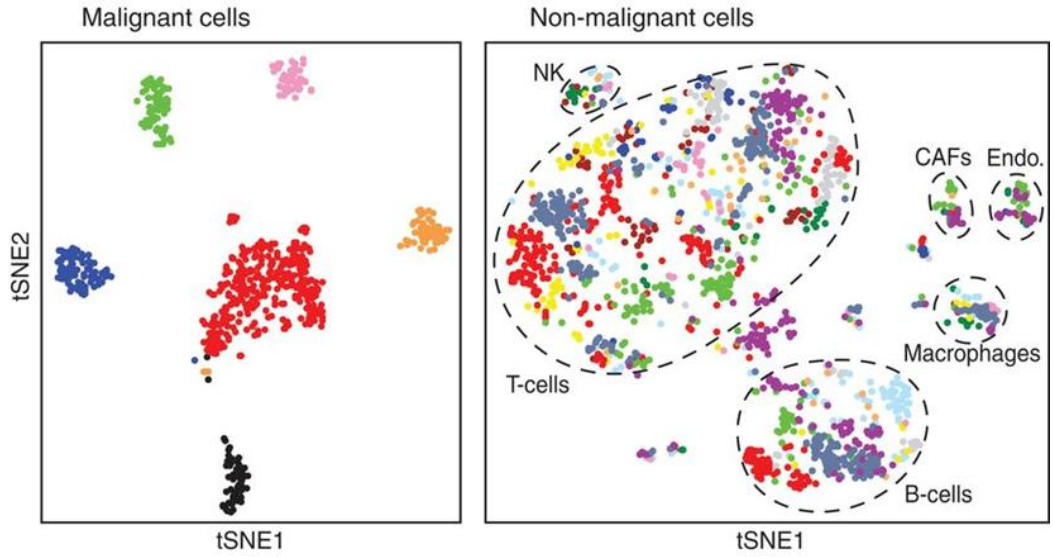

Figure 3: Single-cell expression analysis revealed clusters of malignant and non-malignant cells. *T-distributed Stochastic Neighbor Embedding (T-SNE) plots show malignant cell types from six tumors and non-malignant cells from 11 tumors with annotated cell types. Figure adapted from (Tirosh et al. 2016).*

In melanoma, the first two major phenotypes identified were an invasive/mesenchymal and a proliferative phenotype (Hoek et al. 2008). Those are defined by the expression levels of different transcriptional master regulators that control gene expression and the respective transcriptional program that drive a certain cell phenotype. The mesenchymal phenotype is characterized by low levels of MITF and correlates with high levels of AXL expression whereas the proliferative phenotype is defined by a relatively higher MITF state (Sensi et al. 2011; Tirosh et al. 2016; Konieczkowski et al. 2014). Single-cell RNA sequencing of cells from melanoma patients revealed the inter- and intratumoral heterogeneity in the $MITF^{high}$–AXL^{low} vs $MITF^{low}$–AXL^{high} program (fig. 4), (Tirosh et al. 2016).

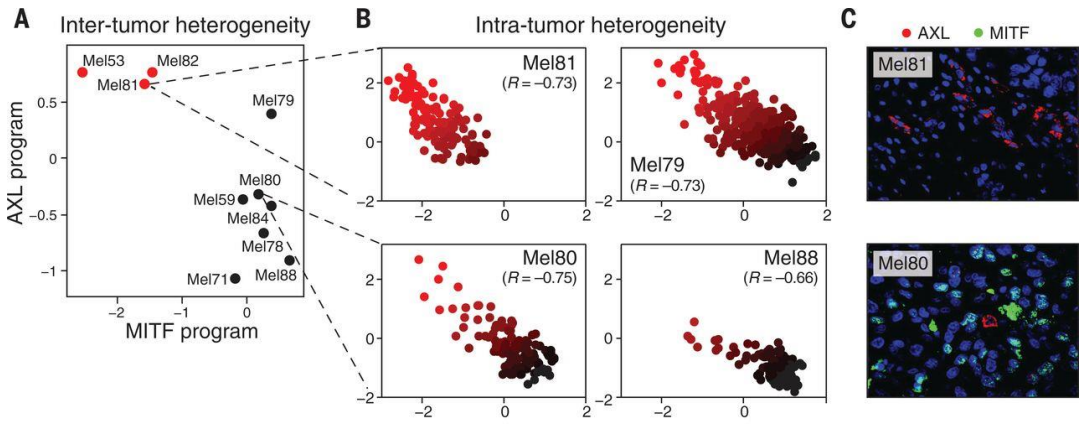

Figure 4: AXL and MITF expression displays inter- and intratumoral heterogeneity. (A) *Average expression of AXL and MITF program within melanoma samples.* ***(B)*** *Negative correlation of AXL and MITF signatures on single-cell level within a tumor.* ***(C)*** *IF staining of* MITF *(green) and* AXL *(red) in two melanoma samples. Figure adapted from (Tirosh et al. 2016).*

Single-cell RNA-sequencing of melanoma cultures also identified main gene regulatory networks that drive either a melanocytic or mesenchymal state and defined an intermediate state between those two. The latter has higher levels of "immune-response-like" transcriptional states and overall displays greater heterogeneity than cells from the melanocytic state. Single-cell regulatory network inference and clustering has led to correlation of specific transcription factors and their target genes being correlated with specific cell states. The melanocytic state has high levels of SOX10, TFAP2A, MITF, IRF4 and SOX4. The mesenchymal state is characterized by high activity of JUN, SOX9, IRF1, FOSL2, ATF5 and NFIB. The intermediate state shares features with both, the melanocytic (SOX10, TFAP2A and MITF) and the mesenchymal cell state (FOSL1, IRF3 and STAT1). The intermediate state shows increased activity of SOX6, NFATC2, EGR3, ELF1 and ETV4. Interestingly, both, the melanocytic and the intermediate states were highly dependent on the expression of SOX10. In a SOX10 knock down experiment the transcriptome collapsed in both cell lines and acquired a mesenchymal-like cell state with comparable transcriptional programs facilitating migration, invasion and development of resistance (Wouters et al. 2020).

But not only the dominance of certain transcription factors play an important role in the context of tumor heterogeneity. The tumor microenvironment (TME) is in continuous contact with the tumor populations and shapes its transcriptional programs by its environmental factors like growth factors and nutrient or oxygen supply (Cheli et al. 2012; Ferguson et al. 2017). The term phenotypic plasticity refers to the capability of genetically identical cells to exhibit several transcriptionally mediated phenotypes. The search for markers of the various phenotypes on the histological level has first brought up different expression of the receptor tyrosine kinase receptor AXL for the mesenchymal phenotype and MITF for the proliferative phenotype (Sensi et al. 2011). Consecutively, the nomenclature changed to $MITF^{high}$–AXL^{low} for the proliferative phenotype and $MITF^{low}$–AXL^{high} for the mesenchymal phenotype. The phenotypes are characterised by different gene signatures. Starting with AXL, the list of gene signatures for the mesenchymal phenotype has been extended by TGF-β and WNT5A. In a microarray assay of melanoma cultures some cultures responded to inhibition of proliferation by TGF-β and some were resistant. The responsive melanoma cultures had low levels of motility whereas the resistant cultures were highly motile. This suggests that TGF-β type and Wnt/β-catenin pathways are differentially regulated and activated

between melanoma samples leading to different motility and metastatic potential of melanoma cells (Hoek et al. 2006; Widmer et al. 2012). The markers for the proliferative phenotype overlap with the gene signature important for melanocyte differentiation and are therefore specific for melanoma. The markers for the mesenchymal phenotype are not specific to melanoma and suggest that this gene signature might also confer an invasive behaviour in other cancer types (Rambow et al. 2015). The markers for the proliferative phenotype correspond with the various cell states that melanocytes undergo during maturation from neural-crest derived precursor cells to mature, differentiated and pigmented melanocytes (Rambow et al. 2018; Tsoi et al. 2018). The state of differentiation as well as the expression of gene signatures associated with immune response, particularly infiltrating lymphocytes can be mapped onto tumour subtypes (Verfaillie et al. 2015; Tirosh et al. 2016).

2.3 Melanoma phenotype plasticity and phenotype switching

Phenotype switching relies on dynamic transcriptional states that allows cells to move between cell states (fig. 5), (Vandamme and Berx 2014). MITF is a major player in this phenotype plasticity and high levels are associated with a proliferative phenotype (Hoek et al. 2008). Upon transition to a mesenchymal phenotype, the suppression or loss of MITF is required, however, the reversible step is a little bit more complicated as the overexpression of MITF in mesenchymal cells does not induce the proliferative phenotype. This leads to the hypothesis that the reversible switch needs other stimuli or changes on the epigenetic level beyond MITF levels (Carreira et al. 2006). Epigenetic profile of proliferative and mesenchymal cells differ from each other (Verfaillie et al. 2015). In the mesenchymal phenotype, MITF and its target genes are repressed and hypermethylated (Lauss et al. 2015). Similarly, an inducible NGFR murine system showed that NGFR drives cancer cells from a proliferative to a mesenchymal slow-cycling phenotype with decrease in tumor growth. Switching off NGFR expression lead to a restored proliferative phenotype and ultimately, was necessary for the tumour progress to metastatic disease (Restivo et al. 2017). The same was shown in Zebrafish- only after EDN-3 induction of a proliferative phenotype the previously invasive cells could metastasize (Kim et al. 2017).

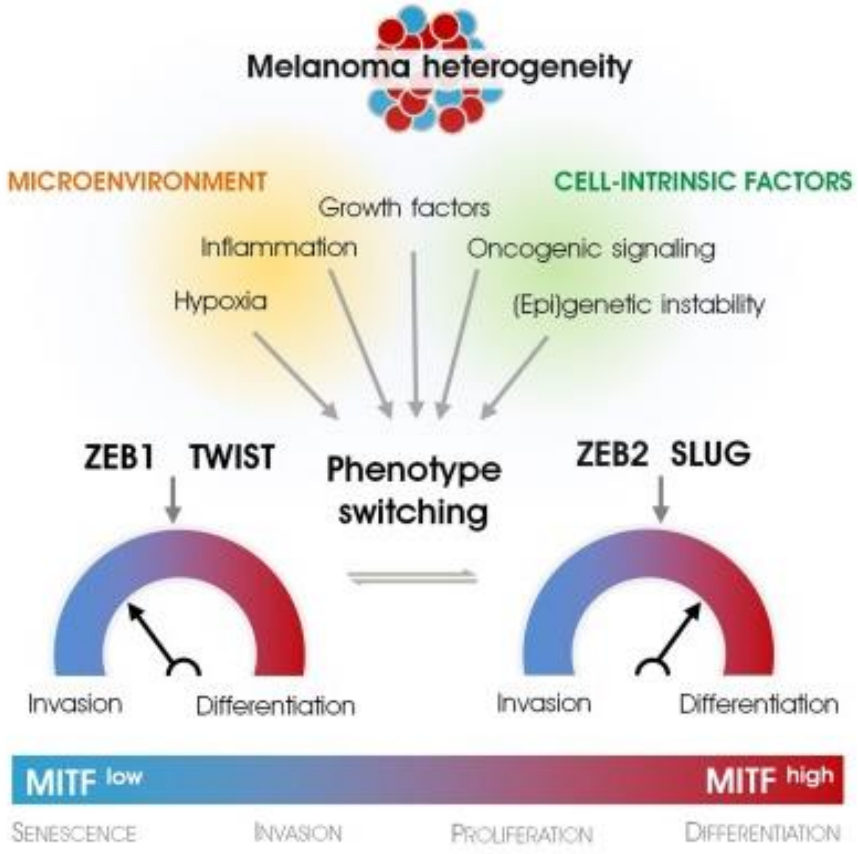

Figure 5: Phenotype switching between invasive and differentiated cell states generates heterogeneity and is triggered by the microenvironment as well as cell-intrinsic factors. *Microenvironmental factors like hypoxia, inflammation and growth factors as well as cell-intrinsic factors like oncogenic signaling and (epi)genetic instability account for the heterogeneity of $MITF^{low}$/invasive and $MITF^{high}$/differentiated cells. Figure adapted from (Vandamme and Berx 2014).*

During tumor development melanocytes transform to melanoma cells exhibiting gene signatures of the proliferative phenotype. They undergo phenotype switching to a mesenchymal phenotype which allows the cells to change their matrix adhesion characteristics, disseminate from the tumor and seed at a metastatic niche. Upon reverse switch to a proliferative phenotype the newly seeded cell can grow out to a metastasis (fig. 6), (Arozarena and Wellbrock 2019).

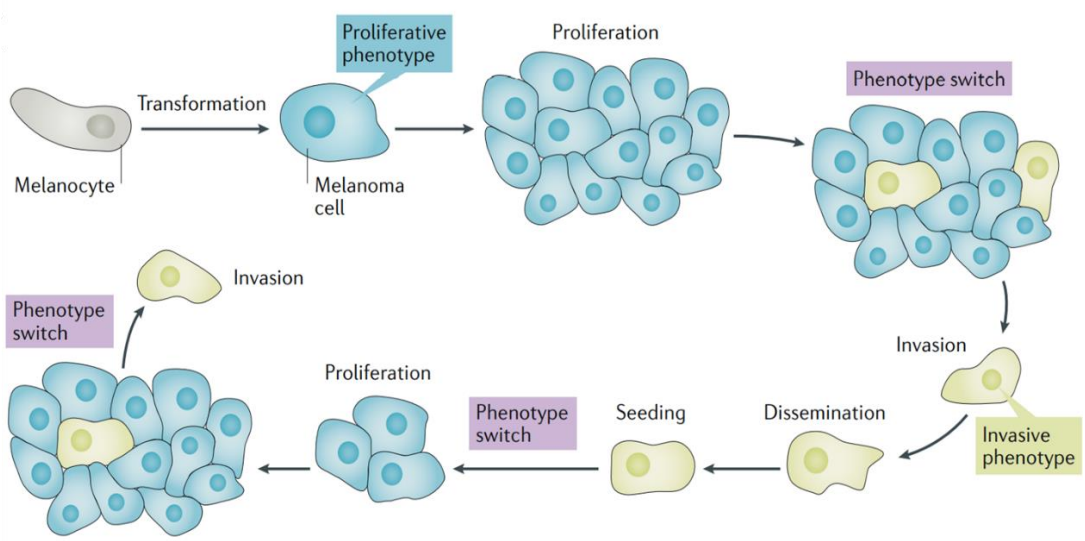

Figure 6: The phenotype-switch model. *The proliferative phenotype drives initial tumor growth and switch to a mesenchymal (invasive) phenotype allows tumor cells to metastasize. At the metastatic niche the switch back to the proliferative phenotype is necessary for full development of metastasis. Figure adapted from (Arozarena and Wellbrock 2019).*

The observation of heterogeneity, not only within tumors and metastasis but also within circulating melanoma cells, leads to the assumption that melanoma cells communicate, progress and metastasize in a cooperative manner. Melanoma cells communicate with each other and their TME. From an intermediate phenotype which comprises cells from both, proliferative and invasive state, cells disseminate heterogeneously and seed and develop into a metastasis cooperatively (fig. 7), (Arozarena and Wellbrock 2019; Chapman et al. 2014).

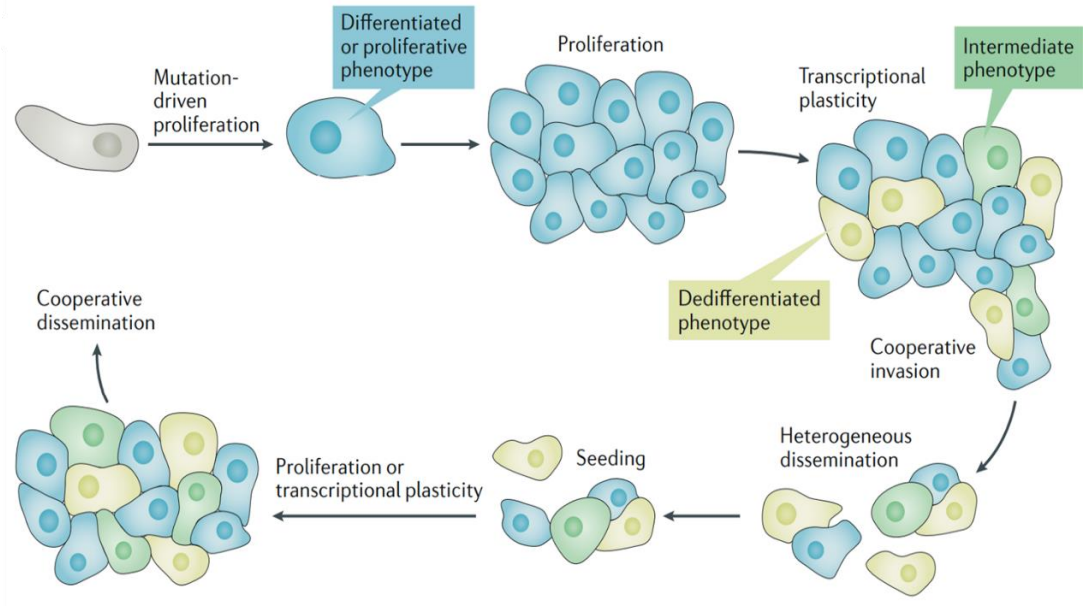

Figure 7: Melanoma cells grow and build metastasis in a cooperative manner. *Cooperativity between melanoma cells and their TME accounts for tumor heterogeneity in all stages of melanoma progression. Figure adapted from (Arozarena and Wellbrock 2019).*

Apart from the cooperative interaction between tumour cells the TME is an important regulator of phenotype plasticity. Nutrients and oxygen availability lead melanoma cells to adapt. Low levels of oxygen push tumors towards a dedifferentiated slow-cycling phenotype that has less oxygen consumption and therefore a survival benefit (Vazquez et al. 2013). This phenotype is also capable of mimicking a vascular endothelium, even in absence of epithelial cells and can thereby lead to neovascularization (Hendrix et al. 2016). The phenotype induced by the hypoxic condition is again mediated by the master regulator MITF, which is suppressed by Hypoxia-induced transcription factor HIF-1a leading to a less differentiation cell state (Feige et al. 2011). Nutrient supply and especially restriction of glucose availability is another driver of a dedifferentiated/ mesenchymal phenotype by transcriptional suppression of MITF (Ferguson et al. 2017; Vazquez et al. 2013). Apart from nutrient and oxygen availability, the cells comprising the TME are important regulators of cancer phenotype. Cancer-associated fibroblasts (CAFs) which are associated with AXL^{high}/ mesenchymal (invasive) gene signatures and negatively correlate with proliferative/ $MITF^{high}$ gene signatures contribute to the TME by remodelling matrix composition and interacting with cancer cells as well as infiltrating leukocytes (Tirosh et al. 2016). Especially in ageing skin CAFs promote an invasive/ mesenchymal phenotype by lowering ECM stiffness by reduced secretion of the important remodeller (Kaur et al. 2019) which is further promoted by the accumulation of UV induced damages over time. Conversely, low abundance of CAFs leads to stiffer ECM and promotes a differentiated phenotype which is reversible by CAF-mediated TGF- β signalling (Kaur et al. 2019; Wulf et al. 2004).

2.4 Resistance models

Melanoma has one of the highest mutational burdens of all cancer types and has a poor prognosis with a 5-year survival rate of 10-20% for patients with advanced disease (Siegel et al. 2019). The development of immune checkpoint inhibitors has greatly improved patient outcomes, however only 10-40% of melanoma patients respond to this therapy (Wolchok et al. 2010; Hamid et al. 2013; Topalian et al. 2012). As 52% of melanoma patients harbor an activating *BRAF* mutation (Hodis et al. 2012), BRAF has become an attractive target for cancer therapy. 60-70% of patients with *BRAF* mutations respond to targeted inhibitors (Larkin et al. 2014; Robert et al. 2015); however, resistance is almost universal within one year (Flaherty et al. 2012; Chapman et al. 2011; Hauschild et al. 2012). Considering the poor prognosis and high mortality rates, the characterisation of resistance mechanisms is an unmet need that may lead to novel therapeutic approaches for patients with clinically advanced melanoma.

2.4.1 Genetic mechanisms of melanoma drug resistance

Several attempts have been made to investigate melanoma resistance to BRAF and MEK inhibitors on a genetic level. Mutation in the RAF downstream proteins MEK1 and MEK2 were identified as resistance mechanisms to both RAF and MEK inhibition. Amplifications of the transcription factor MITF are associated with resistance but cannot be regarded as driver (van Allen et al. 2014). BRAF amplifications are another genetic mechanism of resistance and were observed in 20% of patients treated with BRAF inhibitors (Shi et al. 2012).

Further, resistance to BRAF inhibitors can be acquired by NRAS mutations leading to reactivation of the MAPK pathway. Knockdown reduced growing capabilities in resistant cell lines and overexpression promotes resistance (Nazarian et al. 2010; Jakob et al. 2012).

An RNA interference screen revealed loss of the tumor suppressor and RAS antagonist neurofibromin NF1 as a driver for BRAF inhibitor resistance. Loss of NF1 confers resistance by reactivation of MAPK signalling in many cancer cell lines (Whittaker et al. 2013).

2.4.2 Transcriptional and epigenetic factors contributing to melanoma drug resistance

In a kinase overexpression screen, MAP3K8 (COT/TpI2), which is an agonist of the MAPK pathway confers resistance to a BRAF inhibitor in a BRAF mutant cell line. COT is an upstream regulator of MEK and activates ERK signalling and thereby the MAPK pathway independent from RAF signalling, leading to resistance. Additionally, the expression of COT was found to be a marker of resistance to BRAF inhibitors in various cancer cell lines. A combination therapy to inhibit multiple components of the MAPK pathway is therefore beneficial in many patients (Johannessen et al. 2010).

Sun et al showed that many melanoma patients acquire EGFR expression after becoming resistant to BRAF or MEK inhibitors. Knock down of SOX10 or treatment with TGF-β led to upregulation of EGFR and PDGFR-β and development of resistance. A slow cycling phenotype was established with a gene signature of oncogene-induced senescence. They further supported the concept of tumor heterogeneity with the observation that cells with low levels of SOX10 and high expression of EGFR were enriched in treated samples and this was reversed after retain of the drug (Sun et al. 2014).

Secondary mutations in BRAF were mostly excluded as drivers of resistance to BRAF inhibitors, however, an aberrant splicing variant of the protein was found to be associated with acquired resistance. In physiological condition, activated RAS leads to dimerization of BRAF for further activation of the MAPK signalling pathway. RAS levels are usually low in BRAF mutated tumors and BRAF inhibitors work by binding to and inhibiting BRAF monomers. Aberrant splicing events promote dimerization of BRAF monomers to a greater extend and beyond the BRAF inhibition leading to reactivation of the MAPK signalling pathway (Poulikakos et al. 2011).

Overexpression of PDGFRβ, IGF1R and wild-type NRAS or KRAS were identified as further transcriptional mechanisms to overcome drug treatment (Villanueva et al. 2010; Nazarian et al. 2010; Shi et al. 2014; Lidsky et al. 2014).

2.4.3 Interplay between tumor microenvironment and melanoma drug resistance

Regarding the important role of the TME in tumor heterogeneity and phenotype plasticity, TME factors in the context of BRAF inhibitor resistance have been investigated. The secretion of hepatocyte growth factor (HGF) by tumor stromal cells activates its receptor MET and thereby promotes the reactivation of the MAPK signalling pathway but also the PI(3)K-AKT pathway. Targeting both, the MAPK pathway and HGF restored sensitivity to BRAF inhibition leading to the assumption that also in patients a combination therapy would be beneficial (Straussman et al. 2012).

2.4.4 Drug resistance and phenotype switching

Tracking melanoma phenotypes over time of BRAF inhibitor treatment at the bulk level, a shift towards an $MITF^{high}$ proliferative phenotype can be observed which is followed by the acquisition of a slow-cycling dedifferentiated neural crest state characterized by high expression of NGFR (Smith et al. 2013; Su et al. 2017). The initial increase in $MITF^{high}$ cells can be explained by the phenomenon of rescue from the BRAF inhibition induced cell death by MITF survival signalling (Smith et al. 2016). The neural crest state mirrors the mesenchymal/invasive phenotype and is associated with high expression of the receptor tyrosine kinases NGFR, PDGFR, IGF1R, EGFR and AXL (Rambow et al. 2018; Nazarian et al. 2010; Villanueva et al. 2010; Sun et al. 2014; Konieczkowski et al. 2014).

The concept of clonal evolution in drug resistance (Nowell 1976) is based on the observation that tumor cells have high mutational burdens that together with challenges in nutrient and oxygen availability lead to selection of the “fittest” clone. Genetic instabilities and resulting survival benefits ultimately drive the development of tumors and thus underlines the surge for patient specific precision medicine in cancer treatment. Shaffer et al challenged the concept of clonal evolution by proposing the existence of a small population of cells with “rare cell variability” which are transcriptionally and epigenetically predisposed to develop resistance to drugs. These cell populations are defined by a very high expression of resistance markers which upon drug treatment are epigenetically reprogrammed to move from a transient transcriptional state to a stably resistant cell. They identified loss of SOX10 as first driver to induce that change. Further players in reshaping the transcriptional and epigenetic landscape are the transcription factors JUN, AP-1 and TEAD. In a genetic mutation model, untreated cells undergo genetic mutations to develop resistance and would undergo clonal

selection and expansion during drug treatment leading to the survival of resistant colonies (fig. 8A). The transient gene expression state model suggests that already in an untreated state, cells shift between non-resistant and pre-resistant cell states in a reversible manner (fig. 8B). Drug treatment then leads to transcriptional and epigenetic reprogramming from a transiently pre-resistant cell state to a stably resistant state (Shaffer et al. 2017).

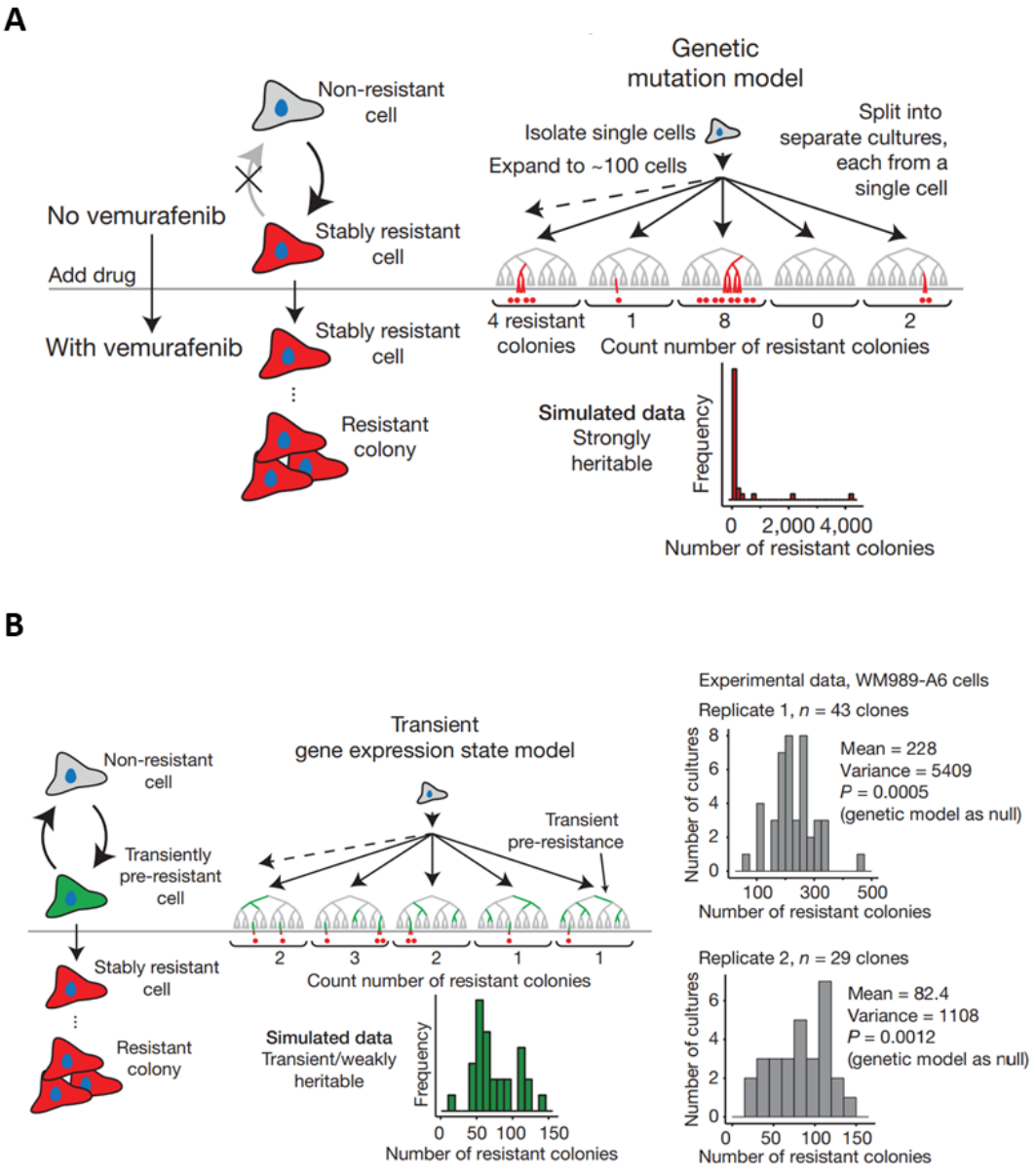

Figure 8: Models for drug resistance predict different outcomes of resistant colonies. (A) *Model for genetic heritability of drug resistance and simulated outcomes of resistant colonies.* ***(B)*** *Model for transient gene expression state and simulated outcomes of resistant colonies. Figure adapted from (Shaffer et al. 2017).*

Rambow et al focused on the small subpopulation of cells that survive drug treatment in a process called minimal residual disease (MRD) (Rambow et al. 2018). They developed a patient-derived xenograft (PDX) murine model that were treated with the BRAF/MEK inhibitor combination Dabrafenib/Trametinib. Phase 0 was defined as start of drug treatment, phase 1 was the tumor response/sensitivity towards the drug, phase 2 was the MRD and phase 3 was acquired resistance (fig. 9A). They followed the respective gene signatures over the time course and identified multiple drug-tolerant transcriptional states that co-existed in the tumor (fig. 9B). Further, the MRD harbored cells from both the $MITF^{high}$ and $MITF^{low}$ state. The main 4 gene sets they identified were neural crest stem cells (NCSC), invasive, "starved"-like melanoma cells (SMCs) and pigmented melanoma cells (fig. 9C). The pseudo-time trajectory analysis shows a shift from a proliferative gene signature to an SMC signature at the branching point (fig. 9D). From there, melanoma cells either develop into a NCSC state or a pigmented state (Rambow et al. 2018).

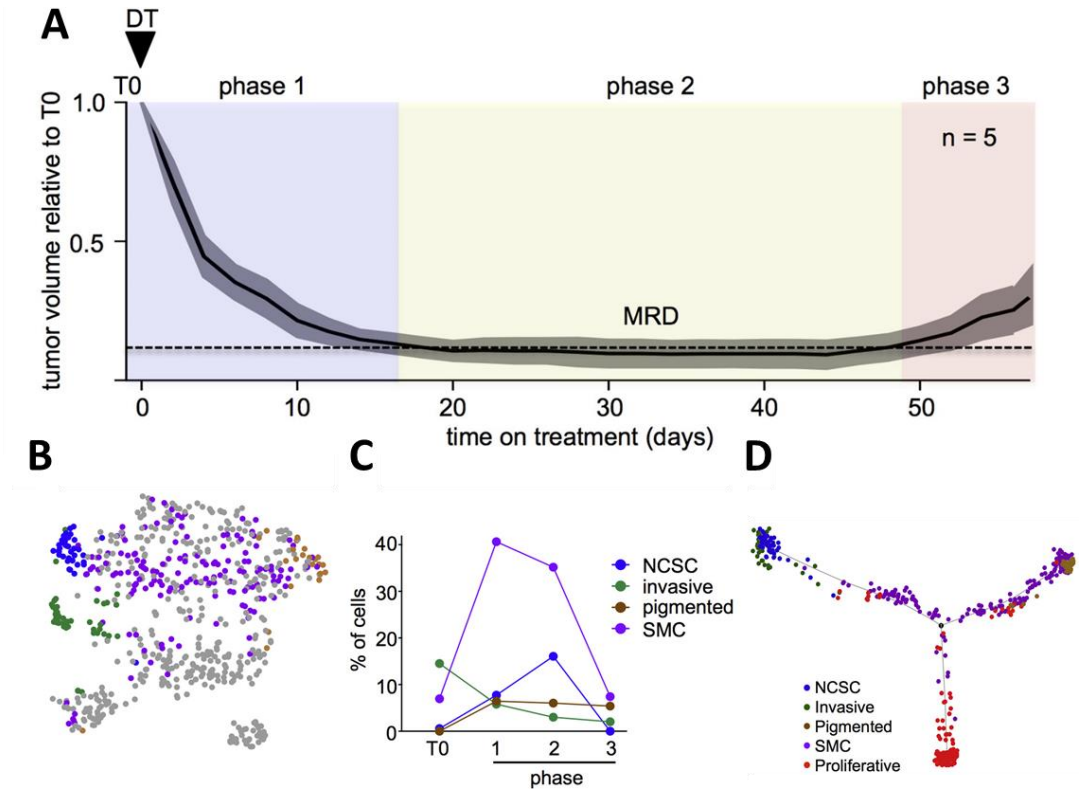

Figure 9: Melanoma cells exhibit dynamic transcriptional cell states and move along two trajectories upon drug treatment in a patient-derived xenograft (PDX) murine model. (A) *Mean melanoma tumor volumes from mice treated with dabrafenib-trametinib.* ***(B)*** *t-SNE plot of scRNA-seq of melanoma samples shows distinct clustering of melanoma cells based on transcriptional cell states.* ***(C)*** *The transcriptional cell states neural crest stem cells (NCSC), invasive cells, pigmented cells and "starved-like" melanoma cells over course of the disease adapt dynamically upon drug treatment.* ***(D)*** *Monocle-based pseudo-time trajectory analysis shows trajectories for resistant cells. Figure adapted from (Rambow et al. 2018).*

2.5 Zebrafish model

The lab has previously established a transgenic (Tg) zebrafish line to model *BRAFV600E* mutant melanoma (fig. 10). In a *tp53*$^{-/-}$ and *mitfa*$^{-/-}$ background, *BRAFV600E* is expressed under an *mitfa* specific promoter. Melanocyte and melanoma development are suppressed by the *mitfa*$^{-/-}$ background. The transposon-based vector miniCoopR contains an *mitfa* minigene that rescues melanocytes and allows expression of mutant *BRAFV600E*. The miniCoopR vector allows rapid cloning and expression of human candidate genes in rescued tissues of the *Tg(mitfa:BRAF(V600E)); p53*$^{-/-}$*; mitfa*$^{-/-}$ strain (*Triples*) when injected into one-cell stage of the *Triples* zebrafish embryos (Kaufman et al. 2016; Ablain et al. 2018; Ceol et al. 2011).

To identify transcriptional and epigenetic mechanisms underlying drug resistance in malignant melanoma *Triples* zebrafish embryos were grown and in around 4 months developed tumors. They were treated daily with the BRAF inhibitor dabrafenib and the change in tumor size was observed. Further, scRNA-seq and scATAC-seq were performed at disease relevant time points, defined to be a DMSO treated control group, the short-term drug treated sensitive tumor, a stage of minimal disease and the resistant tumor that grew back.

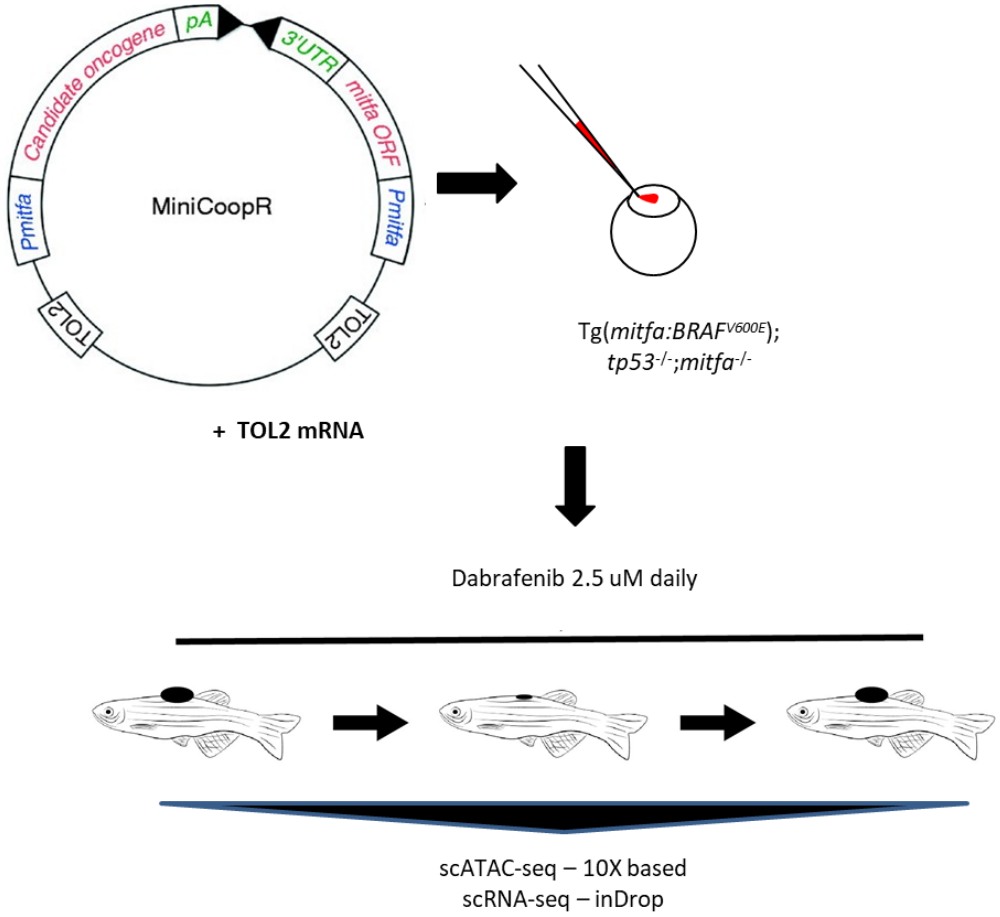

Figure 10: Tg zebrafish line to model BRAFV600E driven melanoma. Tg(*mitfa:BRAF(V600E)*)*; tp53*$^{-/-}$*; mitfa*$^{-/-}$ *zebrafish embryos. BRAFV600E is expressed under an mitfa specific promoter in a tp53*$^{-/-}$ *and mitfa*$^{-/-}$ *background. The miniCoopR vector was injected in the single-cell stage of the Tg(mitfa:BRAF(V600E)); p53*$^{-/-}$*; mitfa*$^{-/-}$ *zebrafish embryos. Upon development of melanomas, fish were drug treated with dabrafenib and parallel scATAC-seq and scRNA-seq were performed on the samples.*

2.6 Aims

To increase the understanding of melanoma biology and find new approaches for treatment, this project focuses on the molecular states that drive inter- and intratumoral heterogeneity and drug resistance in melanoma. We hypothesize that increased tumor heterogeneity is associated with drug resistance and that specific subpopulations of melanoma cells contribute to development of this resistance.

To this end, scRNA-seq and scATAC-seq were performed to transcriptionally and epigenetically define cell populations in response to MAPK pathway inhibition. We were using computer algorithms optimized to identify candidate genes – including transcription factors – and regulatory elements that define specific cellular states through the course of treatment. The laboratory of Dr. Zon has previously established a primary zebrafish model of melanoma that is driven by *BRAFV600E* under control of the *mitfa* promoter, which is specifically expressed in melanocytes, in a *tp53* mutant background that lacks melanocytes (*mitfa*$^{-/-}$*).* Tumors are induced in these zebrafish lacking *mitfa* by injection of a rescue construct that can be modified to introduce reporter transgenes for tracking and monitoring melanoma development by driving expression of a fluorescent protein from the *mitfa* promoter.

Single-cell RNA sequencing (scRNA-seq) was performed to identify gene signatures of cell clusters reflecting populations that (co-)exist in tumors using high throughput droplet-based microfluidics in order to study how transcriptional programs change during drug treatment.

To further research the epigenetic landscape of tumor cells, we utilized single-cell ATAC (Assay for Transposase-Accessible Chromatin) sequencing (scATAC-seq), which maps regions of chromatin accessibility at a genome wide scale. Sequences with increased accessibility as well as transcription factor binding sites can be identified using this technique and can be compared to the scRNA-seq to identify regulatory elements associated with drug resistance.

Using the methods described below, we identified transcriptional programs and regulatory elements associated with the development of drug resistance. Further, we validated our findings in an *in vitro* approach using a drug sensitive and resistant human melanoma cell line, respectively.

3 Materials and Methods

3.1 Injections into single-cell stage of fish embryo

Zebrafish injections were performed as described previously (Ceol et al. 2011). Briefly, 25 pg of *MCR:EGFP* were microinjected together with 25 pg of Tol2 transposase mRNA into one-cell *Triples* zebrafish embryos. Tol2 transposase mRNA was generated using mMESSAGE mMACHINE™ SP6 Transcription Kit according to the manufacturers protocols (ThermoFisher, #AM1340). Embryos were scored for melanocyte rescue at 4-5 days post-fertilization and raised to adulthood (25-30 zebrafish per tank). Adult zebrafish were scored weekly for tumor development.

3.2 Drug treatment of fish

Adult tumor bearing zebrafish were treated daily by overnight (12 hours) immersion in 50 mL of water containing the drug, in petri dishes. Treatment was performed with DMSO or 2.5 µM dabrafenib Free base (LC laboratories, #D-5678).

Samples were taken at four disease relevant time points: control tumors (DMSO treated), short-term treated drug sensitive tumors (~10 days), minimal disease tumors (~3 weeks) and drug resistant tumors. Single-cell RNA sequencing and single-cell ATAC sequencing were performed in parallel.

3.3 Single-cell RNA sequencing

Tumors were macrodissected from zebrafish, manually dissociated with scapple and incubated at room temperature in Ham's F12 media (Gibco, Cat # 11765054) supplemented with Liberase TL (Roche) for 30 mins at room temperature with agitation. The cell suspension was filtered through a 40 micron filter to remove cell clumps (Falcon, cat #352340) prior to proceeding with scRNA-seq or scATAC-seq as below.

Single cell RNA-sequencing was performed by the single cell core, Bauer Core of the Harvard University using the inDrop method (Zilionis et al. 2017; Klein et al. 2015). Sequencing libraries were sequenced on a Nextseq instrument (Illumina) using following read structure: read 1: 86, read 2: 14, Index 1: 8, Index 2:8.

Single-cell RNA-seq data was analysed using R (R Foundation for Statistical Computing 2013) and the R package Seurat (Butler et al. 2018; Stuart et al. 2019) and the R package Monocle (Trapnell et al. 2014; Trapnell et al. 2012; Qiu et al. 2017).

3.4 Single-cell ATAC sequencing

scATAC-seq was performed using 10X Genomics kit (10X Genomics, Chromium Single Cell ATAC Library & Gel Bead Kit, cat #1000081). These libraries were sequenced on a Novaseq instrument (Illumina) using the following read structure: read 1: 50, read 2: 50, index 1: 8, index 2: 16.

scATAC-seq data was processed and analysed in collaboration with the lab of Jason D. Buenrostro (Broad Institute, Harvard University).

3.5 Cell culture and generation of dabrafenib resistant A375 cell line

The human melanoma cell line A375 was cultured in DMEM (Thermofisher, cat# 12430054) + 10% Foetal Bovine Serum (FBS) + Pen/Strep (Thermofisher, cat# 15070063) and were cultured in 5% CO2 at 37°C in cell culture flask T25 or T75. Cells were passaged every 3-5 days.

A dabrafenib resistant A375 melanoma cell line was generated by continuously treating with increasing doses of dabrafenib from 0.1 nM to 100 nM over a period of 3 weeks.

Drug treatments were done using dabrafenib (LC Laboratories, #D-5678) and/or toyocamycin (Sigma, #T3580-10MG) at the specified doses.

3.6 qPCR

Sensitive and resistant cells were seeded at a density of 1 x 10^5 cells in a 6-well plate and treated with dabrafenib and/or toyocamycin 24 hours after seeding. The cells were treated for 5 hours and RNA was extracted using Direct-zol™ RNA Miniprep kit (Zymo Research, # R2050, R2051, R2052, & R2053). The RNA extraction was conducted according to the manufacturers protocols. The final elution step was done with 50 µL of nuclease free water. RNA was stored at -80°C. cDNA was generated using the High Capacity cDNA Reverse Transcription Kit (ThermoFisher, #4368814) according to the manufacturers protocols in a reaction volume of 20 µL. The cDNA was diluted 1:20 in nuclease free water. The cDNA was stored at -20°C. The qPCR reaction was set up in a compatible 96-well plate with a reaction volume of 25 µL. iTaq Universal SYBR Green Supermix (BioRad, #1725120) was used for qPCR master

mix. The primers are listed in tab. 1. Fluorescence was measured on a real-time PCR detection system (Biorad CFX96).

Primer	Sequence
SOX4	GACCTGCTCGACCTGAACC CCGGGCTCGAAGTTAAAATCC
SOX10	TCTGGAGGCTGCTGAACGAA GTAGTGGGCCTGGATGGC
sXBP1	CTGAGTCCGAATCAGGTGCAG ATCCATGGGGAGATGTTCTGG
usXBP1	CAGCACTCAGACTACGTGCA ATCCATGGGGAGATGTTCTGG
tXBP1	TGGCCGGGTCTGCTGAGTCCG ATCCATGGGGAGATGTTCTGG
ATF3	CGGAGCCTGGAGCAAAATGA GGATGGCAAACCTCAGCTCT
CHOP	TGGCCGGGTCTGCTGAGTCCG ATCCATGGGGAGATGTTCTGG
GAPDH	TGCACCACCAACTGCTTAGC GGCATGGACTGTGGTCATGAG

Table 1: Primer sequences for qPCR

Ct values of target gene were normalized to Ct values of GAPDH.

3.7 Viability assay

Sensitive and resistant A375 cells were seeded in a density of 5 x 10^3 cells/well in a 96-well plate. 24 hours after seeding, the cells were drug treated (dabrafenib and/or toyocamycin) and medium was changed after 48 hours. In total, cells were treated for 72 hours. The viability was measured using CellTiter-Glo® 2.0 Cell Viability Assay (Promega, #G9241). The CellTiter-Glo® 2.0 Cell Viability Assay was conducted according to the manufacturers protocols. Fluorescence was measured on a Synergy™ HTX Multi-Mode Microplate Reader (Bio-Tek).

3.8 Bulk ATAC sequencing

Cell preparation

For the cell preparation, 50.000 cells were spun down at 500 x g for 5 min, 4°C. The pellet was washed once with 50 µL of cold 1x PBS and again spun down at 500 x g for 5 min, 4°C. The PBS was carefully removed and pellet was resuspended in 50 µL of cold lysis buffer (10 mM Tris-HCl pH 7.4, 10 mM NaCl, 3 mM MgCl2, 0.1% IGEPAL #CA-360). Cells were spun down

immediately at 500 x g for 10 min, 4°C. The supernatant was discarded and the cell pellet was put on ice.

Transposition reaction

The transposition reaction master mix was prepared by combining the compounds listed in tab. 2.

Compound	**Amount per sample [µL]**
2X TD Buffer (Illumina Nextera DNA Preparation kit (Illumina Cat #FC-121-1030))	25
Transposase enzyme (Illumina Nextera DNA Preparation kit (Illumina Cat #FC-121-1030))	2.5
Nuclease-free water	22.5

Table 2: Transposition reaction master mix

The cell pellet was resuspended in 50 µL of transposition reaction master mix. The transposition reaction was incubated at 37°C for 90 minutes.

The DNA was eluted using MinElute PCR purification kit (Qiagen, # 28004). DNA extraction was conducted according to the manufacturers protocols and DNA was eluted in 10 µL of Elution buffer.

Library amplification

For the library amplification a master mix was set up according to tab. 3.

Compound	**Amount per samples [µL]**
Transposed DNA	10
Nuclease free water	7
Nextera Primer Ad1 (@ 25 u µM)	2.5
Nextera Primer Ad2.[x] (@ 25 µM)	2.5
10X SYBR Green I, diluted in 10 mM Tris-HCl, pH 8 (SYBR Green I dye (Invitrogen #S-7563))	3
NEB PCR Master Mix (NEBNext High-Fidelity 2X PCR master mix (NEB Cat #M0541))	25

Table 3: Library amplification master mix

Nextera Primer Ad1_noMX: AATGATACGGCGACCACCGAGATCTACACTCGTCGGCAGCGTCAGATGTG

Nextera Primer Ad2.1_TAAGGCGA: CAAGCAGAAGACGGCATACGAGATTCGCCTTAGTCTCGTGGGCTCGGAGATGT

Nextera Primer Ad2.2_CGTACTAG: CAAGCAGAAGACGGCATACGAGATCTAGTACGGTCTCGTGGGCTCGGAGATGT

The PCR cycling was run according to steps (1)-(7).

(1) 72°C, 5 min

(2) 98°C, 30 sec

(3) 98°C, 10 sec

(4) 63°C, 30 sec

(5) 72°C, 1 min

(6) Repeat steps 3-5, 4x

(7) Hold at 4°C

The qPCR side reaction was performed to reduce GC and size bias in the library preparation.

The qPCR side reaction was set up according to tab. 4.

Compound	**Amount per samples [µL]**
"5-cycle" PCR reaction from the previous PCR	5
Nuclease-free water	3.9
Nextera Primer Ad1 (@ 25 µM)	0.25
Nextera Primer Ad2.[x] (@ 25 µM)	0.25
10X SYBR Green I	0.6
NEB PCR Master Mix	5

Table 4: Mix for qPCR side reaction

The remaining PCR reaction was kept at 4°C during the qPCR.

The additional number of cycles needed for the remaining 45 µL PCR reaction was determined by:

(1) plotting linear Rn vs. Cycle # of the SYBR amplified product

(2) determining Rn value maxima for the sample

(3) calculating the Cycle# that corresponds to 1/4th of the maxima (this is the number of cycles to add to the PCR reaction)

(4) if the 1/4th value fell between 2 cycle #'s, the smaller integer was chosen

The remaining 45 µL PCR reaction was run to the correct # of cycle as follows:

(1) 98°C, 30 sec
(2) 98°C, 10 sec
(3) 63°C, 30 sec
(4) 72°C, 1 min
(5) Repeat steps 2-4, x times
(6) Hold at 4°C

The amplified library was purified using DNA purification kit (Qiagen, #28104). The library was purified according to the manufacturers protocols and eluted in 20 µL of Elution buffer.

Bead Clean up

Kapa Pure Beads (Roche Sequencing Store, #7983271001) were warmed up to RT and mixed to resuspend. Samples were transferred to 1.7 mL tube and 1.5X volume of Kapa Pure Beads was added and pipetted to mix. Mix was incubated at RT with rocking for 10 mins. Tube was placed on a magnetic rack for 5 mins. Supernatant was discarded and beads were washed with 200 µL of fresh prepared 80% ethanol for 1 min. Ethanol was removed and beads were dried for 5-10 mins. Beads were resuspended in 20 µL of nuclease free water and incubated at 37°C for 10 mins. Tube was put back on the magnetic rack and eluted samples were isolated into new tube.

Qubit

The Qubit dsDNA HS (High Sensitivity) Assay Kit (Thermofisher, #Q32851) was used to measure concentration.

Library QC

A sample of the library was run on TapeStation (2200 TapeStation Instrument, Agilent Technologies). 3 µL of D1000 Sample Buffer (Agilent, Cat#5190-6502) + 1 µL of sample onto D1000 Screen Tape (Agilent, Cat# 5067-5582).

4 Results

4.1 Single-cell RNA sequencing revealed inter- and intratumoral heterogeneity in naïve melanoma samples

Within this chapter the analysis of three primary control samples (GFP1, GFP2 and GFP3), meaning *BRAFV600E* driven tumors that were not drug treated, will be shown and the pipeline discussed. The next chapter includes samples from all disease relevant time points. For this chapter, a dataset of 7705 single melanoma cells from samples from 3 treatment naïve tumor bearing fish were generated using inDrop and sequenced on an illumina NextSeq instrument. Raw reads were converted into a read count file using the inDrops package before being passed onto Seurat. For the analysis of untreated melanoma samples the R package Seurat which is designed for analysis of scRNA-seq data was used. All figures in chapter 4.1 were generated using the R package Seurat (Butler et al. 2018; Stuart et al. 2019; R Foundation for Statistical Computing 2013). The standard pre-processing workflow includes the QC of sequenced cells (fig. 11). The threshold for the number of unique genes per cell (genes/cell) was set between 200 and 2500 as low-quality cells often exhibit very low numbers of unique genes per cell and vice versa for doublets (fig. 11A). Cells which exhibited more than 15000 molecules each (RNA/cell) were filtered out to remove cell multiplets from the dataset (fig. 11B). Another metric that served as QC was the percentage of mitochondrial genes (% mitochondrial RNA) which was set to be less than 5% to filter out low-quality cells with high mitochondrial contamination (fig. 11C).

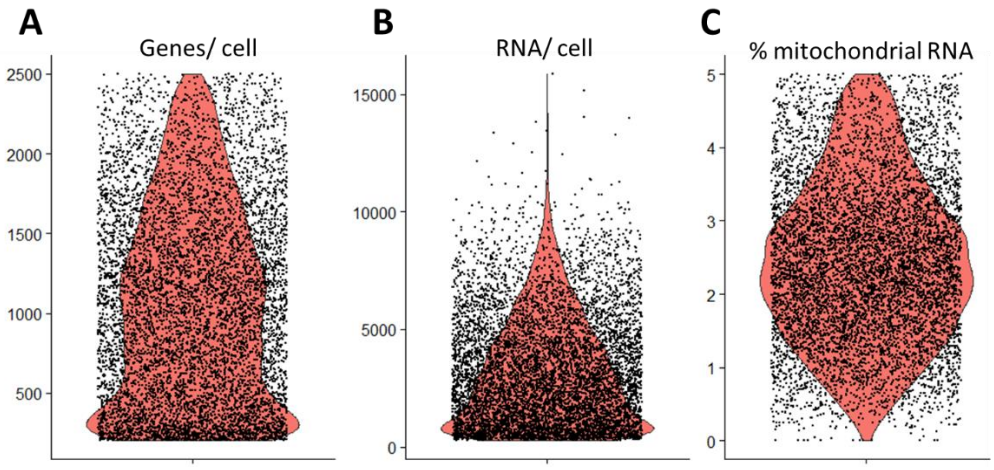

Figure 11: Quality control of single-cell RNA sequencing excludes low quality cells from data analysis. (A) *Cells with less than 200 and more than 2500 unique genes per cell*

(genes/cell), ***(B)*** *more than 15000 RNA molecules per cell (RNA/cell) and* ***(C)*** *more than 5% mitochondrial RNA (% mitochondrial RNA) were filtered out for the downstream analysis.*

The feature scatter shows the correlation of the datasets percentage of mitochondrial genes, the number of RNA molecules per cell and the number of unique genes per cell (fig. 12). With a Pearson's correlation coefficient of 0.07 the percentage of mitochondrial genes and the number of RNA molecules per cell do not correlate (fig. 12A). The number of unique genes per cell and the number of RNA molecules per cell are positively correlated with a Pearson's correlation coefficient of 0.94 (fig. 12B).

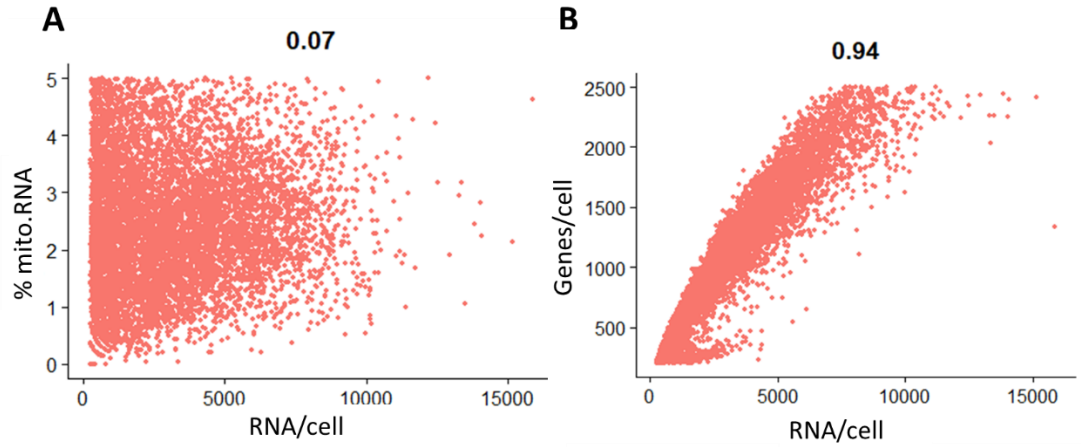

Figure 12: Scatter plot visualizes correlation of QC variables. (A) *The percentage of mitochondrial genes (% mito.RNA) and the number of RNA molecules per cell (RNA/cell) do not correlate (Pearson's correlation coefficient 0.07).* ***(B)*** *The number of unique genes per cell (genes/cell) and the number of RNA molecules per cell show positive correlation (Pearson's correlation coefficient 0.94).*

The normalization was done by normalizing the feature expression by the total expression, multiplying this by 10000 and log-transforming the result. Highly variable features between cells within the dataset were identified and used for the downstream principal component analysis (PCA). In a next step the data was scaled, meaning a linear transformation was applied which sets the mean expression of features to 0 and scales the expression so that the variance across cells is 1. A linear dimensional reduction was performed by PCA. Fig. 13 shows the first two principal components (PCs) of the analysis.

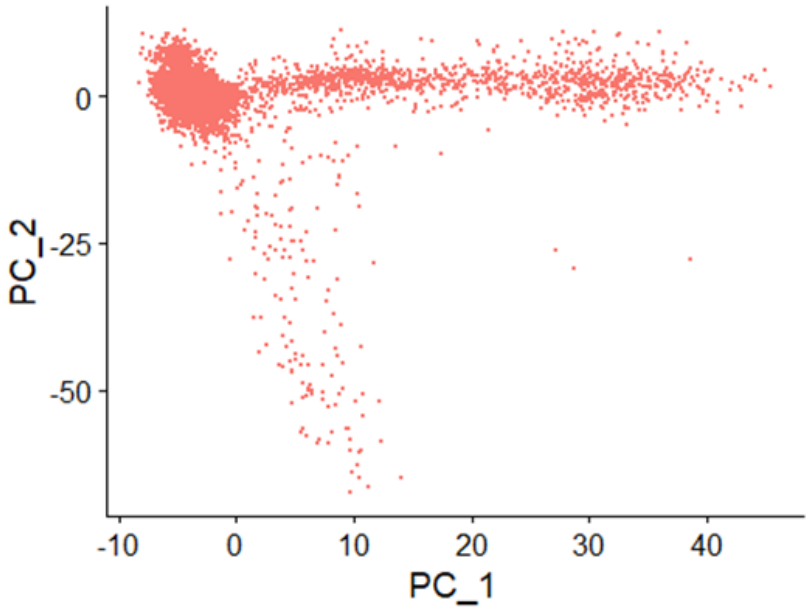

Figure 13: Transcriptional differences cluster cells in first two principal components of the principal component analysis.

The heatmap of the first PC shows the primary source of heterogeneity (fig. 14). The PC is separating melanoma cells which highly express *crestin* and *sox4a*. The other principle component has high expression of the macrophage markers *c1qa*, *c1qb* and *cd74a*. This suggests that cell identity is the strongest driver of heterogeneity within the dataset.

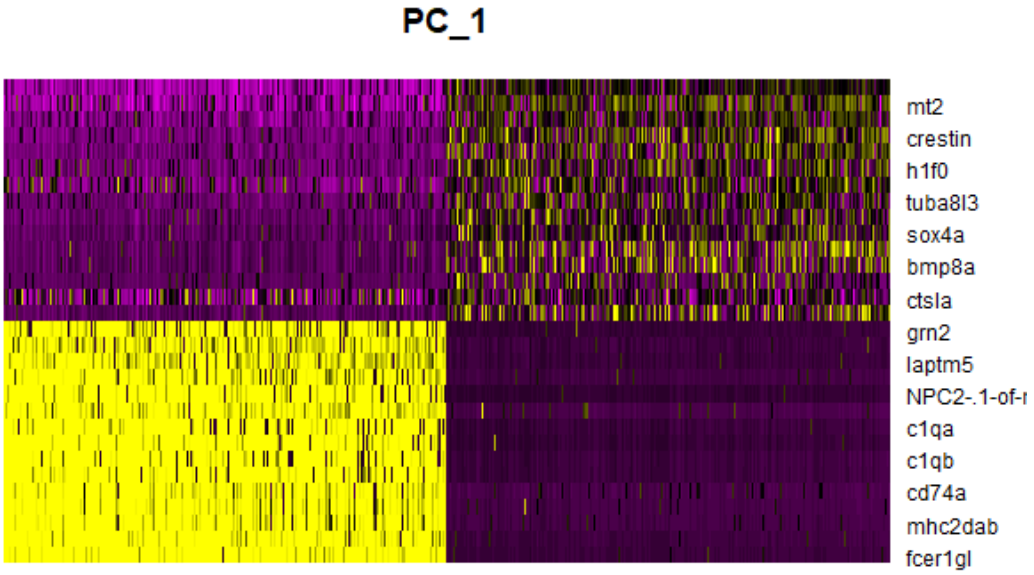

Figure 14: Heatmap of the first PC shows heterogeneity is mainly driven by different transcriptomics of melanoma cells and macrophages. *Linear dimension reduction by PCA separates dataset into main cell types.*

For the identification of significant PCs that determine heterogeneity and for the decision on how many PCs to include in the analysis to get robust results the percentage of variance visualized by the elbow plot was used (fig. 15). The first 18 PCs had a standard deviation greater than 2% and were included in the downstream analysis.

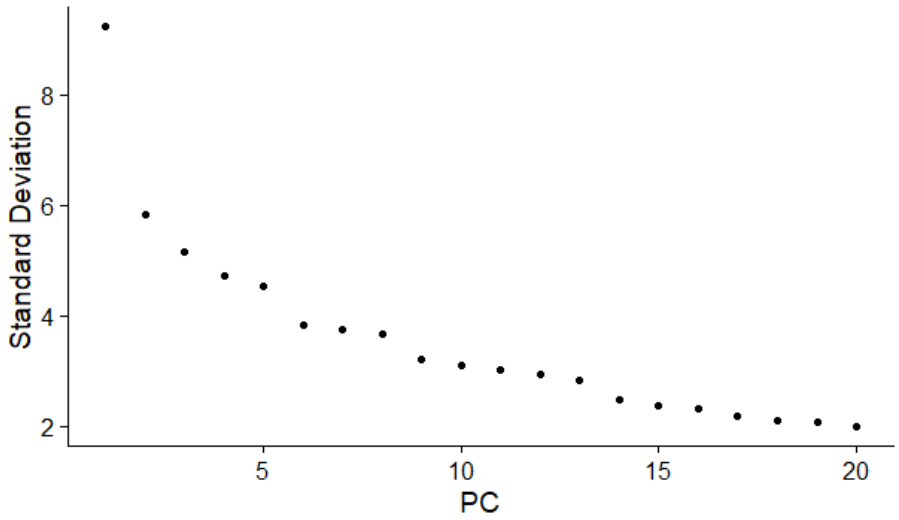

Figure 15: Elbow plot ranks the PCs based on the percentage of variance. *Using a 2% standard deviation as threshold, the first 18 PCs are considered as significant and capture the majority of dimensions.*

The non-linear dimensional reduction calculated cell clusters which are displayed as neighbouring patches in the graphs. Cells with similar transcriptional profiles clustered together which was visualized by uniform manifold approximation and projection (UMAP) for dimension reduction (fig. 16A). Based on the chosen resolution the algorithm calculated 15 cell clusters. Cells formed a separate cluster for each tumor (GFP1, GFP2, GFP3) which shows intra- and intertumoral heterogeneity (fig. 16B).

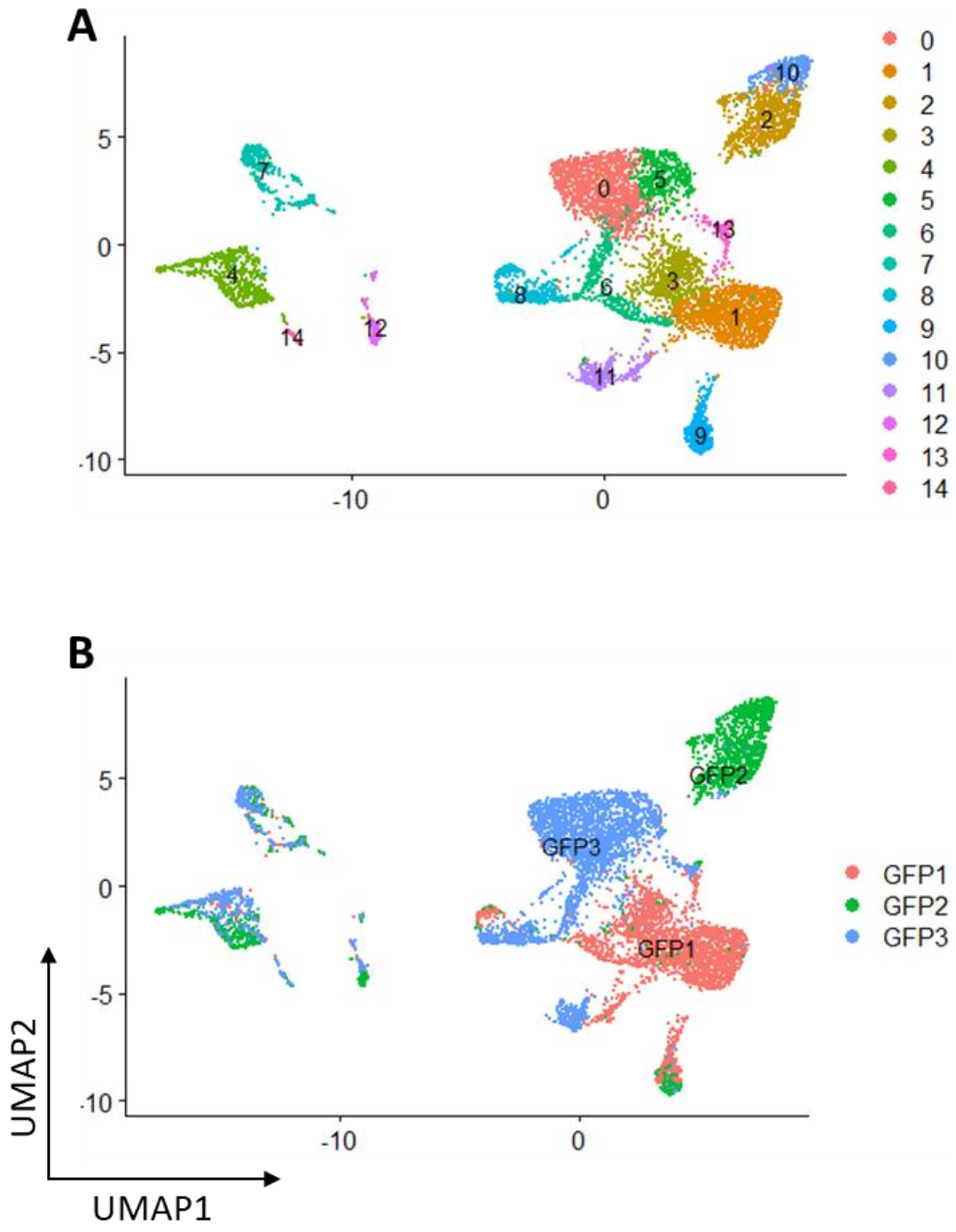

Figure 16: Single-cell expression profiles revealed inter-and intratumoral heterogeneity. ***(A)*** *UMAP shows colour-coded cell clusters calculated by non-linear dimensional reduction.* ***(B)*** *UMAP shows clusters of cells from three colour-coded samples (GFP1, GFP2, GFP3).*

Variably expressed features are biomarkers for each cluster and were visualized by UMAPs (fig. 17). The melanocyte specific biomarkers *mitfa*, *sox10* and *pmela* were highly expressed in subsets of cells reflecting different tumor populations co-existing in melanoma samples. The melanocyte related marker *tyr* was expressed only in few cells.

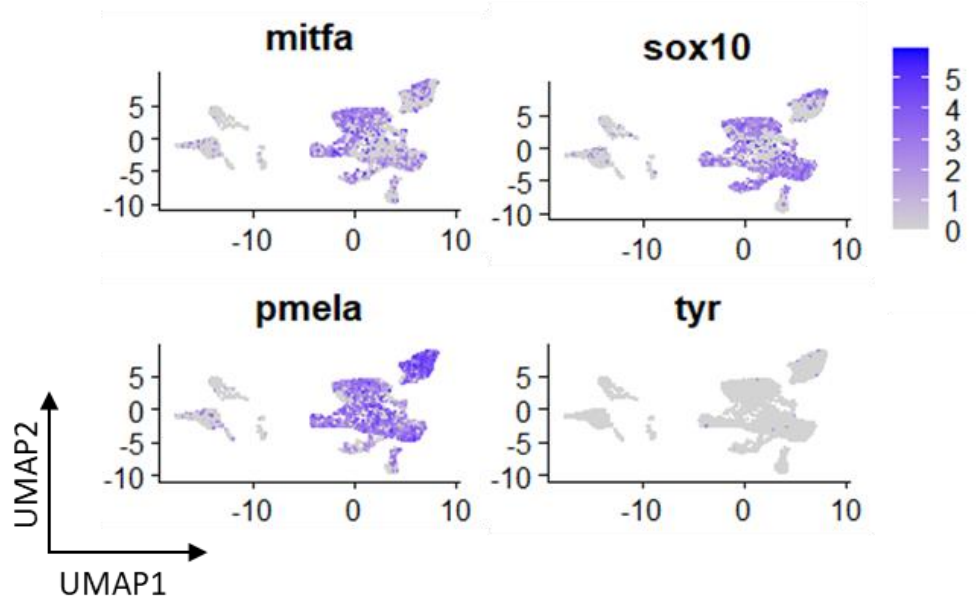

Figure 17: UMAPs of variably expressed features reflect clusters of cells. *The melanocyte specific markers mitfa, sox10, pmela and tyr were differentially expressed between clusters.*

Known cell type markers were used to match the unbiased clustering to known cell types (fig. 18, 19). The identified cell types are highlighted in fig. 18 and include T-cells (*zap70, lck, sla2*), macrophages (*mpeg1.1, marco, mfap4*), neutrophils (*mpx, mmp9, lyz*), keratinocytes (*krt5, epcam, tp63*), fibroblasts (*fn1a, cxcl12a, col1a1a/b*), red blood cells (*alas2, hbba1/2*) and melanoma cells (*mitfa, sox10, pmela, tyr*).

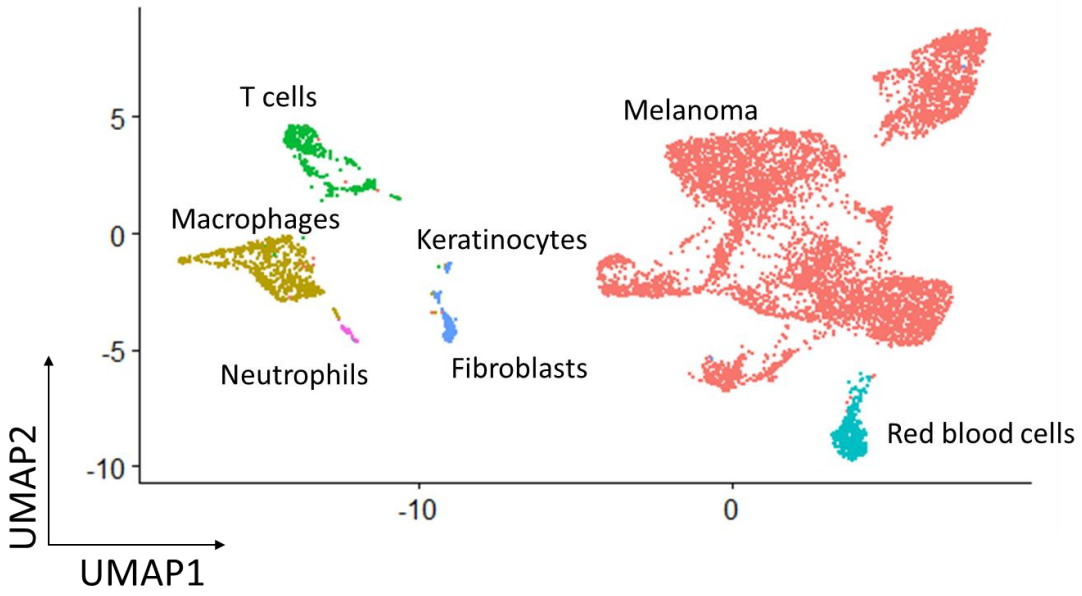

Figure 18: Cell clusters were annotated based on their original cell type. *Cell identities were annotated by distinct or preferential expression of markers for T-cells, macrophages, neutrophils, keratinocytes, fibroblasts, melanoma cells and red blood cells.*

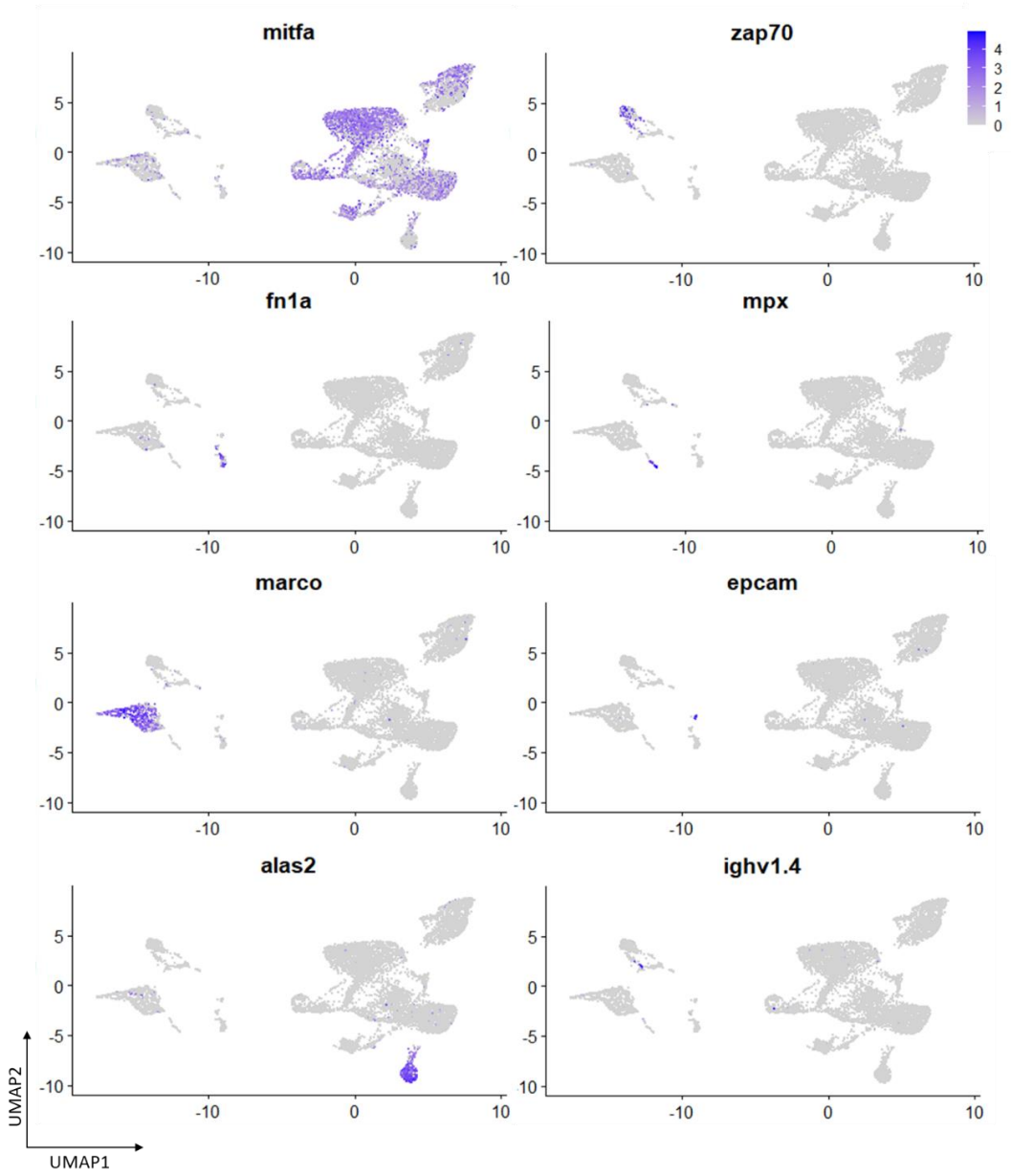

Figure 19: Known markers for cell types were highly enriched in their specific cell clusters. *The UMAPs shows expression of known markers representative for melanoma cells (mitfa), T-cells (zap70), fibroblasts (fn1a), neutrophils (mpx), macrophages (marco), keratinocytes (epcam), red blood cells (alas2) and B-cells (ighv1.4) across the dataset.*

4.2 Drug resistant tumors arise with variable kinetics

BRAFV600E driven melanoma was modelled in Zebrafish. The *Triples* embryos were grown until they developed tumors (around 4 months) followed by daily dabrafenib treatment. The tumor size was checked weekly and drug response curves were generated (fig. 20). The DMSO treated control group had continuous tumor growth whereas tumors of dabrafenib treated fish decreased in size over the first weeks. This state is defined as drug sensitive group. At around 3 weeks on dabrafenib treatment the tumors decreased to a very small size (minimal disease). In the following weeks, some fish eventually developed drug resistance and tumors regrew with variable kinetics.

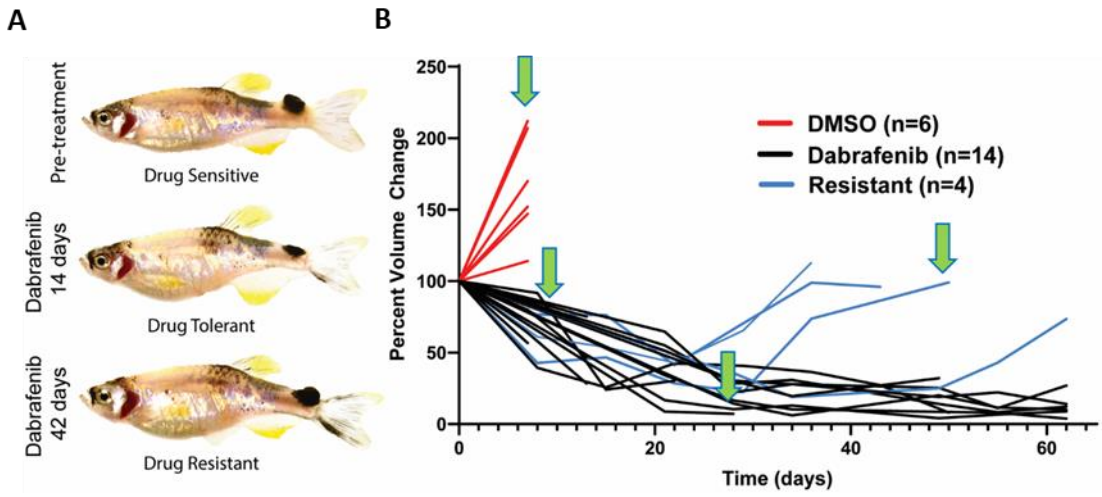

Figure 20: Melanoma tumors decreased in size upon dabrafenib treatment and grew back with variable kinetics after acquiring resistance. (A) *Pre-treatment tumor on the back of the fish decreased in size after 14 days of dabrafenib treatment. The tumor grew back on prolonged dabrafenib treatment and reached its original size.* ***(B)*** *Time of drug treatment is plotted against change in tumor volume. Kinetics of tumor volume shows increase in tumor size of control (DMSO treated) fish (red curve) and decrease of dabrafenib treated fish (blue and black curves). Around day 21 some tumors acquired resistance and grew back (blue curve). Green arrows indicate disease relevant time points: control tumor, drug sensitive tumor, minimal disease and resistant tumor.*

Tumor samples were collected from all four disease relevant time points: untreated control, drug sensitive tumor, minimal disease, and resistant tumors and parallel scRNA-seq and scATAC-seq were conducted.

4.3 Single-cell ATAC sequencing identified distinct normal and heterogeneous epigenetic tumor cell states

Single-cell ATAC sequencing of primary melanomas from DMSO treated control tumors (Control.1), drug sensitive tumors (Sensitive.1, Sensitive.2, Sensitive.3), minimal disease (Minimal Disease.1, Minimal Disease.2) and resistant tumors (Resistant.1, Resistant.2) shows the distinct clustering for all samples (fig. 21A) based on distinct chromatin accessibility. The algorithm identified 23 clusters of distinct landscape of chromatin accessibility (fig. 21B).

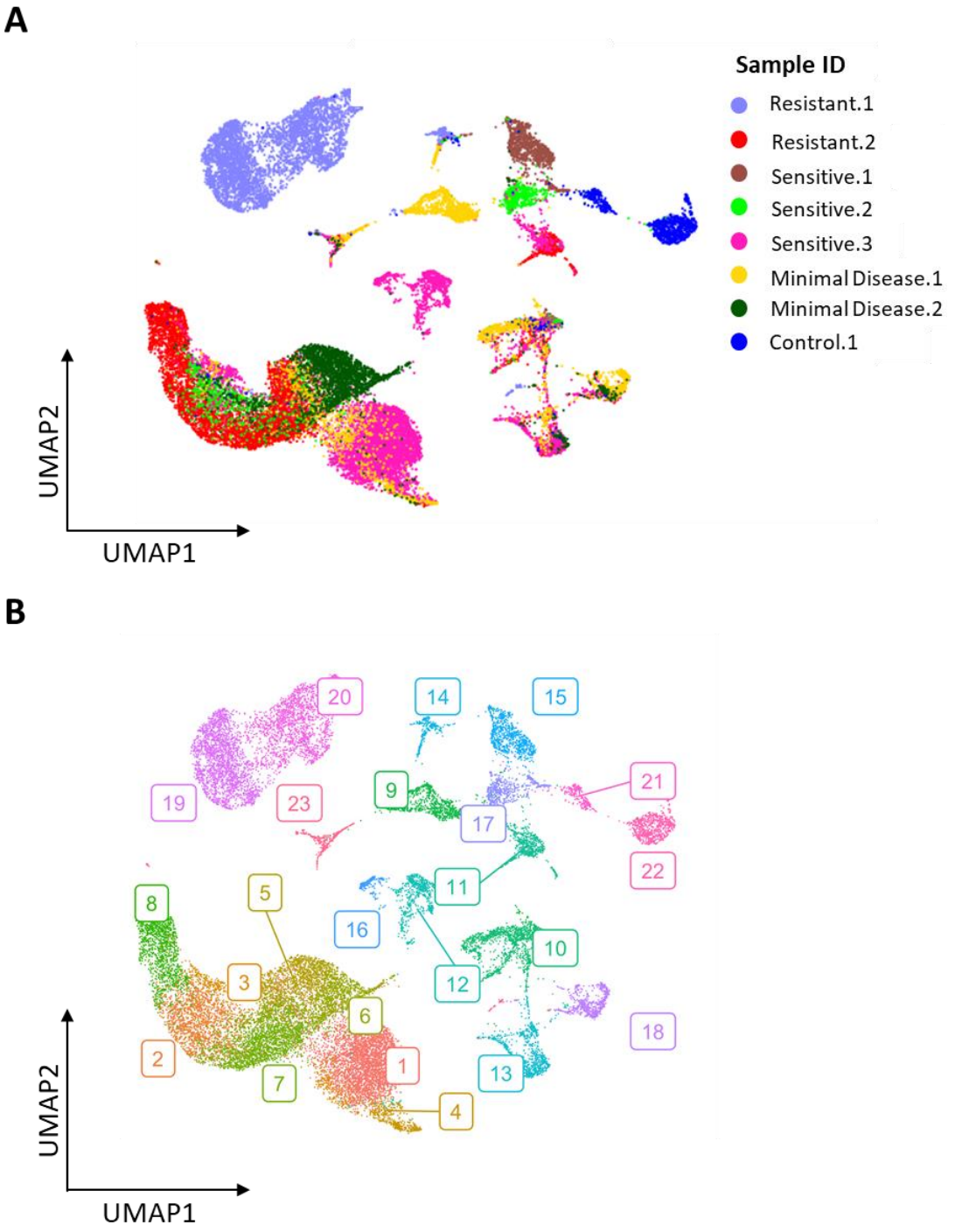

Figure 21: scATAC-seq shows distinct clustering of tumor cells from all four disease relevant time points based on their chromatin accessibility. (A) *Cells are colour-coded based on the disease relevant time point: control tumor (Control.1), sensitive tumors (Sensitive.1, Sensitive.2 and Sensitive.3), minimal disease (Minimal Disease.1 and Minimal Disease.2) and resistant tumors (Resistant.1 and Resistant.2).* ***(B)*** *23 clusters of different chromatin accessibilities were calculated and are visualized by different colour coding.*

Gene accessibility scores on a single cell/cluster basis were calculated using mapped reads to called peaks on the aggregate data within a 2kb window of gene bodies (fig. 22). The original cell types were identified and annotated using known markers for melanoma cells, T-cells, macrophages, red blood cells, B-cells, fibroblasts, epithelial cells and neutrophils. Fibroblasts, macrophages, B-cells, T-cells, red blood cells and epithelial cells show distinct non-overlapping enrichment in their characteristic genes whereas the 11 melanoma clusters were enriched in DNA containing the melanoma-specific genes *pmela, mitfa, sox10* and *tyr* with varying intensities and different compositions.

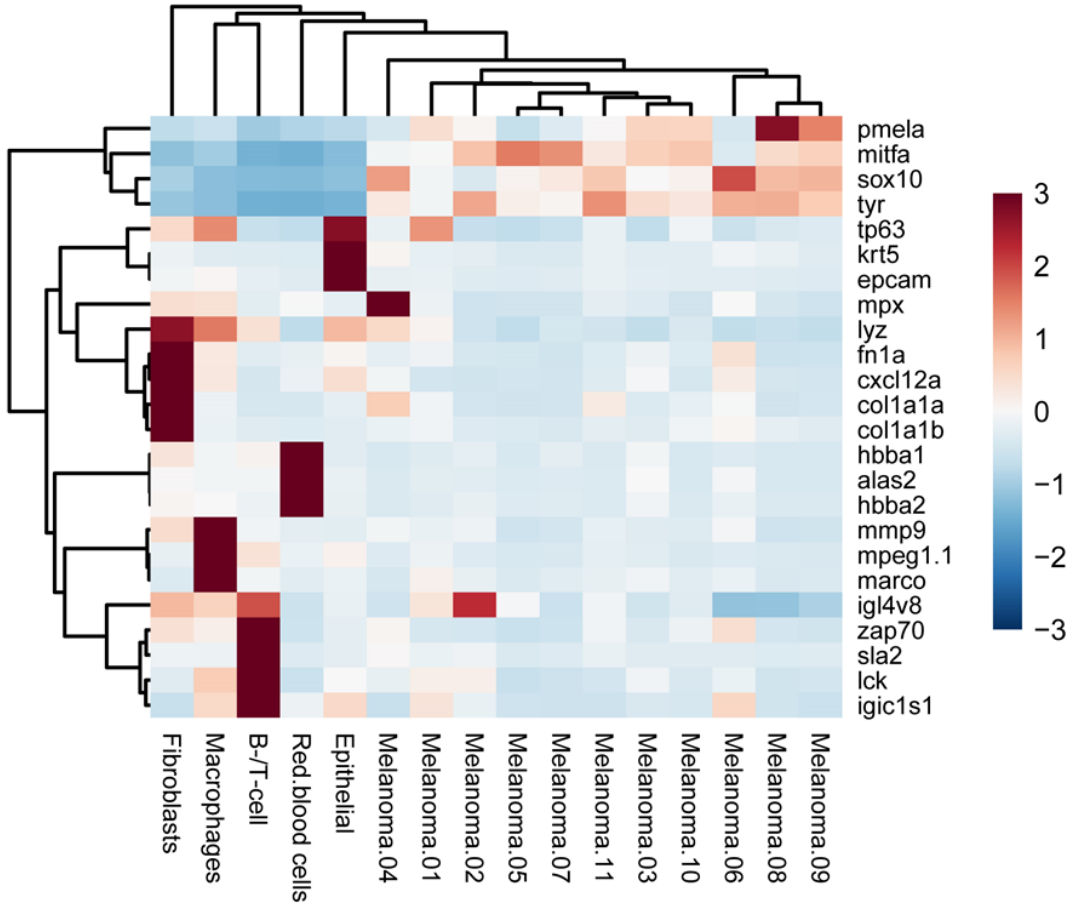

Figure 22: Heatmap shows markers of various cell types and melanoma clusters based on gene accessibility scores. *Known markers were enriched in the various cell types (fibroblasts, macrophages, B-cells, T-cells, epithelial cells and melanoma cells). The melanoma clusters 1-11 (Melanoma.01-Melanoma.11) were enriched in pmela, mitfa, sox10 and tyr with varying intensities.*

To exclude non-melanoma cells from the downstream analysis, the original cell types were identified and annotated using known markers for melanoma cells (highlighted with pink shadow), T-cells, macrophages, red blood cells, B-cells, fibroblasts, epithelial cells and neutrophils and non-melanoma cells were filtered out (fig. 23) for the downstream analysis. Along with the filtering of melanoma cells, the clusters were redefined as 11 candidate melanoma clusters 1-11 (Melanoma.01-Melanoma.11) and reflect the different accessibility of chromatin within the melanoma cells. In order to exclude possible cell doublets from the analysis, clusters were manually curated. Clusters Melanoma.03 and Melanoma.06 were excluded due to dual accessibility.

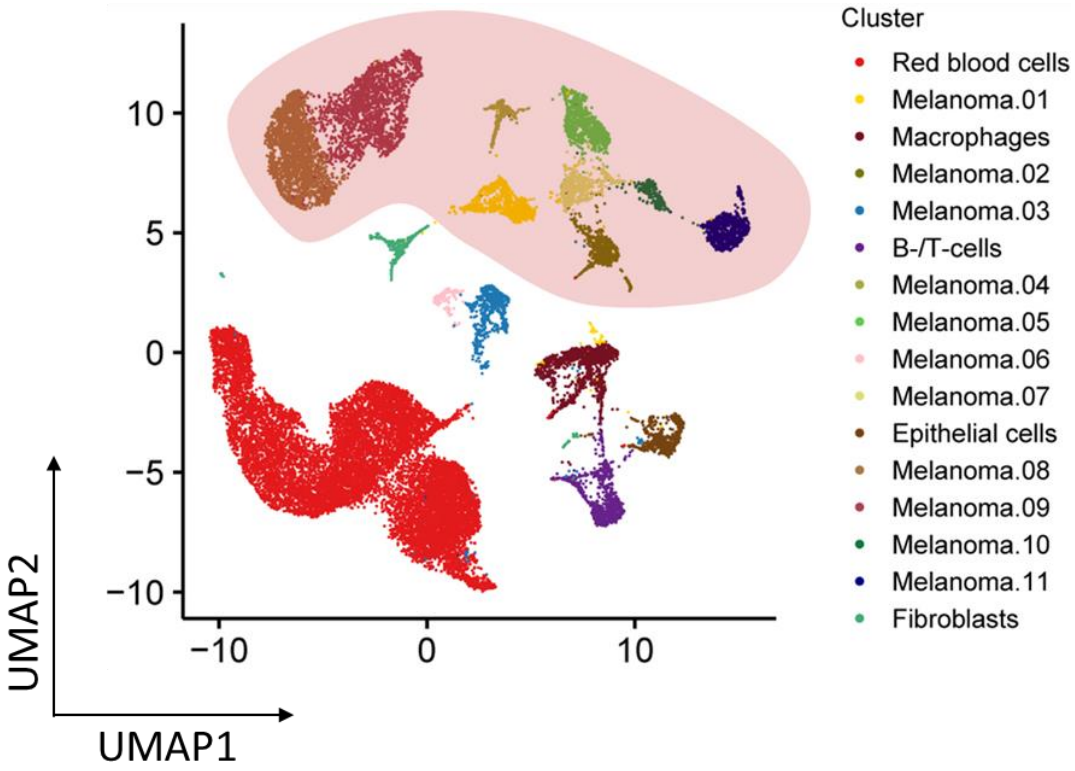

Figure 23: Clusters of differential chromatin accessibility reflect various cell types. *Cell clusters were colour-coded based on the original cell types: Red blood cells, macrophages, B-cells, T-cells, epithelial cells, fibroblasts and melanoma cells. Melanoma cell clusters were redefined as 1-11 (Melanoma.01-Melanoma.11) based on their chromatin accessibility and highlighted with a pink shadow.*

Highlighting specific clusters demonstrated that the disease relevant time points in the UMAP plots tend to cluster with cells from each state and indicates differences in chromatin landscape between samples from the same disease relevant state (fig. 24).

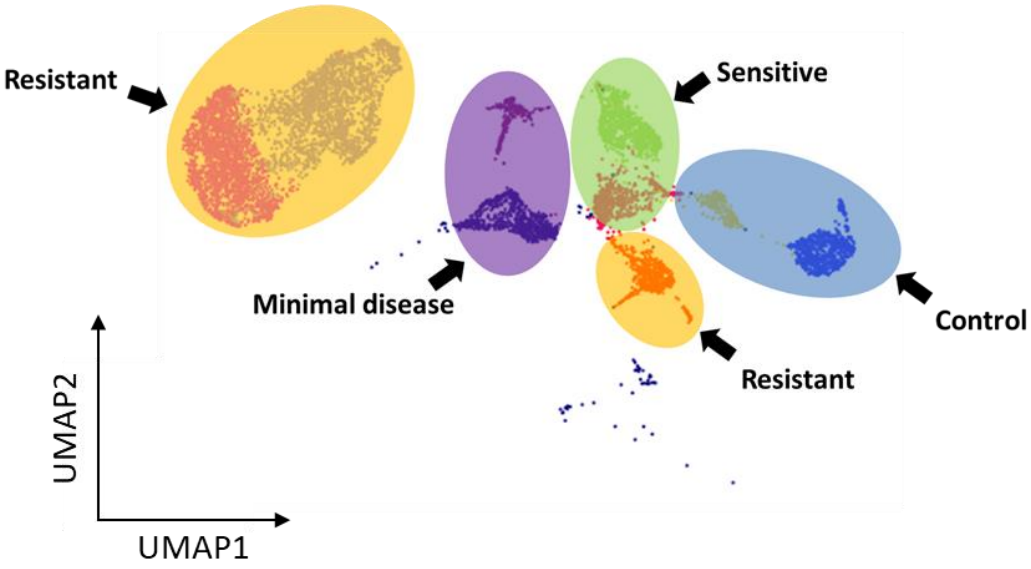

Figure 24: Melanoma cells cluster according to their disease relevant state. *Melanoma cells of control sample, sensitive samples, minimal disease and resistant disease cluster together respectively.*

Colour-coding the calculated clusters (cluster ID, fig. 25A) as well as the origin of the samples (sample ID, fig. 25B) allows comparing of cell origin and epigenetic state. The resistant cells from the tumor Resistant.1 separate into two distinct epigenetic states, the clusters Melanoma.08 and Melanoma.09. There are rare cells within each tumor that account to different clusters. E.g. a subset of cells from Resistant.1 and Minimal Disease.1 cluster together and share the same epigenetic state Melanoma.04. The control cells from Control.1 separate into two distinct epigenetic states Melanoma.10 and Melanoma.11 that are not shared with any other sample. The responsive tumor Sensitive.3 clusters together with Resistant.2 and shares the epigenetic state Melanoma.02. The short-term treated Sensitive.1 and Sensitive.2 fall into one cluster, Melanoma.05 and Melanoma.07 respectively, that are not shared with any other sample.

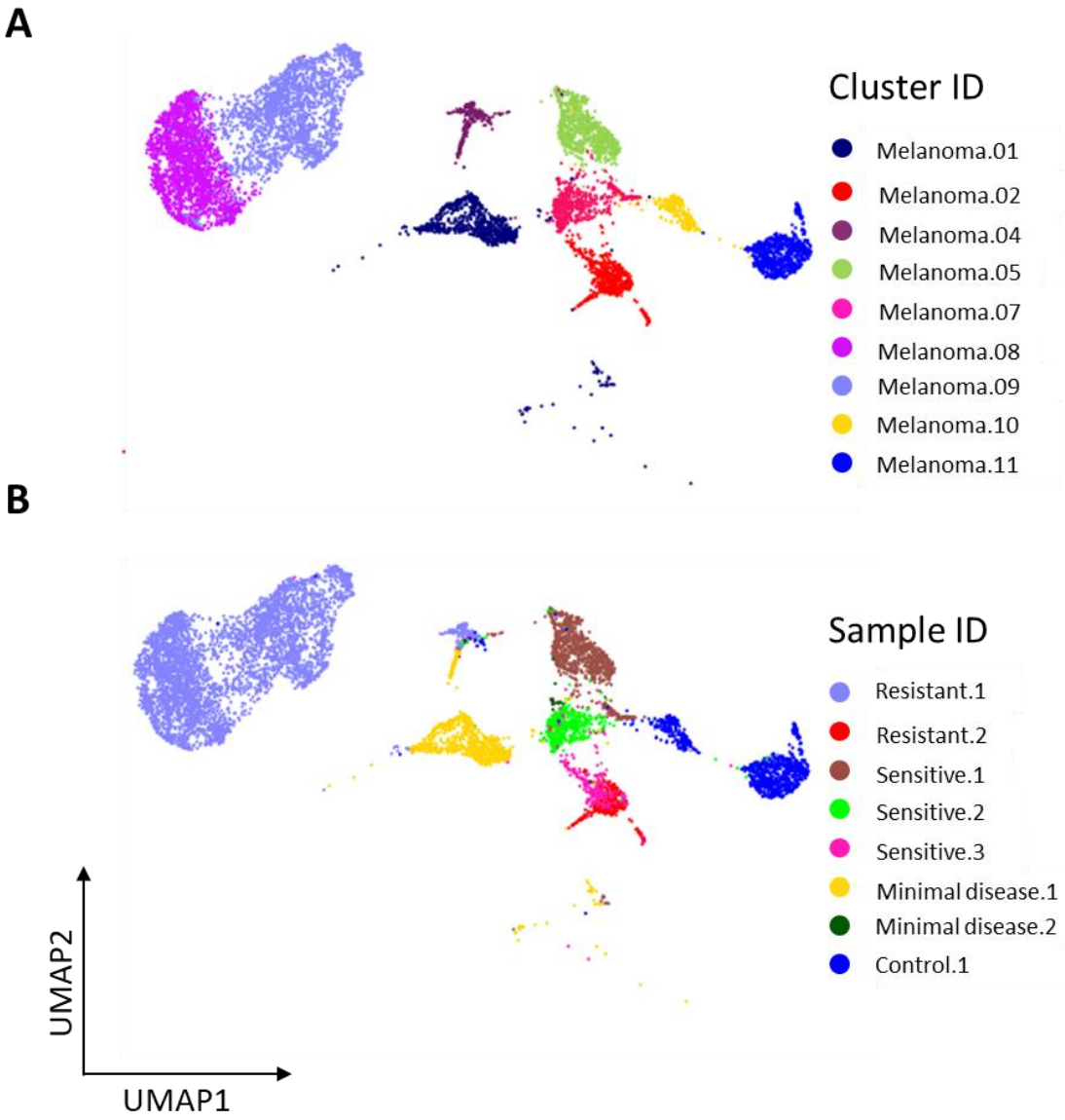

Figure 25: Comparison of calculated cell clusters with original cell samples points towards co-existing epigenetic states in melanoma samples. (A) *The cells are colour-coded based on the calculated cluster IDs Melanoma.01—Melanoma.011 (Melanoma.03 and Melanoma.06 excluded).* ***(B)*** *The cells are colour-coded based on their sample IDs (DMSO treated Control, Sensitive, Minimal disease and Resistant).*

4.4 Motif accessibility defines epigenetic melanoma cell states and suggests “stress-like” state in resistant cells

Melanoma clusters (Melanoma.01-Melanoma.11; 3 and 6 excluded) were assigned to the dominant phenotypes which are control cells, sensitive cells, minimal disease and resistant cells. Control cells are defined by the clusters Melanoma.11 and Melanoma.10, sensitive cells Melanoma.05 and Melanoma.07, minimal disease Melanoma.04 and Melanoma.01 and resistant cells Melanoma.08, Melanoma.09 and Melanoma.02. Hierarchical clustering of highly variable transcription factor motif accessibilities and calculated clusters (Melanoma.01-Melanoma.11; 3 and 6 excluded) shows distinct epigenetic states at various disease relevant time points (fig. 26). Transcription factor motif accessibility was calculated across clusters by examining the presence of specific motifs within called peaks in the aggregate cluster peak file, compared across clusters. A subset of resistant samples was highly enriched in MITF motif accessibility as well as RUNX3, TFAP2C, TEAD3 and SNAI2 motif accessibility. Another subset of minimal disease and resistant samples was defined by highest accessibility of stress related motifs: XBP1, ATF3, ATF6 and CREB3 as well as AP1 factor (FOS and JUNB motif accessibility). A subset of control cells and the short-term treated cells had high accessibility of some transcription factors (SOX4, MITF and TFAP2C, FOS and JUNB) but did not share a whole epigenetic state with the resistant or minimal disease cells.

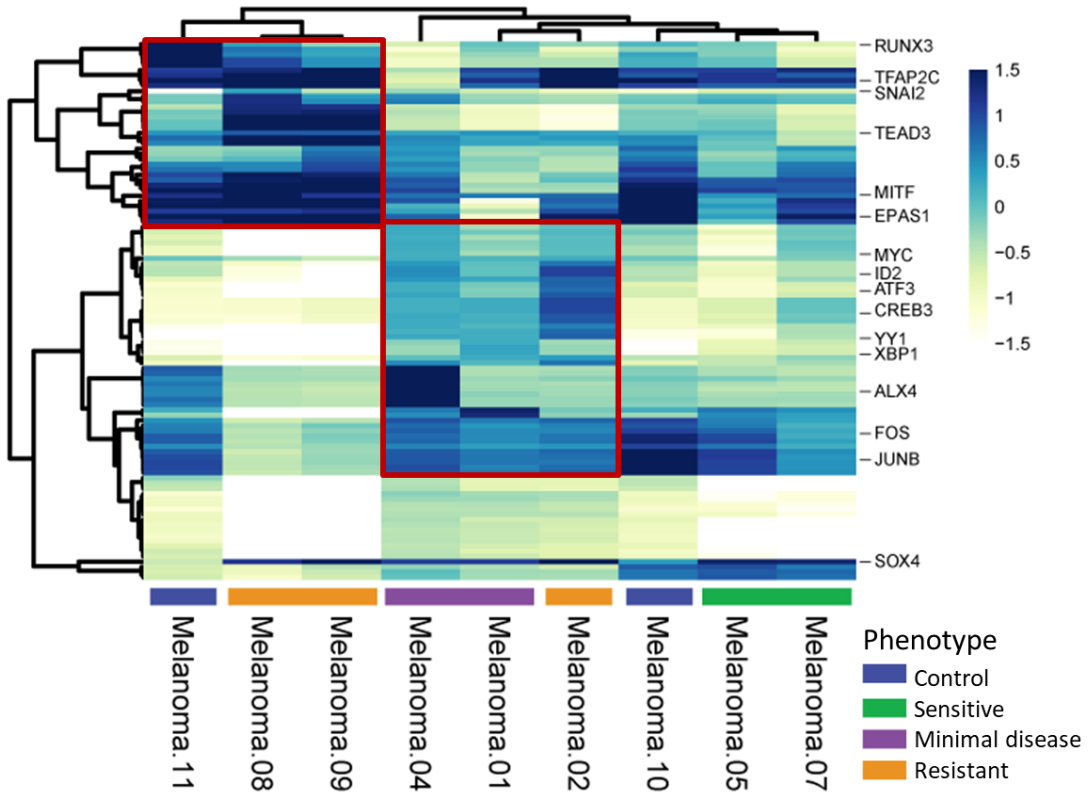

Figure 26: scATAC sequencing reveals "stress-like" state in a subset of resistant melanoma cells. *Transcription factor motif accessibility was clustered hierarchical and dominant phenotypes were assigned (Control, Sensitive, Minimal disease, Resistant). Two major epigenetic states are framed in red.*

4.5 Dabrafenib treatment induces dramatic epigenetic shifts

The volcano plots allow direct comparisons between phenotypes and show the dramatic epigenetic shift that happens upon dabrafenib treatment (fig. 27).

During the short-term treatment especially, differentiation factors like MITF and RUNX1 are lost in the treated cells compared to the control cells. Newly acquired regions are enriched in neural crest motifs like SOX4, SNAI1, SNAI2, ZEB1, CREB3 and ID3 but also the stress related motif ATF6 (fig. 27A).

On prolonged dabrafenib treatement, minimal disease cells lose accessibility of RREB1, PURA and EPAS1 but strengthen their epigenetic stress program. Tumor cells in the minimal disease states show relatively high accessibility at DNA containing the stress related motifs for ATF6, XBP1, ATF3 and the notch signalling factors such as HEY1 (fig. 27B).

Compared to the minimal disease state, resistant cells move towards either direction: a neural crest/ "stress-like" state or a differentiated state. The neural crest/ "stress-like" resistant cells lose accessibility of DNA containing the ALX4 motif, however acquire accessibility of DNA contianing AP2 factor motifs (TFAP2A, TFAP2C) and further increase accessibility of motifs for neural crest factors such as ID2 and CREB3 (fig. 27C).

The differentiated cells are highly accessible at DNA containing the differentiation marker MITF. Accessibility of RREB1 and EPAS1, which was lost during short-term treatment, is restored. The neural crest/ stress factors XBP1, ID2, ATF6 and CREB3 are less accessible in the differentiated resistant cells, compared to the minimal disease cells (fig. 27D).

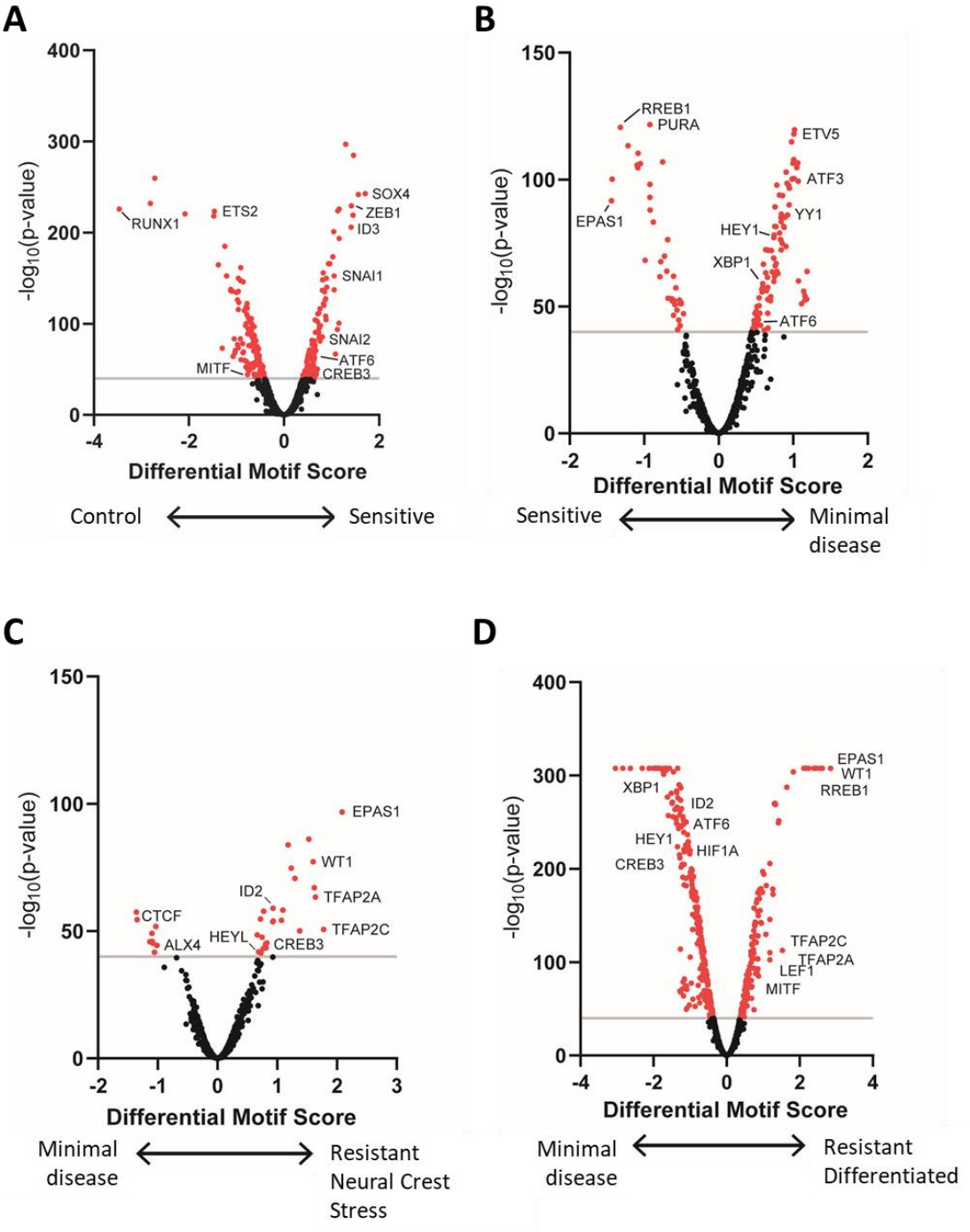

Figure 27: Dabrafenib induces dramatic epigenetic shift. (A) *Volcano plot shows differential motif accessibility for the control cells compared to sensitive cells.* ***(B)*** *Volcano plot shows differential motif accessibility for sensitive cells compared to minimal disease cells.* ***(C)*** *Volcano plot shows differential motif accessibility for the minimal disease cells compared to neural crest/ "stress-like" resistant cells.* ***(D)*** *Volcano plot shows differential motif accessibility for minimal disease cells compared to differentiated, resistant cells. Differential motif score is plotted against -log$_{10}$(p-value) of motif enrichment.*

To more easily visualize transitions between cell states, a heatmap that hierarchically clusters transcription factor motif accessibilities in various calculated clusters with corresponding phenotypes was generated (fig. 28). The dominant phenotypes are control cells, short-term treated sensitive cells, minimal disease and resistant cells. From the control (Melanoma.10 and Melanoma.11) to short term dabrafenib treated cells (Melanoma.07 and Melanoma.05), the accessibility of MITF motifs decreased, whereas stress related motifs like ATF3, ATF6 and XBP1 increased. During the transition from short- term dabrafenib treated cell state to minimal disease (Melanoma.04 and Melanoma.01) the stress related motifs ATF3, ATF6 and XBP1 further gained accessibility and additional neural crest motifs arose (PAX3, SNAI2, MYC). The resistant cells cluster into two distinct epigenetic clusters Melanoma.02 and Melanoma.08/Melanoma.09. The Melanoma.02 cluster is highly accessible for neural crest transcription factors like PAX3, TFAP2D, SOX10 and SOX9 but also stress related motifs like XBP1, ATF6 and ATF3 are highly enriched. The other two clusters Melanoma.08 and Melanoma.09 have rather low accessibility of both, neural-crest and stress related transcription factor motifs, however, they are enriched in MITF motif accessibility, associated with differentiated melanoma. From the minimal disease state to the resistant state either neural crest/ “stress-like” motifs or differentiation motifs were enriched. This transition to a neural crest or “stress-like” state also comprised high accessibility of HES1/HEY, ATF3 and XBP1 motifs.

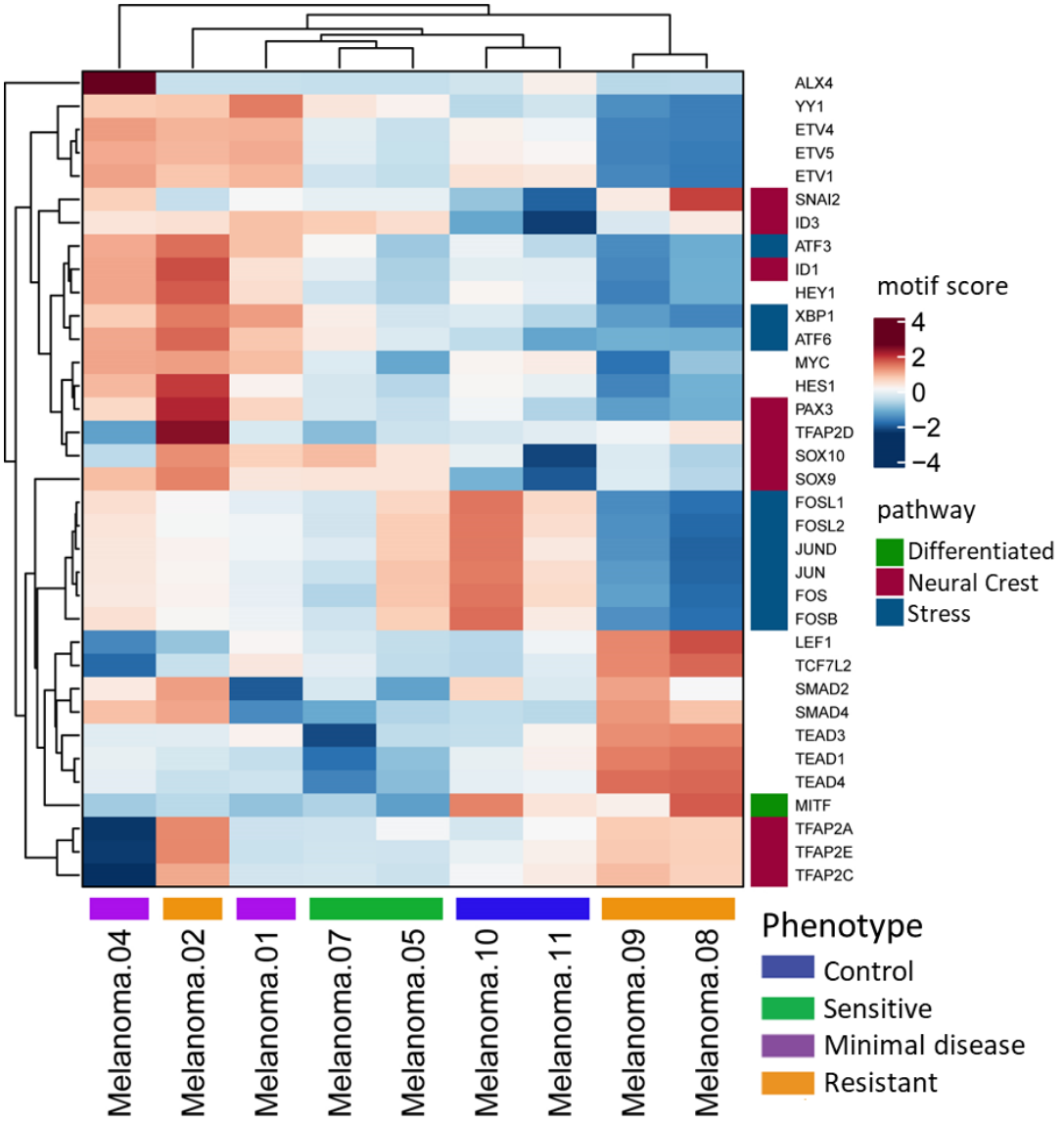

Figure 28: Heatmap shows distinct epigenetic states associated with differentiated melanoma, neural crest or "stress-like" states. *Accessibility of transcription factor motifs associated with differentiated melanoma, neural crest and "stress-like" state was clustered hierarchically and dominant phenotypes were assigned (Control, short-term treated sensitive, minimal disease, resistant).*

4.6 Single-cell RNA sequencing defines transcriptional tumor cell states and supports existence of “stress-like” state in resistant cells

4.6.1 Single-cell RNA sequencing identifies distinct normal and heterogeneous tumor cell states

Single-cell RNA sequencing of primary melanomas from control tumors (DMSO-1, DMSO-2), responsive tumors (Sensitive-1, Sensitive-2), minimal disease (Minimal disease-1, Minimal disease-2) and resistant tumors (Resistant-1, Resistant-2) and dimensional reduction show the distinct clustering of transcriptional profiles for all samples (fig. 29).

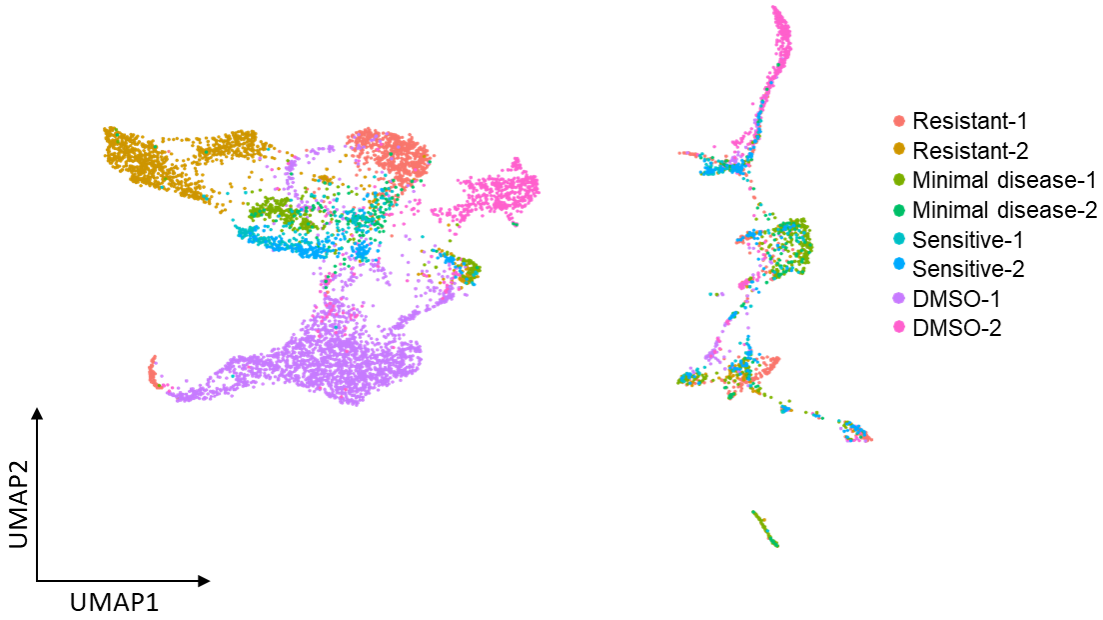

Figure 29: Single-cell RNA sequencing shows distinct clustering of tumor cells from all disease relevant time points based on their transcriptional profiles. *Cells are colour-coded based on the disease relevant time point: control tumors (DMSO-1, DMSO-2), sensitive tumors (Sensitive-1, Sensitive-2) minimal disease (Minimal disease-1, Minimal disease-2) and resistant tumors (Resistant-1, Resistant-2).*

To exclude non-melanoma cells from the downstream analysis, the original cell types were identified using known markers for melanoma cells, T-cells, macrophages, red blood cells, B-cells, fibroblasts, epithelial cells and neutrophils and non-melanoma cells were filtered out (fig. 30).

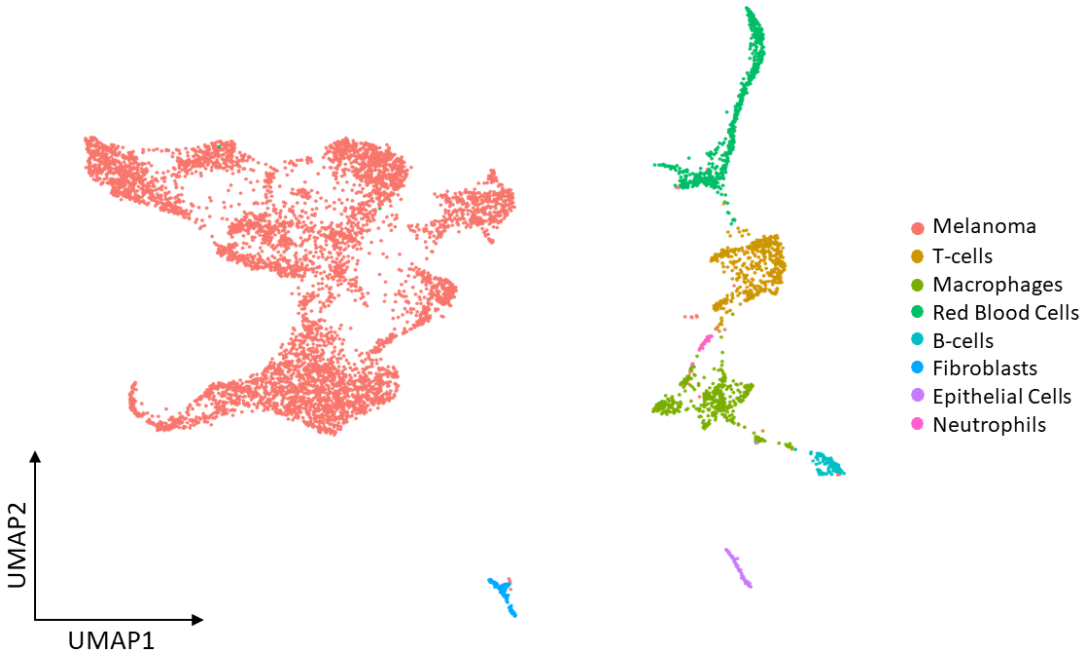

Figure 30: Transcriptionally defined cell types cluster together. *Cell clusters were colour-coded based on the cells original cell types: Melanoma cells, red blood cells, macrophages, B-cells, T-cells, epithelial cells, fibroblasts.*

Colour-coding the cells based on their disease-relevant time point sensitive cells and minimal disease cells, resistant cells and DMSO treated control cells shows the distinct clustering and transcriptional states of the various phenotypes (fig. 31).

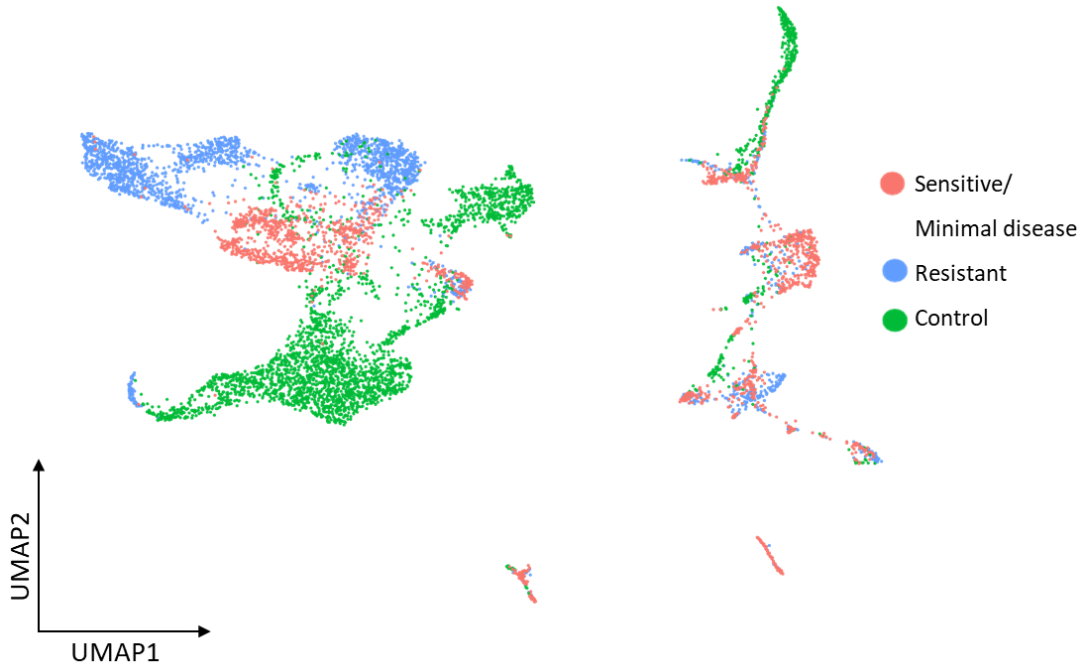

Figure 31: Cells cluster according to their disease relevant state. *Sensitive and minimal disease cells, resistant cells and DMSO control cells exhibit distinct transcriptional programs.*

4.6.2 Dabrafenib treatment leads to transcriptional shift in melanoma cells

Gene transcription of the various cell types was analysed in Seurat as above and 21 clusters were identified (fig. 32). The anticipated shift from the DMSO control cell state, over the dabrafenib sensitive state to the minimal disease and resistant cell state is indicated with black arrows.

Figure 32: Dynamic cell state adaptation to dabrafenib. *Transcriptional cell states were merged into 20 transcriptional clusters. Black arrows indicate dynamics of gene expression.*

Monocle-based pseudo-time trajectory analysis was performed to investigate the transcriptional shift upon drug treatment and development of resistance (fig. 33). Treatment with dabrafenib depletes cells from a proliferative state, which is highly enriched in cells from the untreated control samples. Sensitive cells are moving towards both extremes with many cells sharing an intermediate state. The resistant cells make up for the two most extreme transcriptional cell states.

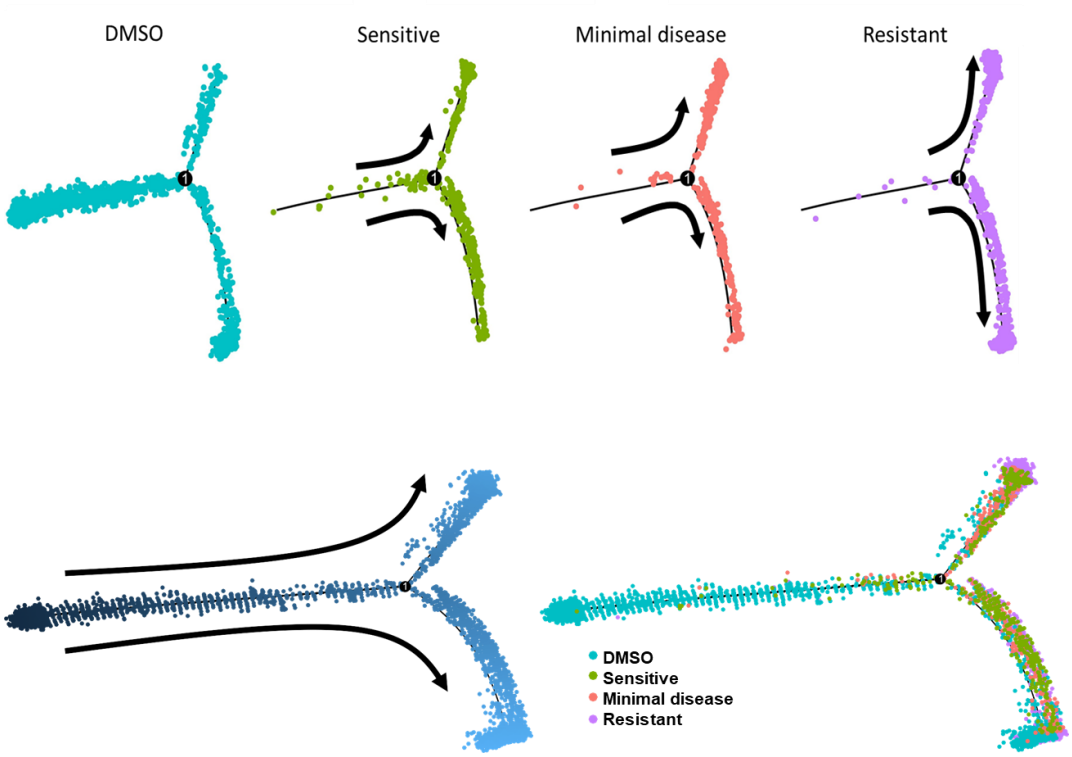

Figure 33: Cell states undergo gradual change on prolonged dabrafenib treatment. *Monocle-based pseudo-time trajectory analysis of scRNA-seq data from tumor samples from all disease relevant time points (DMSO control, sensitive, minimal disease, resistant) show transcriptional shift over the course of the treatment.*

The heatmap in fig. 34 visualizes the distinct transcriptional states along the pseudo-time trajectory. The pre-branch cell population has high levels of *ccnb1, mcm2* and *pcna*, which are markers for mitosis, proliferation and DNA replication. This population can be assigned to the previously identified proliferative cell type. The mitfa-high subgroup has high expression of *mitfa* and *mycb* and notable low expression of *sox10* and *fosab*. Markers of the neural crest cell state are *snai2* and *tfap2a*, but also the stress markers *xbp1*, *jun* and *fosab.*

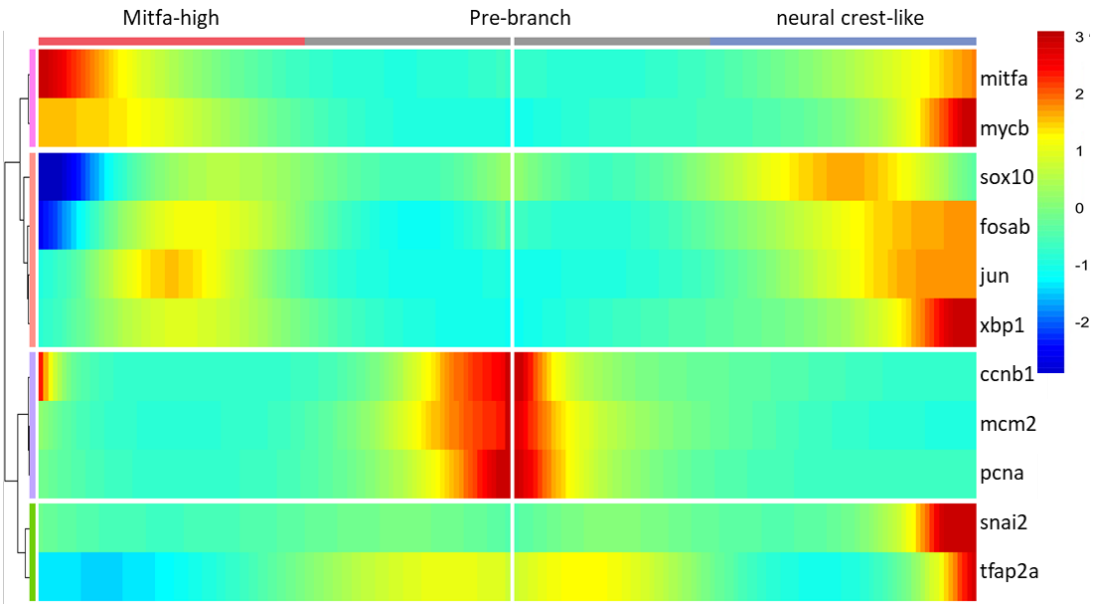

Figure 34: In a transcriptional pseudo-time simulation cells are either in a mitfa-high or in a neural crest/ "stress-like" state. *The heatmap hierarchically clusters variable features of the mitfa-high, the pre-branch and the neural crest cell state and group them into four major transcriptional states.*

The neural crest markers *id2a* and *mycb* and the stress related markers *xbp1* and *bhlhe41* are differentially expressed in melanoma cells with highest expression in resistant tumors (fig. 35). *Id2a* and *mycb* are more consistently expressed in both post-branch states, compared to the stress markers *xbp1* and *bhlhe41*.

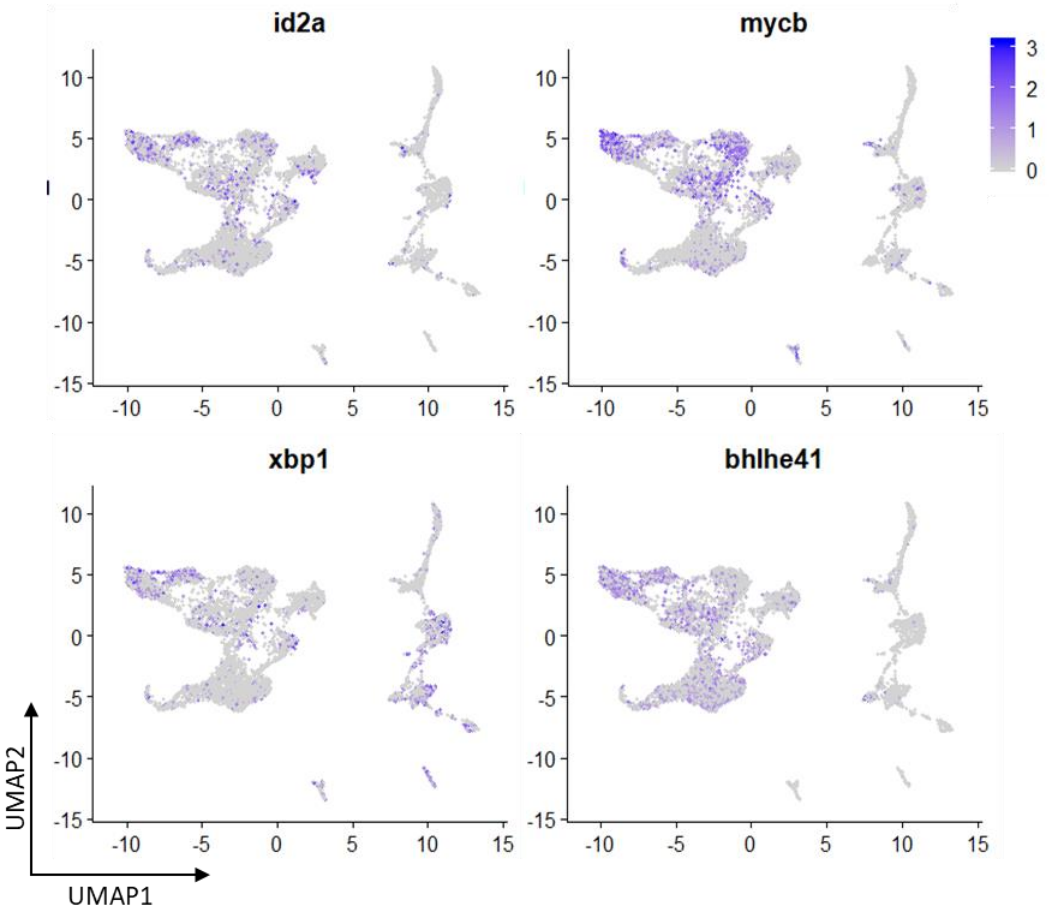

Figure 35: Resistant tumors have distinct expression of neural crest and stress related markers. *Expression of the neural crest markers id2a and mycb and the stress related markers xbp1 and bhlhe41 is visualized in UMAP plots.*

4.7 *In vitro* validation of "stress- like" state as driver for resistance

4.7.1 Generation of dabrafenib resistant A375 cell line

To validate the "stress-like" state *in vitro*, we generated a dabrafenib resistant cell line. The human melanoma cell line A375 was continuously treated with increasing doses of dabrafenib from 0.1 nM to 100 nM over a period of 3 weeks (fig. 36).

Both, the scATAC-seq and scRNA-seq data suggest *xbp1* as a major driver of resistant cell heterogeneity. *XBP1* is a target of ATF6 and mediates unfolded protein response (UPR) activated by ER stress (Yoshida et al. 2001). Consequently, we focused on ER stress and its inhibition in our *in vitro* validation experiments.

Figure 36: Scheme of generation of drug resistant cell line. *A375 cells were continuously treated with increasing doses of dabrafenib from 0.1 nM to 100 nM over a period of 3 weeks.*

4.7.2 Sensitive and resistant melanoma cells respond differently to pharmacologic ER stress inhibition

The sensitivity of the generated dabrafenib resistant cell line and the control cell line (treated with DMSO) to the ER stress inhibitor toyocamycin, which has been described as an inhibitor of XBP1 splicing (Ri et al. 2012) was compared (fig. 37). Cells were seeded and treated with varying concentrations of toyocamycin (15-60 nM) and viability was measured 72 hours after treatment. With increasing concentrations of toyocamycin, both cell lines showed decreased viability. With higher doses of toyocamycin (30 and 60 nM) the resistant cells showed higher sensitivity compared to the sensitive cells.

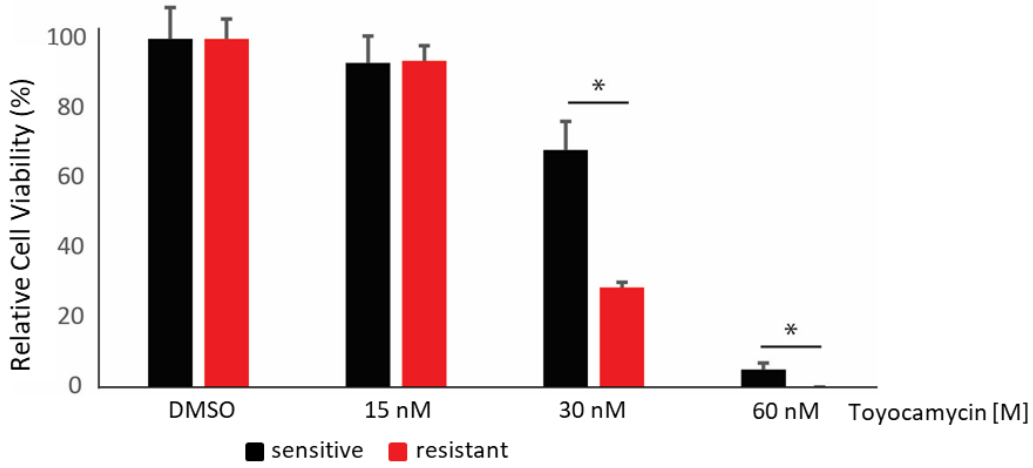

Figure 37: Sensitive and resistant A375 melanoma cells show different response to the ER stress inhibitor toyocamycin. *Sensitive and resistant A375 cells were seeded and treated with increasing concentrations of toyocamycin (15-60 nM) and viability was measured 72 hours after treatment. Asterisks indicate significant difference between sensitive and resistant cells (two-sided t-test, *p<0.05)*

4.7.3 Markers of neural crest/ "stress-like" state are differentially expressed in sensitive and resistant melanoma cells

To validate the "stress-like" state in resistant cells on the transcriptional level, expression of stress markers was measured in resistant and sensitive A375 melanoma cells. Sensitive and

resistant cells were seeded and treated with DMSO as a control, dabrafenib (100 nM) and toyocamycin (30 nM) combination or toyocamycin (30 nM) alone for 5 hours. Expression of the stress marker *XBP1* was quantified using qPCR (fig. 38). The amount of total *XBP1 (tXBP1*) was higher in the resistant cell line compared to the sensitive cell line indicating a higher degree of stress. Upon dabrafenib treatment, the spliced *XBP1* (sXBP1) decreased in the sensitive cells and increased in resistant cells. The combination of dabrafenib and toyocamycin treatment decreased levels of *sXBP1* in both cell lines and toyocamycin alone did not affect *sXBP1* levels.

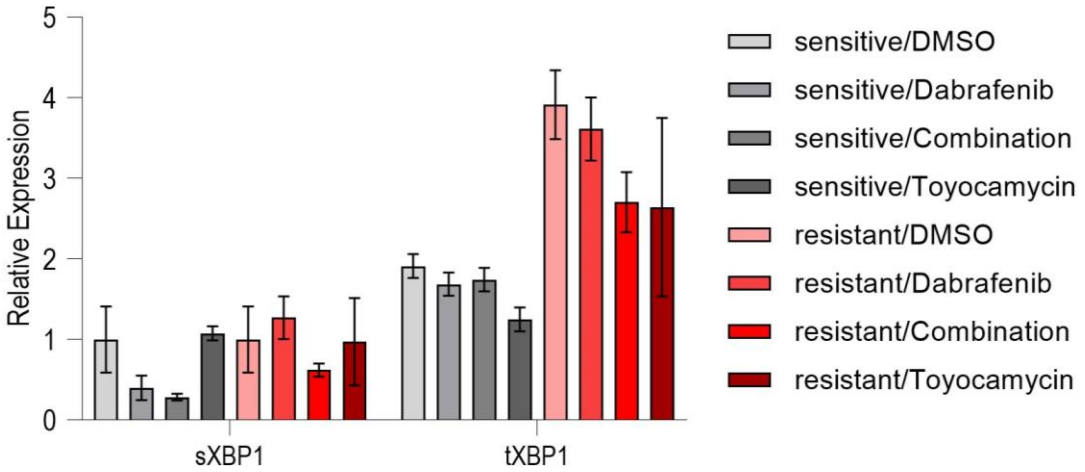

Figure 38: qPCR shows different levels of XBP1 in sensitive and resistant cells upon drug treatment. *Sensitive and resistant A375 melanoma cells were seeded and treated with DMSO as a control, 100 nM dabrafenib, 100 nM dabrafenib and 30 nM toyocamycin combination or 30 nM toyocamycin alone for 5 hrs. Levels of spliced xbp1 (sXPB1) and total xbp1 (tXBP1) were measured using qPCR and normalized to Ct values of gapdh. Expression of sXBP1 was normalized to the sensitive/DMSO sample. Error bars indicate standard deviation of three replicates.*

The neural crest markers *SOX4* (fig. 39) and *SOX10* (fig. 40) and the stress markers *ATF3* (fig. 41) and *DDIT3* (fig. 42) were also subjected to qPCR. Again, sensitive and resistant cells were seeded and treated with DMSO as a control, dabrafenib, dabrafenib and toyocamycin combination and toyocamycin alone. In the sensitive cell line there was an increase in *SOX4* upon dabrafenib treatment and dabrafenib and toyocamycin combination treatment, but not in only toyocamycin treated cells. In the resistant cell line, an increase in *SOX4* levels was observed when treating with dabrafenib or toyocamycin, however, the combination treatment had lower *SOX4* levels.

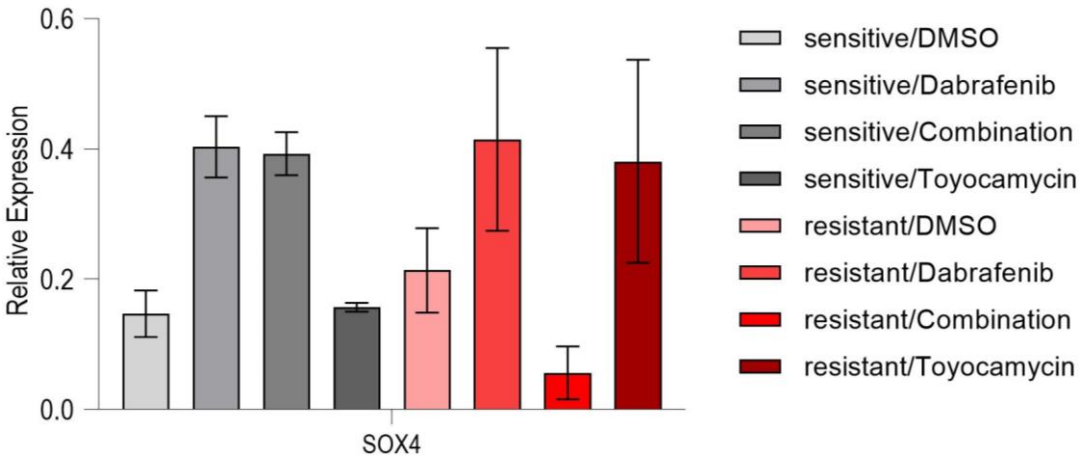

Figure 39: qPCR shows different levels of SOX4 in sensitive and resistant cells upon drug treatment. *Sensitive and resistant A375 melanoma cells were seeded and treated with DMSO as a control, 100 nM dabrafenib, 100 nM dabrafenib and 30 nM toyocamycin combination or 30 nM toyocamycin alone for 5 hrs. Levels of SOX4 were measured using qPCR and normalized to Ct values of gapdh. Error bars indicate standard deviation of three replicates.*

Levels of *SOX10* did not change dramatically in the sensitive cell line upon drug treatment, however, in resistant cells the dabrafenib treatment lead to increased levels of *SOX10*, but not in the dabrafenib/ toyocamycin combination treatment.

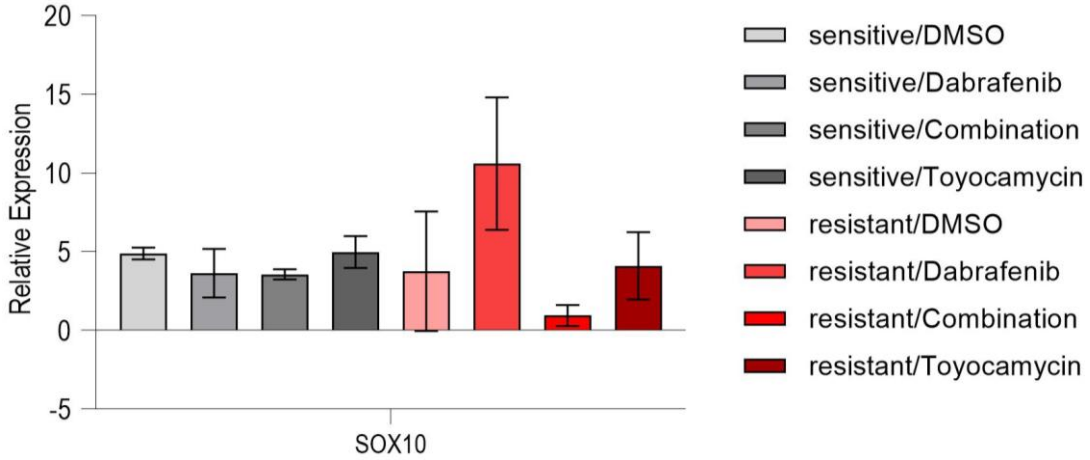

Figure 40: qPCR shows different levels of SOX10 in sensitive and resistant cells upon drug treatment. *Sensitive and resistant A375 melanoma cells were seeded and treated with DMSO as a control, 100 nM dabrafenib, 100 nM dabrafenib and 30 nM toyocamycin combination or 30 nM toyocamycin alone for 5 hrs. Levels of SOX10 were measured using qPCR and normalized to Ct values of gapdh. Error bars indicate standard deviation of three replicates.*

Levels of *ATF3* increased in sensitive cells with dabrafenib and dabrafenib/toyocamycin combination treatment but not with the toyocamycin treatment alone. In resistant cells, there is almost no increase in the dabrafenib treated cells and levels were decreased upon the

dabrafenib/ toyocamycin combination treatment. The cells treated with toyocamycin alone showed highest levels of *ATF3*.

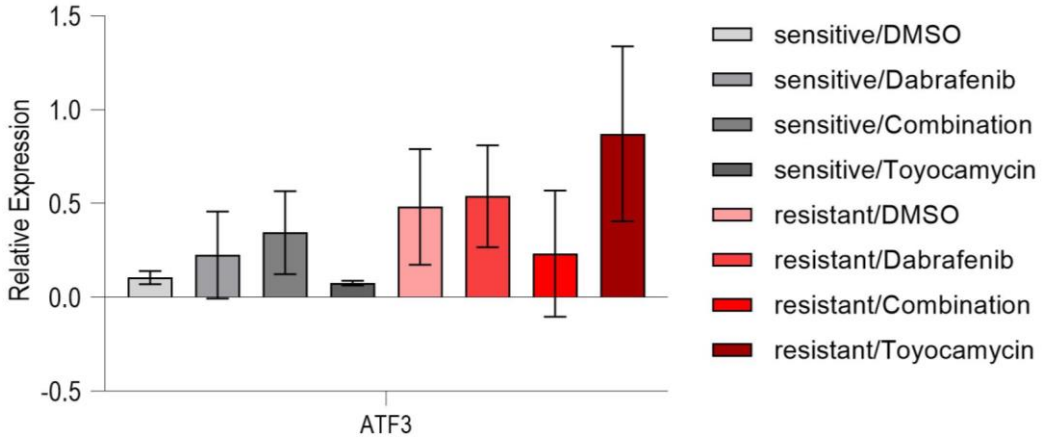

Figure 41: qPCR shows different levels of ATF3 in sensitive and resistant cells upon drug treatment. *Sensitive and resistant A375 melanoma cells were seeded and treated with DMSO as a control, 100 nM dabrafenib, 100 nM dabrafenib and 30 nM toyocamycin combination or 30 nM toyocamycin alone for 5 hrs. Levels of ATF3 were measured using qPCR and normalized to Ct values of gapdh. Error bars indicate standard deviation of three replicates.*

Levels of the stress marker *DDIT3* increased in sensitive cells with both, dabrafenib and dabrafenib/toyocamycin combination treatment. The resistant cells had clearly higher levels of *DDIT3* upon dabrafenib treatment, however, the dabrafenib/toyocamycin combination treatment reversed that effect. The toyocamycin treatment alone did not seem to have an effect on *DDIT3* in both cell lines, as anticipated since *DDIT3* is not a downstream target of XBP1.

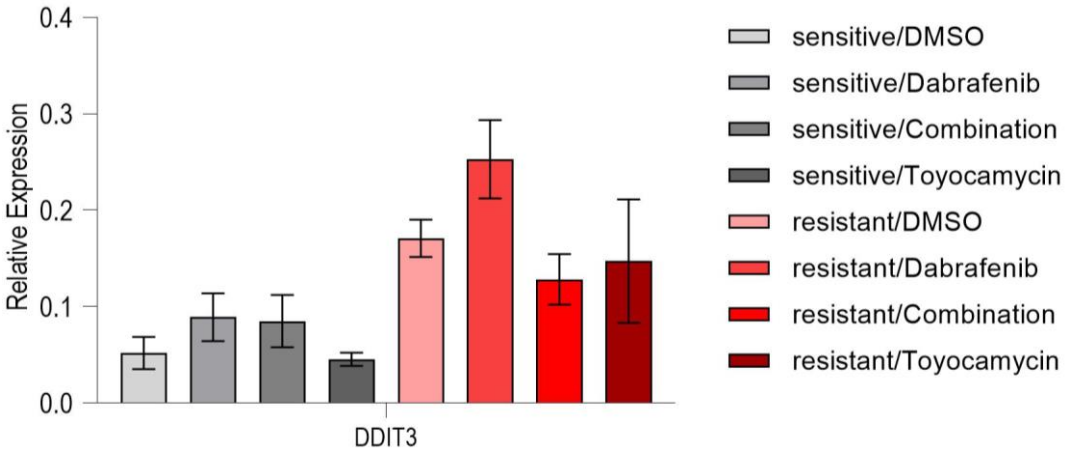

Figure 42: qPCR shows different levels of DDIT3 in sensitive and resistant cells upon drug treatment. *Sensitive and resistant A375 melanoma cells were seeded and treated with DMSO as a control, 100 nM dabrafenib, 100 nM dabrafenib and 30 nM toyocamycin combination or 30 nM toyocamycin alone for 5 hrs. Levels of DDIT3 were measured using qPCR and normalized to Ct values of gapdh. Error bars indicate standard deviation of three replicates.*

4.7.4 Bulk ATAC-sequencing confirms “stress-like” state in resistant cells

To validate the “stress- like” state on an epigenetic level, bulk ATAC sequencing of the sensitive and resistant A375 cells was performed without any further drug treatment (fig. 43-45). Reads from the sequencing were subjected to pre-alignment quality control following alignment to the reference genome. The accessible regions (peaks) were identified using MACS2 as peak caller. The accessibility of regions of candidate genes in sensitive and resistant cells were then compared using Integrative Genomics Viewer (Robinson et al. 2011). Peaks are coloured in blue and red bars indicate identified peak. Difference is calculated by subtracting the areas under the peaks. Higher accessibility in the resistant cell line is depicted as orange differential peak and negative values are coloured green. In the resistant cell line, the region around the neural-crest marker *ATF4* was more accessible compared to the sensitive cell line (fig. 43). The markers for the “stress-like” state *ATF3, DDIT3* (fig. 43); *HSPA9, HSP90B1, HSPA5, HYOU* (fig. 44); *HSPA8, JUNB, JUND* and *UBB* (fig. 45) showed higher accessibility in the resistant cell line.

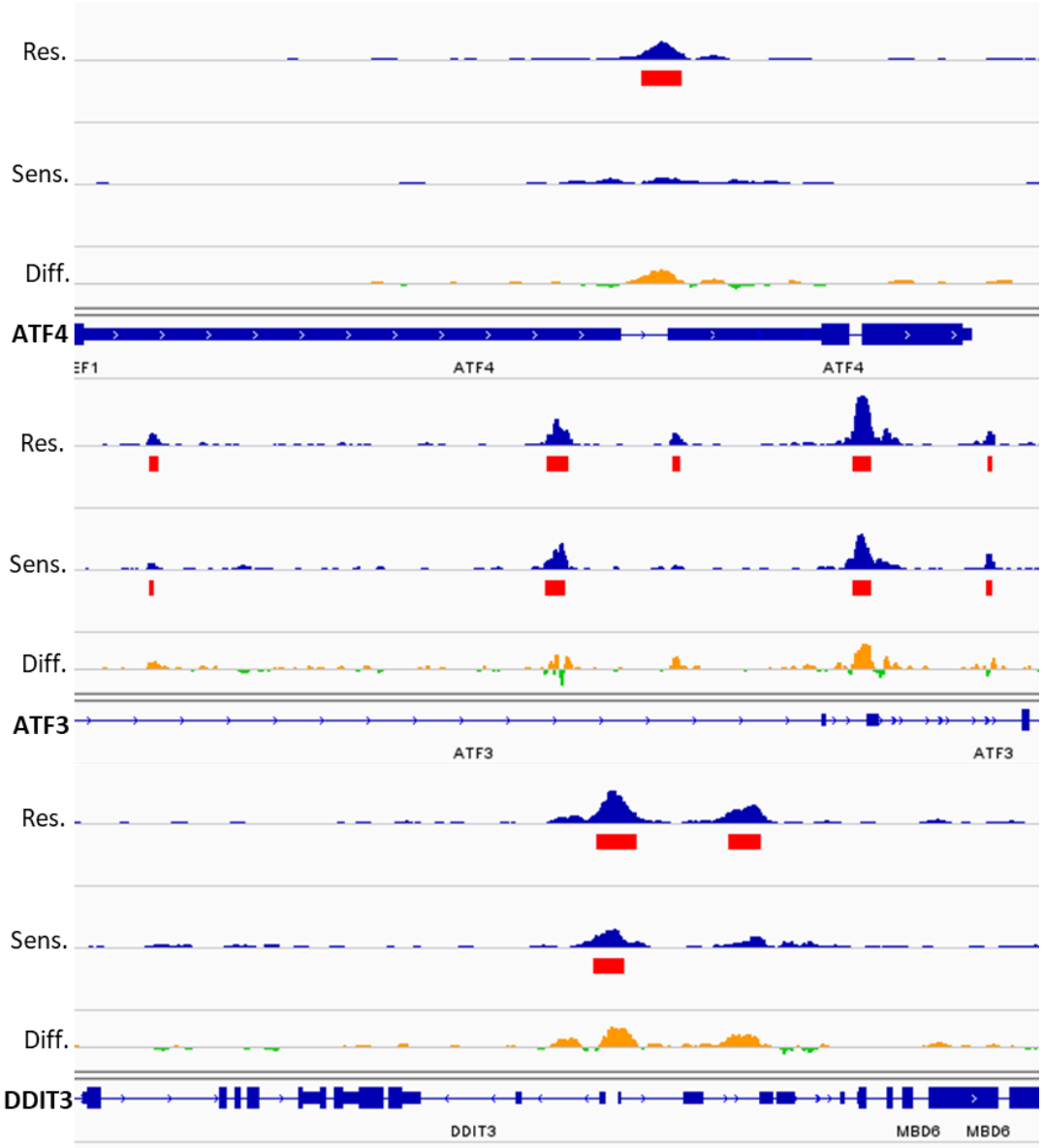

Figure 43: Chromatin regions around ATF3, ATF4 and DDIT3 show higher accessibility in resistant cells. *Sensitive and resistant cell lines were subjected to bulk ATAC-sequencing, peaks were called using MACS2 and accessibility was visualized using Integrative Genomics Viewer. Accessibility of the neural crest marker ATF4 and the stress related markers ATF3 and DDIT3 was assessed. Peaks of accessibility: blue, identified peaks: red bars, difference: orange (positive values), green (negative values). Res: resistant cells, Sens: sensitive cells, Diff: difference.*

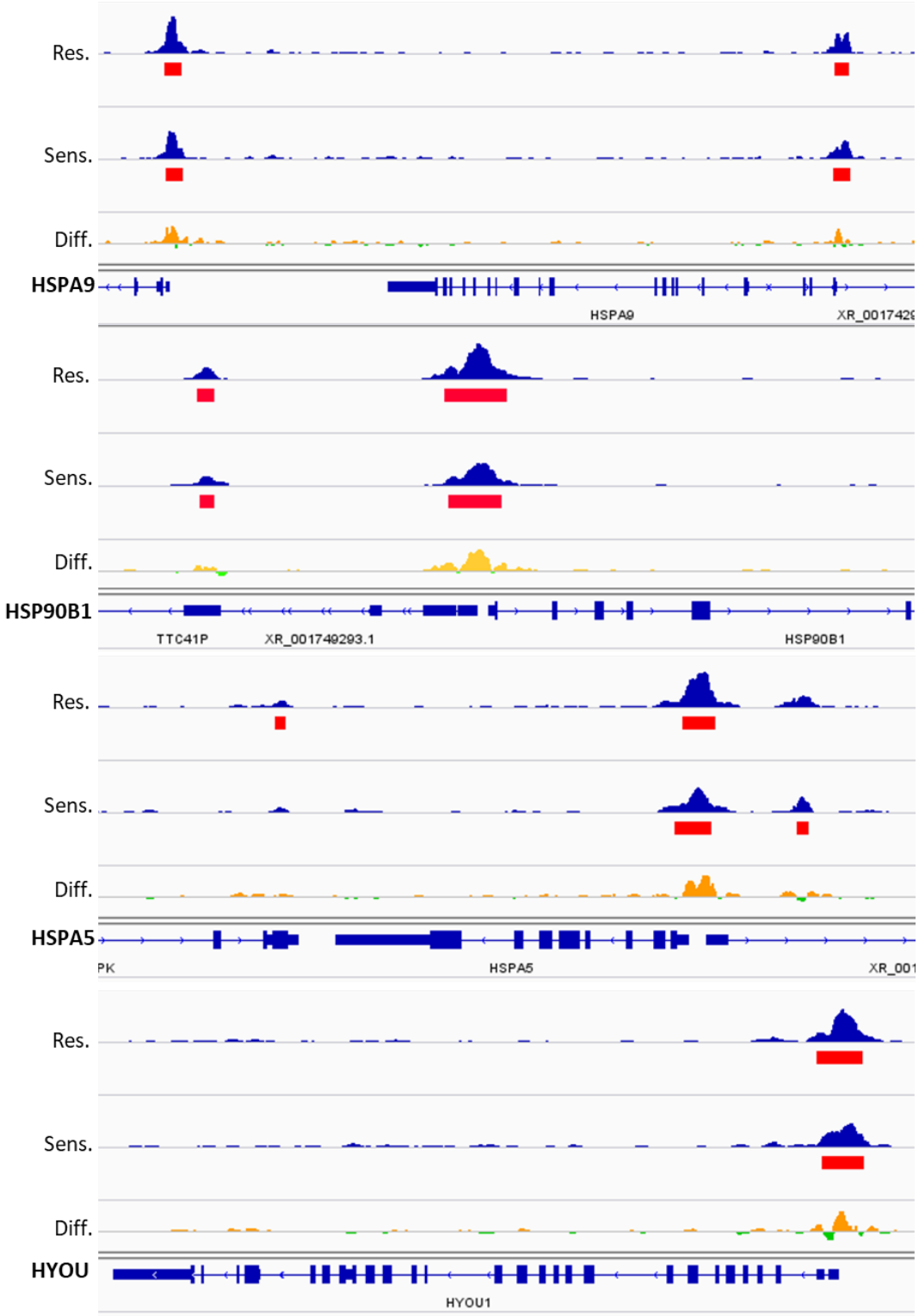

Figure 44: Chromatin regions around HSPA9, HSP90B1, HSPA5 and HYOU show higher accessibility in resistant cells. *Sensitive and resistant cell lines were subjected to bulk ATAC-sequencing, peaks were called using MACS2 and accessibility was visualized using Integrative Genomics Viewer. Accessibility of the stress marker HSPA9, HSP90B1, HSPA5 and HYOU was assessed. Peaks of accessibility: blue, identified peaks: red bars, difference: orange (positive values), green (negative values). Res: resistant cells, Sens: sensitive cells, Diff: difference.*

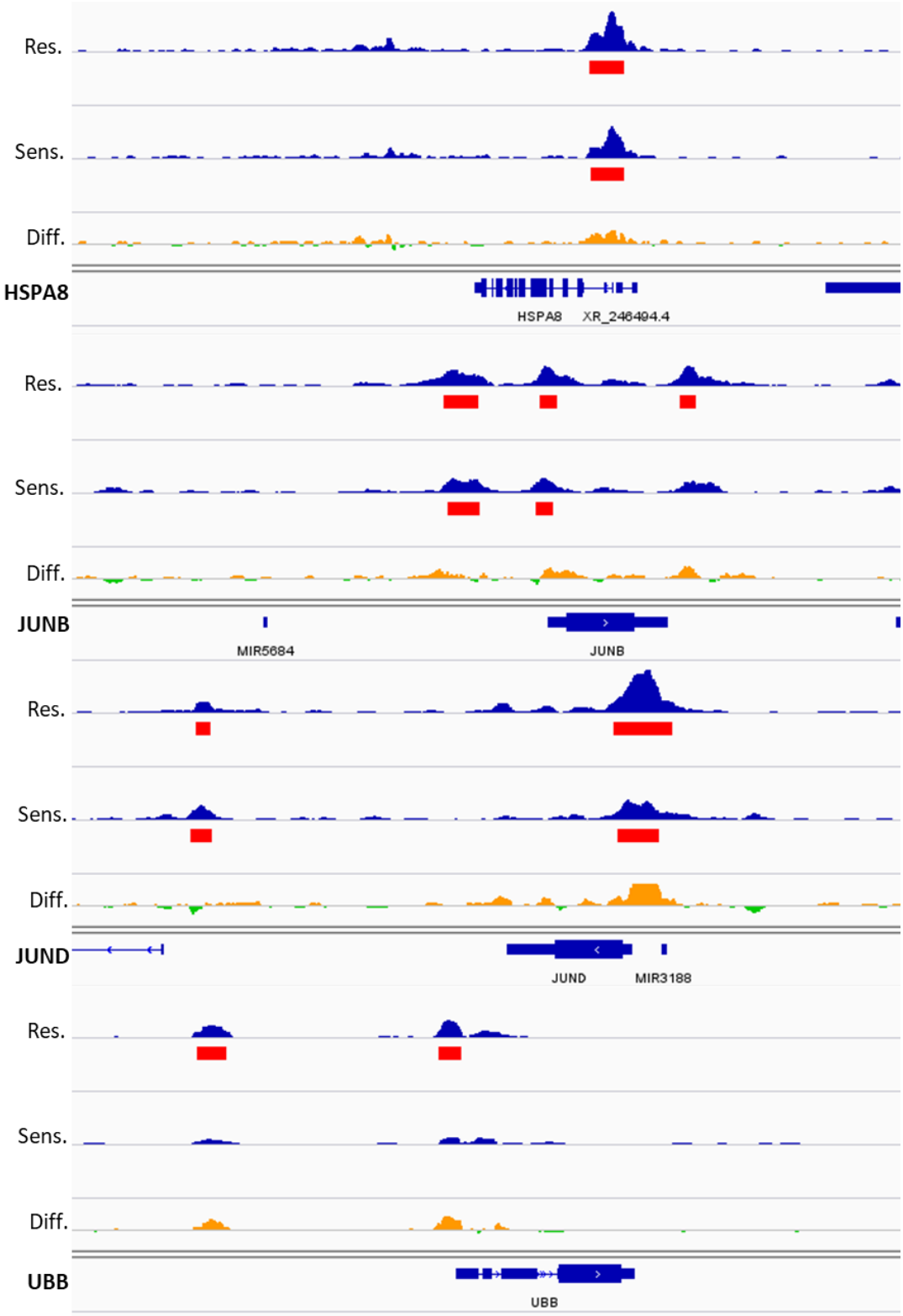

Figure 45: Chromatin regions around HSPA8, JUNB, JUND and UBB show higher accessibility in resistant cells. *Sensitive and resistant cell lines were subjected to bulk ATAC-sequencing, peaks were called using MACS2 and accessibility was visualized using Integrative Genomics Viewer. Accessibility of the stress markers HSPA8, JUNB, JUND and UBB was assessed. Peaks of accessibility: blue, identified peaks: red bars, difference: orange (positive values), green (negative values). Res: resistant cells, Sens: sensitive cells, Diff: difference.*

5 Discussion

5.1 Single-cell RNA sequencing revealed inter- and intratumoral heterogeneity in naïve melanoma samples

BRAFV600E driven melanomas were generated in a *Tg(mitfa:BRAFV600E);tp53*$^{-/-}$*; mitfa*$^{-/-}$ zebrafish line and samples of three treatment naïve tumors were used to generate scRNA-seq libraries with the inDrop platform. All libraries were sequenced on an illumina Nextseq instrument and 7705 single melanoma cells from all three samples were collectively analysed using the R package Seurat.

The pre-processing analysis showed that most cells were of high quality and passed the thresholds for quality control (fig. 11). Most cells had between 200 and 2500 unique genes per cell, less than 15000 RNA molecules per cell and less than 5% mitochondrial RNA reads. Those measures were used to filter out low quality cells, multiplets and cells with high mitochondrial read numbers.

The scatter plots visualize that the number of unique genes per cell and RNA molecules per cell correlated, whereas the percentage of mitochondrial RNA and number of RNA molecules per cell did not show a correlation (fig. 12).

The heatmap of the first principal component (fig. 14) illustrates genes that mainly drive heterogeneity and discriminates the dataset. The two major transcriptional states that can be separated are characterized by markers for melanoma cells and immune cells, respectively. *Crestin* and *sox4a* are markers for melanoma cells and the *c1qa* and *c1qb* complement factors allow to narrow down the immune cells to macrophages. This pattern was similarly seen in other principle components that primarily seemed to separate specific cell types.

According to the standard deviations of the various principal components (fig. 15), the first 18 PCs were used for further downstream analysis.

Dimensional reduction demonstrates that naïve melanomas form distinct and partly overlapping clusters for each sample (fig. 16). The tumors show both unique and conserved cell clusters, that suggest a high degree of both inter- and intratumoral heterogeneity at baseline even in an inbred and genetically well-defined animal model of melanoma which is known to have a low genetic mutation burden (Yen et al. 2013).

Similar to what Rambow et al. were observing (Rambow et al. 2018), our data shows that even prior to initial treatment, naïve melanoma cells show significant inter- and intratumoral heterogeneity. In contrast to the melanoma cells, non-melanoma stromal cells were readily identified using established transcriptional markers, suggesting that the majority of tumor heterogeneity is driven by the tumor cells proper-prior to initiation of therapy.

Further, our scRNA-seq data suggests specific transcriptional cell states already in naïve melanoma. E.g. the melanoma markers *mitfa* and *sox10* were differentially expressed in melanoma cells. This leads to the assumption that specific tumor states pre-existing in naïve melanoma shape the development and progress of melanoma by the acquisition of distinct transcriptional subpopulations.

5.2 Dabrafenib resistant tumors arise with variable kinetics

The kinetics of drug response in *BRAFV600E* driven tumors was followed in the *Triple* zebrafish line (fig. 20). From the injection into the single-cell stage of the embryo it took approximately 4 months for fish to develop tumors. The fish were treated daily with dabrafenib and the tumor response was monitored weekly. As anticipated, tumors in the DMSO treated control group increased in size until they were sacrificed due to their tumor burden. The short period from tumor development to a large tumor burden further underlines the aggressiveness of this cancer type and the fish model. As was expected, the tumors of the dabrafenib treated group decreased in size over the first 3 weeks. As in human patients, resistance arose with variable kinetics over the course of several months that varied between animals. The high rate of resistance in zebrafish correlate with the poor prognosis that is seen in human melanoma patients suggesting that initial drug tolerance may not be mediated by genetic means given the known low mutational burden in these tumors (Yen et al. 2013) and that transcriptional and epigenetic adaptation maybe an important mediator in the development of drug resistance. Thus, this model provides an opportunity to examine these changes with single cell resolution to identify additional therapy options for patients.

5.3 Single-cell ATAC sequencing identifies distinct normal and heterogeneous tumor cell states

BRAFV600E driven tumors were modelled in the *Triples* line and samples were taken from four disease relevant time points: control DMSO treated tumors, short-term treated drug sensitive tumors, minimal disease, and drug resistant tumors. Differences in chromatin accessibility were investigated using scATAC-seq to identify epigenetic states associated with specific disease relevant time points. The tumors clustered into groups based on their epigenetic landscape and accessibility of specific motifs associated with various clusters were identified (fig. 21). Much as in the treatment naïve setting, the data suggests that a single tumor can harbor melanoma cells in several multiple epigenetic states, even under the selective pressure of drug treatment. Interestingly, subsets of cells from resistant tumors and minimal disease clustered together (fig. 22). This suggests that the minimal disease state represents a transition state from responsive to resistant tumors.

Our results seem to support the concept of tumor heterogeneity with cells from various epigenetic states co-existing within a tumor. Shaffer et al (Shaffer et al. 2017) proposed the model of transient gene expression. Non-genetic rare cell variability accounts for drug response by epigenetic reprogramming of those cells. Essentially, pre-resistant melanoma cells move in and out of the transient pre-resistance state and upon drug treatment turn into fully resistant cells. We believe that minimal disease state that we and others (Rambow et al. 2018) have observed represents an intermediate or pre-resistant cell state that acquire most, but not all, of the epigenetic features needed to contribute to development of overt drug resistance given relatively minor shifts we see in a subset of resistance tumors from the minimal disease state.

5.3.1 Motif accessibility defines melanoma cell states and suggests “stress-like” state in resistant cells

Accessibility of various motifs was analysed and clusters of differential motifs were calculated for all four disease relevant time points. Resistant cells cluster into two major epigenetic states based on different motif accessibilities: an MITF related motif cluster and a “stress-like” motif cluster (fig. 26). MITF is a master regulator of melanocyte development and high expression correlates with a high degree of melanocyte maturation and differentiation. The MITF related motif is associated with high accessibility of RUNX3, TEAD3, MITF and EPAS1. Those motifs are in line with previous findings of the $MITF^{high}$ or differentiated

cell state (Hoek et al. 2008). The TFAP2C and SNAI2 motifs were previously identified as markers for the neural crest-like state and were highly enriched throughout treatment with dabrafenib – suggesting that expression of neural crest factors may underly the epigenetic and transcriptional response to MAPK pathway inhibition within the model. The tumor suppressor RUNX3 is a downstream target of the TGF-β signalling pathway and besides regulating angiogenesis and cell death it has been shown to inhibit migration and invasion in melanoma (Zhang et al. 2017).

The other motifs XBP1, ATF3, ATF6, CREB3, ALX4, ID2, MYC and the AP2 factors FOS and JUNB point toward a "stress-like" state in a subset of resistant cells. Those findings are in line with the "stress-like" cancer cell state Baron et al found in melanoma cells on the transcriptional level (Baron et al. 2020). The neural crest marker MYC is enriched in a subset of resistant cells. This leads to the assumption that resistant cells either move towards a highly differentiated cell state characterized by high MITF accessibility or a neural crest-like/ "stress-like" state characterized by low MITF accessibility and high accessibility of DNA containing several neural crest (TFAP2A, ID2, MYC) and stress related motifs (ATF3, ATF6, XBP1). The short-term treated drug sensitive phenotype clusters shared high motif accessibility of both states, which suggest a common epigenetic and transcriptional response to MAPK pathway inhibition that allows these cells to not "commit" to a specific cell state. Notably, the AP-2 factor motifs are highly enriched in the short-term treated phenotype clusters suggesting that the neural crest cell state is an early response to MAPK pathway inhibition. Cells of the minimal disease state exclusively shared stress-like motifs which points to the likelihood that over the course of the drug treatment, eventually, cells fully acquire a "stress-like" state that allows them to survive prolonged MAPK pathway inhibition and provide the basis for the development of resistance. As previously discussed, this suggests that minimal disease cells are a result of transient gene expression that epigenetically acquire a state of drug tolerance that develops into full resistance upon prolonged drug treatment. Of note, this theory is not mutually exclusive from the acquisition of specific genetic mutations that may lead to drug resistance.

Moreover, the control cells share motifs of both states with higher abundance of the $MITF^{high\text{-}accessibility}$ state. This suggests that the $MITF^{high\text{-}accessibility}$ state is not exclusive to the resistant cells whereas the stress motif is a cell state specifically acquired upon drug treatment. A subset of the control cells is highly accessible for markers for the $MITF^{high\text{-}accessibility}$

and neural crest state which underlines the intratumoral heterogeneity. Those findings would seem to show that the “stress-like” state provides cells with a survival benefit.

5.3.2 Dabrafenib induces dramatic epigenetic shifts

Comparing two phenotypes based on motif enrichment scores allowed to identify motifs that show differential accessibility at the respective time points (fig. 27, 28). This was done to follow the epigenetic changes that occur over the course of the treatment and to find candidate drivers that shape the chromatin landscape upon development of drug resistance. Comparing the control cells versus the short-term treated drug sensitive state, the first showed high accessibility of RUNX1, MITF and ETS2 motifs. Losing accessibility of those motifs upon drug treatment is in line with the gradual dedifferentiation of melanoma cells others have observed (Tsoi et al. 2018; Rambow et al. 2018). The short-term treated drug sensitive cells are enriched in accessibility for the neural crest related motifs SOX4, SNAI1 and SNAI2 and the stress related factor ATF6 and AP1 related motifs (JUN, FOS, etc.). The initial decrease in MITF accessibility and the increased accessibility of neural crest and stress associated motifs indicates the shift towards a neural crest-like state early on in the course of the disease. Over prolonged dabrafenib treatment, the accessibility of stress-related motifs further increased and motifs for ATF3/6, XBP1 and HEY1 are more accessible in the minimal disease state compared to the short-term treated drug sensitive state. As discussed previously, the fully resistant state can be discriminated into two major epigenetic states: a differentiated resistant disease ($MITF^{high\text{-}accessibility}$) and a neural crest-like/ “stress-like” resistant disease. Compared to minimal disease cells, both have higher accessibility of sites containing motifs for AP-2 factors including TFAP2A and TFAP2C. The stress motifs XBP1 and ATF6 are specific for the neural crest-like/ “stress-like” state whereas the differentiated resistant cell state is defined by high accessibility of the differentiation marker MITF. This supports the hypothesis of drug responsive cells that acquire a “stress-like” cell state that allows survival in response to MAPK pathway inhibition. This is consistent with a model described by Tsoi et al suggesting a gradual gene expression shift upon BRAF inhibition in melanoma cells (Tsoi et al. 2018). Their data points towards a treatment-induced shift of differentiation following a trajectory over a neural crest-like cell state and a transitory cell state to a melanocytic cell state. Our data suggests the dedifferentiation of drug responsive cells and minimal disease cells and subsets of resistant cells which differentiate after developing resistance.

It can be concluded that resistant cells are in either of two major epigenetic states with intra- and intertumoral heterogeneity: an MITF$^{high\text{-}accessibility}$ state and a neural crest/ “stress-like” state. The latter is gradually acquired early on in the course of drug treatment and is likely a crucial epigenetic feature in both initial tumor response to MAPK pathway inhibition, cell survival and the development of overt drug resistance. Meanwhile, the relationship between the MITF$^{high\text{-}accessibility}$ state and the minimal disease state is less clear as they appear to have very different epigenetic phenotypes. The two states seem to be mutually exclusive from one another in the resistant phenotype, whereas the sensitive and minimal disease are overlapping and could potentially use co-operativity to fully acquire drug resistance.

5.4 Single-cell RNA sequencing defines transcriptional tumor cell states and supports existence of “stress-like” state in resistant cells

Single-cell RNA sequencing was performed in parallel to transcriptionally define tumor cells from control tumors, short-term treated drug sensitive tumors, minimal disease tumors and resistant tumors. As anticipated from the scATAC-seq data, the scRNA-seq data analysis showed distinct clustering of tumor cells from the respective time points with significant degrees of both inter- and intratumoral heterogeneity (fig. 29). Again, known markers were used to identify melanoma cells, T-cells, macrophages, red blood cells, B-cells, fibroblasts, epithelial cells and neutrophils and exclude non-melanoma cells from the further analysis (fig. 30).

To reconstruct the pseudo-time trajectory of melanoma cells, a monocle-based trajectory analysis was conducted (fig. 33). Our findings are in line with previous results and confirm the co-existence of two major transcriptional states in resistant melanoma cells: an *mitfa*-high state and a neural crest-like/ “stress-like” state (fig. 34). The pre-branch cells are in a proliferative state, that have high levels of *mcm2*, *pcna* and *cdk1*, all of which are involved in DNA replication, proliferation and cell cycle progression. This constitutes a refinement of the previous clustering by Hoek et al who combined differentiated and proliferative cells in the MITF^{high} cell type (Hoek et al. 2008). Our trajectory analysis demonstrates that proliferating and differentiated cells exhibit transcriptionally distinct clusters. The proliferative state is likely a transient cell state from where cells upon drug treatment exit the cell cycle and move towards either a differentiated or neural-crest/ “stress-like” state. Transcriptionally, the MITF^{high} cell state can be compared with the previously defined differentiated cell state. The other branch of the analysis can be further described as neural crest or “stress-like”

state. The scATAC-seq data showed two major epigenetic states- an MITF$^{high\text{-}accessibility}$ and a neural crest/ “stress-like” state. The scRNA-seq data is in good agreement with the scATAC-seq data and presents a refinement of the identified cell states. The neural crest state is transcriptionally defined by high expression of *snai2* and *tfap2a* which correlates with the scATAC-seq data. The stress-related factors *fosab*, *jun* and *xbp1* from the scRNA-seq highly overlap with the “stress-like” state found on the epigenetic level.

5.5 *In vitro* validation of the “stress-like” state as driver of resistance

Many markers of the “stress-like” state like the AP-1 factors *fos* and *jun* are involved in a variety of stress responses but others like *xbp1, atf4* or *atf6* suggest endoplasmic reticulum stress is a major mediator of this state (Szegezdi et al. 2006). Therefore, we focused on ER stress for the validation of the “stress-like” state in the following experiments.

A375 human melanoma cells were continuously treated with increasing doses of dabrafenib from 0.1 nM to 100 nM over a period of 3 weeks to generate a drug resistance cell line. This resistant cell line as well as a drug sensitive cell line were used for the *in vitro* validation of the “stress-like” state in resistant tumor cells.

5.5.1 Sensitive and resistant melanoma cells respond differently to pharmacologic ER stress inhibition

According to the scATAC-seq data, accessibility of DNA containing the stress related XBP1 motif is highly enriched in a subset of resistant melanoma cells. The scRNA-seq data confirmed those results so in order to interfere with the stress state, the drug toyocamycin which interferes with ER stress by inhibiting XBP1 splicing (Ri et al. 2012) was used. The differential drug response of sensitive and resistant cells was measured using a viability assay (fig. 37). On low doses (0-15 nM) of toyocamycin both cell lines showed comparable drug response. On higher doses (30-60 nM) the resistant cell line showed significantly reduced viability compared to the sensitive cell line. This lends support to previous findings of a “stress-like” state benefitting survival in resistant cells (Baron et al. 2020).

Our findings are in line with previous publications on ER stress in resistant melanoma. Induction of a “stress-like” state confers resistance under both MEK and BRAF inhibition and combined inhibition of BRAF and autophagy restored drug sensitivity in BRAFi-resistant xenografts (Ma et al. 2014; Baron et al. 2020). The BRAF inhibitor vemurafenib was shown to decrease levels of antiapoptotic proteins and induce ER stress- mediated apoptosis which

was reversed upon knock down of ATF4, an important regulator of ER stress (Beck et al. 2013).

The vulnerability of subsets of cells towards iron dependent oxidative stress and the differential drug response over the course of treatment and differentiation states underlines the importance of a "stress-like" state in the pathogenesis of melanoma progression (Tsoi et al. 2018), although our data points towards ER stress rather than oxidative stress. These differences can be explained in part by overlapping regulators of the various stress states. Further, viewing the sum of cellular processes that are happening in parallel, it is very likely that a general stress state is acquired, involving ER stress, oxidative stress or mitochondrial stress.

5.5.2 Markers of "stress-like" state are differentially expressed in sensitive and resistant melanoma cells upon ER stress and BRAF inhibition

The expression of stress-related markers was investigated in the sensitive and resistant cell line with 5 hours dabrafenib, toyocamycin and combination (dabrafenib + toyocamycin) treatment. *XBP1* with is fundamental role in ER stress was of major interest, so the total levels and the spliced levels of *XBP1* were measured (fig. 38). The resistant cell line seems to have higher basal levels of total *XBP1* which points towards a "stress-like" state in those cells. The levels of total X*BP1* did not vary in the sensitive cell line, but the levels of spliced *XBP1* decreased with dabrafenib and combination treatment. Contrary to expectations, the levels of spliced *XBP1* were higher in sensitive cells treated with toyocamycin alone. In the resistant cell line total *XBP1* was expressed to a lower level upon combination and toyocamycin treatment. For spliced *XBP1* the combination treatment was found to be most potent in decreasing the levels.

The neural crest associated markers *SOX4* and *SOX10* increased upon dabrafenib and combination treatment, but not toyocamycin alone, in sensitive cells (fig. 39, 40). This is consistent with the *in vivo* data showing dabrafenib treatment selecting for cells in a more neural crest-like state. In the resistant cells, there was an increase in *SOX4* and *SOX10* upon dabrafenib and toyocamycin treatment, however, levels dramatically decreased on the combination treatment. This suggests that the resistant cells are at least somewhat dependent on ER stress as a signal to reinforce the neural crest state.

The stress markers *ATF3 and DDIT3* increased in sensitive cells with dabrafenib and combination treatment (fig. 41, 42). Again, this suggests an increase in stress state mainly due to dabrafenib. The toyocamycin treatment decreased *ATF3* and *DDIT3* levels to a minimum. In

resistant cells, there was a drop in *ATF3* and *DDIT3* levels upon combination treatment which is in line with the observations for the neural crest markers *SOX4* and *SOX10*.

Toyocamycin is a potent inhibitor of IRE-1a mediated XBP1 splicing, but the levels of the neural crest marker *SOX4* and the stress marker *ATF3* were higher than expected in resistant cells treated with toyocamycin. The observed increase could be interpreted as being a result of resistant cells which need further growth inhibition (provided by the addition of dabrafenib) to reduce levels of those markers or a drug dependency that has developed over prolonged dabrafenib treatment.

The decreased levels of the neural crest markers *SOX4* and *SOX10* and the stress related markers *ATF3* and *DDIT3* on the combination treatment could lead to the hypothesis of reversibility of the "stress-like" state upon combination of dabrafenib with a stress inhibitor. As toyocamycin alone did not seem to have a decreasing effect on the levels of neural crest and stress markers, it could be possible that the basal stress level is rather low and triggered upon dabrafenib treatment.

5.5.3 Bulk ATAC-sequencing confirms "stress-like" state in resistant cells

As part of the validation of the epigenetic "stress-like" state, bulk ATAC-seq was performed on the resistant and sensitive cell lines (fig. 43-45). The accessibility of markers for the neural crest state and the "stress-like" state were compared between the cell lines. The neural crest marker *ATF4* and the stress related markers *ATF3, DDIT3, HSPA9, HSP90B1, HSPA5, YOU*, *HSPA8, JUNB, JUND* and *UBB* showed higher accessibility in resistant cells than in sensitive cells. This is in good agreement with the scATAC-seq and scRNA-seq data and strengthens our confidence of the existence of a "stress-like" state in resistant cells.

HSPA5 is a main regulator of ER stress involved in the correct folding of proteins and quality control in the ER lumen. *HSP90* was identified as a marker for progression of melanoma and inhibitors are in clinical trials (McCarthy et al. 2008). We found that the ER stress regulator *HSP90B1* was higher accessible in resistant melanoma cells. *HSPA9* is related to mitochondrial stress and *YOU* is an oxygen-regulated protein suppressing hypoxia-induced apoptotic cell death (Honrath et al. 2017). The higher accessibility of factors for various stress types suggest an interplay between ER and mitochondrial/oxygen stress in resistant cells.

5.6 Conclusion, future work and outlook

Using our Zebrafish model system, we proved the successful *in vivo* modelling of drug resistance to BRAF inhibition in a *BRAFV600E* driven melanoma. As in human patients, the high number of samples that developed resistance underlines the importance of further research of the mechanisms driving resistance and the work on new approaches of therapy.

Defining the resistant cell state on a transcriptional and epigenetic level on single-cell basis has revealed inter- and intratumoral heterogeneity and allowed us to further characterize the cell states that were previously defined by Hoek et al. and Rambow et al. Our data shows that many epigenetic states co-exist within the same tumor and revealed the differential accessibility of chromatin according to various disease states. The emergence of a dominant "stress-like" epigenetic state at the point of minimal disease is of immense clinical importance and can be regarded as a step towards enhancing our understanding of epigenetic mechanisms underlying drug resistance in malignant melanoma as this would be the ideal point to intervene clinically.

Further, we have succeeded in validating the "stress-like" state on the transcriptional level. We have obtained comprehensive results demonstrating the trajectory of melanoma cells upon developing resistance. Proliferation and differentiation were previously combined in the $MITF^{high}$ cell state however, we have found that cells from a proliferative phenotype upon prolonged dabrafenib treatment either move towards a differentiated or a neural crest/ "stress-like" cell state.

As both, the scRNA-seq and scATAC-seq data suggested XBP1, a major player in ER stress, as a main factor contributing to intratumoral heterogeneity, the effects of inhibition of ER stress were investigated. Inhibiting the stress-state resulted in lower viability of dabrafenib resistant cells compared to sensitive cells. Also, the levels of markers of the neural crest and stress-like cell state responded differently to ER stress inhibition and dabrafenib treatment. All in all, the levels in sensitive cells showed lower fluctuation of stress markers. In resistant cells, especially the dabrafenib and toyocamycin combination treatment potently reduced markers for the neural crest and "stress-like" state. Taken together, these findings suggest that the stress-like state is a crucial feature of cells to develop resistance and grow under BRAF inhibition. Furthermore, it seems like drug sensitivity could be restored on stress inhibition. Further data collection is required to more specifically narrow down the stress-like state and its interplay with the other cell states.

The *in vitro* validation of the "stress-like" cell state was an important methodology and allowed us to exclude the previous hypothesis that the stress-like cell state is an artifact from scRNA-seq data due to cell dissociation and sorting methods (van den Brink et al. 2017). Our bulk ATAC-seq data shows that several regions of markers for the "stress-like" state (*XBP1, ATF3, ATF6, DDIT3, UBB*) are more accessible in resistant cells compared to sensitive cells which is in line with our scRNA-seq and scATAC-seq data.

We have provided comprehensive results following the transcriptional and epigenetic landscape of melanoma cells from an untreated state over a sensitive phenotype to a minimal disease state and resistant state.

Although we have contributed to further definition of the disease relevant states in melanoma the specific mechanisms of the "stress-like" state to confer drug resistance remains to be elucidated.

Future work will focus on the *in vivo* validation of candidate genes by overexpression experiments. Another interesting approach would be to use both, dabrafenib and a stress inhibitor in an *in vivo* experiment and follow up tumor progress.

6 References

Ablain, Julien; Xu, Mengshu; Rothschild, Harriet; Jordan, Richard C.; Mito, Jeffrey K.; Daniels, Brianne H. et al. (2018): Human tumor genomics and zebrafish modeling identify SPRED1 loss as a driver of mucosal melanoma. In *Science* 362 (6418), pp. 1055–1060. DOI: 10.1126/science.aau6509.

Arozarena, Imanol; Wellbrock, Claudia (2019): Phenotype plasticity as enabler of melanoma progression and therapy resistance. In *Nature reviews. Cancer* 19 (7), pp. 377–391. DOI: 10.1038/s41568-019-0154-4.

Baron, Maayan; Tagore, Mohita; Hunter, Miranda V.; Kim, Isabella S.; Moncada, Reuben; Yan, Yun et al. (2020): The Stress-Like Cancer Cell State Is a Consistent Component of Tumorigenesis. In *Cell systems* 11 (5), pp. 536–546. DOI: 10.1016/j.cels.2020.08.018.

Beck, Daniela; Niessner, Heike; Smalley, Keiran S. M.; Flaherty, Keith; Paraiso, Kim H. T.; Busch, Christian et al. (2013): Vemurafenib potently induces endoplasmic reticulum stress-mediated apoptosis in BRAFV600E melanoma cells. In *Science signaling* 6 (260), ra7. DOI: 10.1126/scisignal.2003057.

Burrell, Rebecca A.; McGranahan, Nicholas; Bartek, Jiri; Swanton, Charles (2013): The causes and consequences of genetic heterogeneity in cancer evolution. In *Nature* 501 (7467), pp. 338–345. DOI: 10.1038/nature12625.

Butler, Andrew; Hoffman, Paul; Smibert, Peter; Papalexi, Efthymia; Satija, Rahul (2018): Integrating single-cell transcriptomic data across different conditions, technologies, and species. In *Nature biotechnology* 36 (5), pp. 411–420. DOI: 10.1038/nbt.4096.

Carreira, Suzanne; Goodall, Jane; Denat, Laurence; Rodriguez, Mercedes; Nuciforo, Paolo; Hoek, Keith S. et al. (2006): Mitf regulation of Dia1 controls melanoma proliferation and invasiveness. In *Genes & Development* 20 (24), pp. 3426–3439. DOI: 10.1101/gad.406406.

Ceol, Craig J.; Houvras, Yariv; Jane-Valbuena, Judit; Bilodeau, Steve; Orlando, David A.; Battisti, Valentine et al. (2011): The histone methyltransferase SETDB1 is recurrently amplified in melanoma and accelerates its onset. In *Nature* 471 (7339), pp. 513–517. DOI: 10.1038/nature09806.

Chapman, Anna; Del Fernandez Ama, Laura; Ferguson, Jennifer; Kamarashev, Jivko; Wellbrock, Claudia; Hurlstone, Adam (2014): Heterogeneous tumor subpopulations cooperate to drive invasion. In *Cell reports* 8 (3), pp. 688–695. DOI: 10.1016/j.celrep.2014.06.045.

Chapman, Paul B.; Hauschild, Axel; Robert, Caroline; Haanen, John B.; Ascierto, Paolo; Larkin, James et al. (2011): Improved survival with vemurafenib in melanoma with BRAF V600E mutation. In *The New England journal of medicine* 364 (26), pp. 2507–2516. DOI: 10.1056/NEJMoa1103782.

Cheli, Y.; Giuliano, S.; Fenouille, N.; Allegra, M.; Hofman, V.; Hofman, P. et al. (2012): Hypoxia and MITF control metastatic behaviour in mouse and human melanoma cells. In *Oncogene* 31 (19), pp. 2461–2470. DOI: 10.1038/onc.2011.425.

Costin, Gertrude-E; Hearing, Vincent J. (2007): Human skin pigmentation: melanocytes modulate skin color in response to stress. In *FASEB journal : official publication of the Federation of American Societies for Experimental Biology* 21 (4), pp. 976–994. DOI: 10.1096/fj.06-6649rev.

Davies, Helen; Bignell, Graham R.; Cox, Charles; Stephens, Philip; Edkins, Sarah; Clegg, Sheila et al. (2002): Mutations of the BRAF gene in human cancer. In *Nature* 417 (6892), pp. 949–954. DOI: 10.1038/nature00766.

Diepgen, Thomas L.; Mahler, V. (2002): The epidemiology of skin cancer. In *The British journal of dermatology* 146 Suppl 61, pp. 1–6. DOI: 10.1046/j.1365-2133.146.s61.2.x.

D'Orazio, John; Jarrett, Stuart; Amaro-Ortiz, Alexandra; Scott, Timothy (2013): UV radiation and the skin. In *International Journal of Molecular Sciences* 14 (6), pp. 12222–12248. DOI: 10.3390/ijms140612222.

Feige, Erez; Yokoyama, Satoru; Levy, Carmit; Khaled, Mehdi; Igras, Vivien; Lin, Richard J. et al. (2011): Hypoxia-induced transcriptional repression of the melanoma-associated oncogene MITF. In *Proceedings of the National Academy of Sciences of the United States of America* 108 (43), E924-33. DOI: 10.1073/pnas.1106351108.

Ferguson, Jennifer; Smith, Michael; Zudaire, Isabel; Wellbrock, Claudia; Arozarena, Imanol (2017): Glucose availability controls ATF4-mediated MITF suppression to drive melanoma cell growth. In *Oncotarget* 8 (20), pp. 32946–32959. DOI: 10.18632/oncotarget.16514.

Flaherty, Keith T.; Infante, Jeffery R.; Daud, Adil; Gonzalez, Rene; Kefford, Richard F.; Sosman, Jeffrey et al. (2012): Combined BRAF and MEK inhibition in melanoma with BRAF V600 mutations. In *The New England journal of medicine* 367 (18), pp. 1694–1703. DOI: 10.1056/NEJMoa1210093.

Gandini, Sara; Sera, Francesco; Cattaruzza, Maria Sofia; Pasquini, Paolo; Picconi, Orietta; Boyle, Peter; Melchi, Carmelo Francesco (2005): Meta-analysis of risk factors for cutaneous melanoma: II. Sun exposure. In *European journal of cancer* 41 (1), pp. 45–60. DOI: 10.1016/j.ejca.2004.10.016.

Hamid, Omid; Robert, Caroline; Daud, Adil; Hodi, F. Stephen; Hwu, Wen-Jen; Kefford, Richard et al. (2013): Safety and tumor responses with lambrolizumab (anti-PD-1) in melanoma. In *The New England journal of medicine* 369 (2), pp. 134–144. DOI: 10.1056/NEJMoa1305133.

Hauschild, Axel; Grob, Jean-Jacques; Demidov, Lev V.; Jouary, Thomas; Gutzmer, Ralf; Millward, Michael et al. (2012): Dabrafenib in BRAF-mutated metastatic melanoma: a multicentre, open-label, phase 3 randomised controlled trial. In *The Lancet* 380 (9839), pp. 358–365. DOI: 10.1016/S0140-6736(12)60868-X.

Hayward, Nicholas K.; Wilmott, James S.; Waddell, Nicola; Johansson, Peter A.; Field, Matthew A.; Nones, Katia et al. (2017): Whole-genome landscapes of major melanoma subtypes. In *Nature* 545 (7653), pp. 175–180. DOI: 10.1038/nature22071.

Hendrix, Mary J. C.; Seftor, Elisabeth A.; Seftor, Richard E. B.; Chao, Jun-Tzu; Chien, Du-Shieng; Chu, Yi-Wen (2016): Tumor cell vascular mimicry: Novel targeting opportunity in melanoma. In *Pharmacology & therapeutics* 159, pp. 83–92. DOI: 10.1016/j.pharmthera.2016.01.006.

Heppner, G. H. (1984): Tumor heterogeneity. In *Cancer research* 44 (6), pp. 2259–2265.

Hodis, Eran; Watson, Ian R.; Kryukov, Gregory V.; Arold, Stefan T.; Imielinski, Marcin; Theurillat, Jean-Philippe et al. (2012): A landscape of driver mutations in melanoma. In *Cell* 150 (2), pp. 251–263. DOI: 10.1016/j.cell.2012.06.024.

Hoek, Keith S.; Eichhoff, Ossia M.; Schlegel, Natalie C.; Döbbeling, Udo; Kobert, Nikita; Schaerer, Leo et al. (2008): In vivo switching of human melanoma cells between proliferative and invasive states. In *Cancer research* 68 (3), pp. 650–656. DOI: 10.1158/0008-5472.CAN-07-2491.

Hoek, Keith S.; Schlegel, Natalie C.; Brafford, Patricia; Sucker, Antje; Ugurel, Selma; Kumar, Rajiv et al. (2006): Metastatic potential of melanomas defined by specific gene expression profiles with no BRAF signature. In *Pigment cell research* 19 (4), pp. 290–302. DOI: 10.1111/j.1600-0749.2006.00322.x.

Honrath, Birgit; Metz, Isabell; Bendridi, Nadia; Rieusset, Jennifer; Culmsee, Carsten; Dolga, Amalia M. (2017): Glucose-regulated protein 75 determines ER-mitochondrial coupling and sensitivity to oxidative stress in neuronal cells. In *Cell Death Discovery* 3, p. 17076. DOI: 10.1038/cddiscovery.2017.76.

Jakob, John A.; Bassett, Roland L.; Ng, Chaan S.; Curry, Jonathan L.; Joseph, Richard W.; Alvarado, Gladys C. et al. (2012): NRAS mutation status is an independent prognostic factor in metastatic melanoma. In *Cancer* 118 (16), pp. 4014–4023. DOI: 10.1002/cncr.26724.

Johannessen, Cory M.; Boehm, Jesse S.; Kim, So Young; Thomas, Sapana R.; Wardwell, Leslie; Johnson, Laura A. et al. (2010): COT drives resistance to RAF inhibition through MAP kinase pathway reactivation. In *Nature* 468 (7326), pp. 968–972. DOI: 10.1038/nature09627.

Kaufman, Charles K.; Mosimann, Christian; Fan, Zi Peng; Yang, Song; Thomas, Andrew J.; Ablain, Julien et al. (2016): A zebrafish melanoma model reveals emergence of neural crest identity during melanoma initiation. In *Science* 351 (6272), aad2197. DOI: 10.1126/science.aad2197.

Kaur, Amanpreet; Ecker, Brett L.; Douglass, Stephen M.; Kugel, Curtis H.; Webster, Marie R.; Almeida, Filipe V. et al. (2019): Remodeling of the Collagen Matrix in Aging Skin Promotes Melanoma Metastasis and Affects Immune Cell Motility. In *Cancer discovery* 9 (1), pp. 64–81. DOI: 10.1158/2159-8290.CD-18-0193.

Kim, Isabella S.; Heilmann, Silja; Kansler, Emily R.; Zhang, Yan; Zimmer, Milena; Ratnakumar, Kajan et al. (2017): Microenvironment-derived factors driving metastatic plasticity in melanoma. In *Nature communications* 8, p. 14343. DOI: 10.1038/ncomms14343.

Klein, Allon M.; Mazutis, Linas; Akartuna, Ilke; Tallapragada, Naren; Veres, Adrian; Li, Victor et al. (2015): Droplet barcoding for single-cell transcriptomics applied to embryonic stem cells. In *Cell* 161 (5), pp. 1187–1201. DOI: 10.1016/j.cell.2015.04.044.

Konieczkowski, David J.; Johannessen, Cory M.; Abudayyeh, Omar; Kim, Jong Wook; Cooper, Zachary A.; Piris, Adriano et al. (2014): A melanoma cell state distinction influences sensitivity to MAPK pathway inhibitors. In *Cancer discovery* 4 (7), pp. 816–827. DOI: 10.1158/2159-8290.CD-13-0424.

Larkin, James; Ascierto, Paolo A.; Dréno, Brigitte; Atkinson, Victoria; Liszkay, Gabriella; Maio, Michele et al. (2014): Combined vemurafenib and cobimetinib in BRAF-mutated melanoma. In *The New England journal of medicine* 371 (20), pp. 1867–1876. DOI: 10.1056/NEJMoa1408868.

Lauss, Martin; Haq, Rizwan; Cirenajwis, Helena; Phung, Bengt; Harbst, Katja; Staaf, Johan et al. (2015): Genome-Wide DNA Methylation Analysis in Melanoma Reveals the Importance of CpG Methylation in MITF Regulation. In *The Journal of investigative dermatology* 135 (7), pp. 1820–1828. DOI: 10.1038/jid.2015.61.

Levy, Carmit; Khaled, Mehdi; Fisher, David E. (2006): MITF: master regulator of melanocyte development and melanoma oncogene. In *Trends in molecular medicine* 12 (9), pp. 406–414. DOI: 10.1016/j.molmed.2006.07.008.

Lidsky, Michael; Antoun, Gamil; Speicher, Paul; Adams, Bartley; Turley, Ryan; Augustine, Christi et al. (2014): Mitogen-activated protein kinase (MAPK) hyperactivation and enhanced NRAS expression drive acquired vemurafenib resistance in V600E BRAF melanoma cells. In *The Journal of Biological Chemistry* 289 (40), pp. 27714–27726. DOI: 10.1074/jbc.M113.532432.

Ma, Xiao-Hong; Piao, Sheng-Fu; Dey, Souvik; McAfee, Quentin; Karakousis, Giorgos; Villanueva, Jessie et al. (2014): Targeting ER stress-induced autophagy overcomes BRAF inhibitor resistance in melanoma. In *The Journal of clinical investigation* 124 (3), pp. 1406–1417. DOI: 10.1172/JCI70454.

Marusyk, Andriy; Almendro, Vanessa; Polyak, Kornelia (2012): Intra-tumour heterogeneity: a looking glass for cancer? In *Nature Reviews Cancer* 12 (5), pp. 323–334. DOI: 10.1038/nrc3261.

McCarthy, M. M.; Pick, E.; Kluger, Y.; Gould-Rothberg, B.; Lazova, R.; Camp, R. L. et al. (2008): HSP90 as a marker of progression in melanoma. In *Annals of oncology : official journal of the European Society for Medical Oncology* 19 (3), pp. 590–594. DOI: 10.1093/annonc/mdm545.

Nazarian, Ramin; Shi, Hubing; Wang, Qi; Kong, Xiangju; Koya, Richard C.; Lee, Hane et al. (2010): Melanomas acquire resistance to B-RAF(V600E) inhibition by RTK or N-RAS upregulation. In *Nature* 468 (7326), pp. 973–977. DOI: 10.1038/nature09626.

Nowell, P. C. (1976): The clonal evolution of tumor cell populations. In *Science* 194 (4260), pp. 23–28. DOI: 10.1126/science.959840.

Ploper, Diego; Robertis, Edward M. de (2015): The MITF family of transcription factors: Role in endolysosomal biogenesis, Wnt signaling, and oncogenesis. In *Pharmacological research* 99, pp. 36–43. DOI: 10.1016/j.phrs.2015.04.006.

Poulikakos, Poulikos I.; Persaud, Yogindra; Janakiraman, Manickam; Kong, Xiangju; Ng, Charles; Moriceau, Gatien et al. (2011): RAF inhibitor resistance is mediated by dimerization of aberrantly spliced BRAF(V600E). In *Nature* 480 (7377), pp. 387–390. DOI: 10.1038/nature10662.

Qiu, Xiaojie; Mao, Qi; Tang, Ying; Wang, Li; Chawla, Raghav; Pliner, Hannah A.; Trapnell, Cole (2017): Reversed graph embedding resolves complex single-cell trajectories. In *Nature methods* 14 (10), pp. 979–982. DOI: 10.1038/nmeth.4402.

R Foundation for Statistical Computing (2013): R: A language and environment for statistical computing. Vienna, Austria: R Core Team. Available online at URL http://www.R-project.org/.

Rambow, Florian; Job, Bastien; Petit, Valérie; Gesbert, Franck; Delmas, Véronique; Seberg, Hannah et al. (2015): New Functional Signatures for Understanding Melanoma Biology from Tumor Cell Lineage-Specific Analysis. In *Cell reports* 13 (4), pp. 840–853. DOI: 10.1016/j.celrep.2015.09.037.

Rambow, Florian; Rogiers, Aljosja; Marin-Bejar, Oskar; Aibar, Sara; Femel, Julia; Dewaele, Michael et al. (2018): Toward Minimal Residual Disease-Directed Therapy in Melanoma. In *Cell* 174 (4), 843-855.e19. DOI: 10.1016/j.cell.2018.06.025.

Restivo, Gaetana; Diener, Johanna; Cheng, Phil F.; Kiowski, Gregor; Bonalli, Mario; Biedermann, Thomas et al. (2017): low neurotrophin receptor CD271 regulates phenotype switching in melanoma. In *Nature communications* 8 (1), p. 1988. DOI: 10.1038/s41467-017-01573-6.

Ri, M.; Tashiro, E.; Oikawa, D.; Shinjo, S.; Tokuda, M.; Yokouchi, Y. et al. (2012): Identification of Toyocamycin, an agent cytotoxic for multiple myeloma cells, as a potent inhibitor of ER stress-induced XBP1 mRNA splicing. In *Blood Cancer Journal* 2 (7), e79. DOI: 10.1038/bcj.2012.26.

Robert, Caroline; Karaszewska, Boguslawa; Schachter, Jacob; Rutkowski, Piotr; Mackiewicz, Andrzej; Stroiakovski, Daniil et al. (2015): Improved overall survival in melanoma with combined dabrafenib and trametinib. In *The New England journal of medicine* 372 (1), pp. 30–39. DOI: 10.1056/NEJMoa1412690.

Robinson, James T.; Thorvaldsdóttir, Helga; Winckler, Wendy; Guttman, Mitchell; Lander, Eric S.; Getz, Gad; Mesirov, Jill P. (2011): Integrative genomics viewer. In *Nature biotechnology* 29 (1), pp. 24–26. DOI: 10.1038/nbt.1754.

Sensi, Marialuisa; Catani, Mara; Castellano, Giancarlo; Nicolini, Gabriella; Alciato, Federica; Tragni, Gabrina et al. (2011): Human cutaneous melanomas lacking MITF and melanocyte differentiation antigens express a functional Axl receptor kinase. In *The Journal of investigative dermatology* 131 (12), pp. 2448–2457. DOI: 10.1038/jid.2011.218.

Shaffer, Sydney M.; Dunagin, Margaret C.; Torborg, Stefan R.; Torre, Eduardo A.; Emert, Benjamin; Krepler, Clemens et al. (2017): Rare cell variability and drug-induced reprogramming as a mode of cancer drug resistance. In *Nature* 546 (7658), pp. 431–435. DOI: 10.1038/nature22794.

Shi, Hubing; Hugo, Willy; Kong, Xiangju; Hong, Aayoung; Koya, Richard C.; Moriceau, Gatien et al. (2014): Acquired resistance and clonal evolution in melanoma during BRAF inhibitor therapy. In *Cancer discovery* 4 (1), pp. 80–93. DOI: 10.1158/2159-8290.CD-13-0642.

Shi, Hubing; Moriceau, Gatien; Kong, Xiangju; Lee, Mi-Kyung; Lee, Hane; Koya, Richard C. et al. (2012): Melanoma whole-exome sequencing identifies (V600E)B-RAF amplification-mediated acquired B-RAF inhibitor resistance. In *Nature communications* 3, p. 724. DOI: 10.1038/ncomms1727.

Siegel, Rebecca L.; Miller, Kimberly D.; Jemal, Ahmedin (2019): Cancer statistics, 2019. In *CA: a cancer journal for clinicians* 69 (1), pp. 7–34. DOI: 10.3322/caac.21551.

Smith, Michael P.; Brunton, Holly; Rowling, Emily J.; Ferguson, Jennifer; Arozarena, Imanol; Miskolczi, Zsofia et al. (2016): Inhibiting Drivers of Non-mutational Drug Tolerance Is a Salvage Strategy for Targeted Melanoma Therapy. In *Cancer cell* 29 (3), pp. 270–284. DOI: 10.1016/j.ccell.2016.02.003.

Smith, Michael P.; Ferguson, Jennifer; Arozarena, Imanol; Hayward, Robert; Marais, Richard; Chapman, Anna et al. (2013): Effect of SMURF2 targeting on susceptibility to MEK inhibitors in melanoma. In *Journal of the National Cancer Institute* 105 (1), pp. 33–46. DOI: 10.1093/jnci/djs471.

Straussman, Ravid; Morikawa, Teppei; Shee, Kevin; Barzily-Rokni, Michal; Qian, Zhi Rong; Du, Jinyan et al. (2012): Tumour micro-environment elicits innate resistance to RAF inhibitors through HGF secretion. In *Nature* 487 (7408), pp. 500–504. DOI: 10.1038/nature11183.

Stuart, Tim; Butler, Andrew; Hoffman, Paul; Hafemeister, Christoph; Papalexi, Efthymia; Mauck, William M. et al. (2019): Comprehensive Integration of Single-Cell Data. In *Cell* 177 (7), 1888-1902.e21. DOI: 10.1016/j.cell.2019.05.031.

Su, Yapeng; Wei, Wei; Robert, Lidia; Xue, Min; Tsoi, Jennifer; Garcia-Diaz, Angel et al. (2017): Single-cell analysis resolves the cell state transition and signaling dynamics associated with melanoma drug-induced resistance. In *Proceedings of the National Academy of Sciences of the United States of America* 114 (52), pp. 13679–13684. DOI: 10.1073/pnas.1712064115.

Sun, Chong; Wang, Liqin; Huang, Sidong; Heynen, Guus J. J. E.; Prahallad, Anirudh; Robert, Caroline et al. (2014): Reversible and adaptive resistance to BRAF(V600E) inhibition in melanoma. In *Nature* 508 (7494), pp. 118–122. DOI: 10.1038/nature13121.

Szegezdi, Eva; Logue, Susan E.; Gorman, Adrienne M.; Samali, Afshin (2006): Mediators of endoplasmic reticulum stress-induced apoptosis. In *EMBO reports* 7 (9), pp. 880–885. DOI: 10.1038/sj.embor.7400779.

The Cancer Genome Atlas Network (2015): Genomic Classification of Cutaneous Melanoma. In *Cell* 161 (7), pp. 1681–1696. DOI: 10.1016/j.cell.2015.05.044.

Tirosh, Itay; Izar, Benjamin; Prakadan, Sanjay M.; Wadsworth, Marc H.; Treacy, Daniel; Trombetta, John J. et al. (2016): Dissecting the multicellular ecosystem of metastatic melanoma by single-cell RNA-seq. In *Science* 352 (6282), pp. 189–196. DOI: 10.1126/science.aad0501.

Tobin, Desmond J. (2006): Biochemistry of human skin--our brain on the outside. In *Chemical Society reviews* 35 (1), pp. 52–67. DOI: 10.1039/b505793k.

Topalian, Suzanne L.; Hodi, F. Stephen; Brahmer, Julie R.; Gettinger, Scott N.; Smith, David C.; McDermott, David F. et al. (2012): Safety, activity, and immune correlates of anti-PD-1 antibody in cancer. In *The New England journal of medicine* 366 (26), pp. 2443–2454. DOI: 10.1056/NEJMoa1200690.

Trapnell, Cole; Cacchiarelli, Davide; Grimsby, Jonna; Pokharel, Prapti; Li, Shuqiang; Morse, Michael et al. (2014): The dynamics and regulators of cell fate decisions are revealed by pseudotemporal ordering of single cells. In *Nature biotechnology* 32 (4), pp. 381–386. DOI: 10.1038/nbt.2859.

Trapnell, Cole; Roberts, Adam; Goff, Loyal; Pertea, Geo; Kim, Daehwan; Kelley, David R. et al. (2012): Differential gene and transcript expression analysis of RNA-seq experiments with TopHat and Cufflinks. In *Nature protocols* 7 (3), pp. 562–578. DOI: 10.1038/nprot.2012.016.

Tsao, Hensin; Chin, Lynda; Garraway, Levi A.; Fisher, David E. (2012): Melanoma: from mutations to medicine. In *Genes & Development* 26 (11), pp. 1131–1155. DOI: 10.1101/gad.191999.112.

Tsoi, Jennifer; Robert, Lidia; Paraiso, Kim; Galvan, Carlos; Sheu, Katherine M.; Lay, Johnson et al. (2018): Multi-stage Differentiation Defines Melanoma Subtypes with Differential Vulnerability to Drug-Induced Iron-Dependent Oxidative Stress. In *Cancer cell* 33 (5), 890-904.e5. DOI: 10.1016/j.ccell.2018.03.017.

van Allen, Eliezer M.; Wagle, Nikhil; Sucker, Antje; Treacy, Daniel J.; Johannessen, Cory M.; Goetz, Eva M. et al. (2014): The genetic landscape of clinical resistance to RAF inhibition in metastatic melanoma. In *Cancer discovery* 4 (1), pp. 94–109. DOI: 10.1158/2159-8290.CD-13-0617.

van den Brink, Susanne C.; Sage, Fanny; Vértesy, Ábel; Spanjaard, Bastiaan; Peterson-Maduro, Josi; Baron, Chloé S. et al. (2017): Single-cell sequencing reveals dissociation-induced gene expression in tissue subpopulations. In *Nature methods* 14 (10), pp. 935–936. DOI: 10.1038/nmeth.4437.

Vandamme, Niels; Berx, Geert (2014): Melanoma cells revive an embryonic transcriptional network to dictate phenotypic heterogeneity. In *Frontiers in oncology* 4, p. 352. DOI: 10.3389/fonc.2014.00352.

Vazquez, Francisca; Lim, Ji-Hong; Chim, Helen; Bhalla, Kavita; Girnun, Geoff; Pierce, Kerry et al. (2013): PGC1α expression defines a subset of human melanoma tumors with increased mitochondrial capacity and resistance to oxidative stress. In *Cancer cell* 23 (3), pp. 287–301. DOI: 10.1016/j.ccr.2012.11.020.

Verfaillie, Annelien; Imrichova, Hana; Atak, Zeynep Kalender; Dewaele, Michael; Rambow, Florian; Hulselmans, Gert et al. (2015): Decoding the regulatory landscape of melanoma reveals TEADS as regulators of the invasive cell state. In *Nature communications* 6, p. 6683. DOI: 10.1038/ncomms7683.

Villanueva, Jessie; Vultur, Adina; Lee, John T.; Somasundaram, Rajasekharan; Fukunaga-Kalabis, Mizuho; Cipolla, Angela K. et al. (2010): Acquired resistance to BRAF inhibitors mediated by a RAF kinase switch in melanoma can be overcome by cotargeting MEK and IGF-1R/PI3K. In *Cancer cell* 18 (6), pp. 683–695. DOI: 10.1016/j.ccr.2010.11.023.

Whittaker, Steven R.; Theurillat, Jean-Philippe; van Allen, Eliezer; Wagle, Nikhil; Hsiao, Jessica; Cowley, Glenn S. et al. (2013): A genome-scale RNA interference screen implicates NF1 loss in resistance to RAF inhibition. In *Cancer discovery* 3 (3), pp. 350–362. DOI: 10.1158/2159-8290.CD-12-0470.

Widmer, Daniel S.; Cheng, Phil F.; Eichhoff, Ossia M.; Belloni, Benedetta C.; Zipser, Marie C.; Schlegel, Natalie C. et al. (2012): Systematic classification of melanoma cells by phenotype-specific gene expression mapping. In *Pigment cell & melanoma research* 25 (3), pp. 343–353. DOI: 10.1111/j.1755-148X.2012.00986.x.

Wolchok, Jedd D.; Weber, Jeffrey S.; Hamid, Omid; Lebbé, Celeste; Maio, Michele; Schadendorf, Dirk et al. (2010): Ipilimumab efficacy and safety in patients with advanced melanoma: a retrospective analysis of HLA subtype from four trials. In *Cancer Immunity : a Journal of the Academy of Cancer Immunology* 10, p. 9.

Wouters, Jasper; Kalender-Atak, Zeynep; Minnoye, Liesbeth; Spanier, Katina I.; Waegeneer, Maxime de; Bravo González-Blas, Carmen et al. (2020): Robust gene expression programs underlie recurrent cell states and phenotype switching in melanoma. In *Nature cell biology* 22 (8), pp. 986–998. DOI: 10.1038/s41556-020-0547-3.

Wulf, Hans Christian; Sandby-Møller, Jane; Kobayasi, Takasi; Gniadecki, Robert (2004): Skin aging and natural photoprotection. In *Micron* 35 (3), pp. 185–191. DOI: 10.1016/j.micron.2003.11.005.

Yang, Guang; Rajadurai, Anpuchchelvi; Tsao, Hensin (2005): Recurrent patterns of dual RB and p53 pathway inactivation in melanoma. In *The Journal of investigative dermatology* 125 (6), pp. 1242–1251. DOI: 10.1111/j.0022-202X.2005.23931.x.

Yen, Jennifer; White, Richard M.; Wedge, David C.; van Loo, Peter; Ridder, Jeroen de; Capper, Amy et al. (2013): The genetic heterogeneity and mutational burden of engineered melanomas in zebrafish models. In *Genome biology* 14 (10), R113. DOI: 10.1186/gb-2013-14-10-r113.

Yoshida, Hiderou; Matsui, Toshie; Yamamoto, Akira; Okada, Tetsuya; Mori, Kazutoshi (2001): XBP1 mRNA Is Induced by ATF6 and Spliced by IRE1 in Response to ER Stress to Produce a Highly Active Transcription Factor. In *Cell* 107 (7), pp. 881–891. DOI: 10.1016/S0092-8674(01)00611-0.

Zhang, Xin; Wang, Linghui; Zeng, Xianlu; Fujita, Takashi; Liu, Wenguang (2017): Runx3 inhibits melanoma cell migration through regulation of cell shape change. In *Cell biology international* 41 (9), pp. 1048–1055. DOI: 10.1002/cbin.10824.

Zilionis, Rapolas; Nainys, Juozas; Veres, Adrian; Savova, Virginia; Zemmour, David; Klein, Allon M.; Mazutis, Linas (2017): Single-cell barcoding and sequencing using droplet microfluidics. In *Nature protocols* 12 (1), pp. 44–73. DOI: 10.1038/nprot.2016.154.

7 Acknowledgements

First of all, I want to thank Prof. Leonard Zon for accepting me in his research group and giving me the chance to work on this fascinating topic. Len is an amazing mentor for researchers and students from various backgrounds and helped me shaping my idea and vision of great science. He not only guided me in my research project but helped me navigating in the joyous, yet competitive world of research and science.

I would like to express my special thanks to my supervisor Dr. Jeffrey Mito for introducing me to the topic and teaching me a lot of techniques. He consistently allowed me to work on my own responsibility and strengthened my passion for science. Jeff went to great lengths in keeping me engaged when physical working in the lab was restricted and helped me overcome various obstacles I have been facing through my research remotely.

I want to acknowledge all the other Zon lab members for including me in the team and providing feedback and help whenever needed.

This project constituted a major step in my professional and personal development and I highly appreciate all the skills that I gained and improved during my time in the Zon lab.

I must express my very profound gratitude to my parents and to my friends for providing me with unfailing support and continuous encouragement throughout my time in Boston and through the process of researching and writing this thesis.

Erklärung:

Ich erkläre, dass die vorliegende Diplomarbeit/Masterarbeit von mir selbst verfasst wurde und ich keine anderen als die angeführten Behelfe verwendet bzw. mich auch sonst keiner unerlaubter Hilfe bedient habe.

Ich versichere, dass ich diese Diplomarbeit/Masterarbeit bisher weder im In- noch im Ausland (einer Beurteilerin/einem Beurteiler zur Begutachtung) in irgendeiner Form als Prüfungsarbeit vorgelegt habe.

Weiters versichere ich, dass die von mir eingereichten Exemplare (ausgedruckt und elektronisch) identisch sind.

Declaration:

I hereby declare that the submitted Master thesis was written by myself and that I did not use any aids other than those indicated, none of which are unauthorised.

I assure that I have not previously submitted this Master thesis or its contents in any form for assessment as part of an examination either in Austria or abroad.

Furthermore, I assure that all copies submitted by myself (electronic and printed) are identical.

date: 21.02.2021 signature: Melanie Albrecht